

NO-A188 112

SOLID-STATE THRESHOLD ACCELEROMETER CHIP(U) MOTOROLA

1/2

INC SCOTTSDALE AZ GOVERNMENT ELECTRONICS GROUP

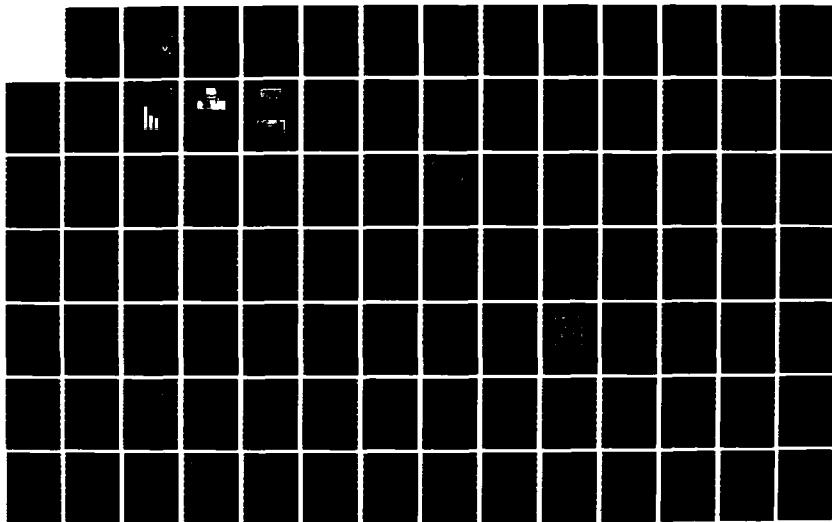
L FARACO ET AL 28 MAR 87 HDL-CR-86-146-1

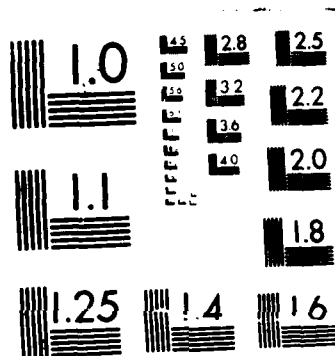
UNCLASSIFIED

DARLO2-85-C-0146

F/G 19/1

NL





MICROCOPY RESOLUTION TEST CHART
NATIONAL BUREAU OF STANDARDS 1963-A

HDL-CR-86-146-1
March 1987

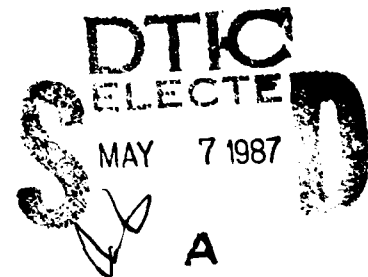
AD-A180 112

Solid-State Threshold Accelerometer Chip: Final Report

by Lou Farace & Al Meyer

Prepared by:
Motorola Inc.
Government Electronics Group
Tactical Electronics Division
8220 E. Roosevelt St
Scottsdale, AZ 85252

Under contract
DAAL02-85-C-0146



U.S. ARMY Laboratory Command
Harry Diamond Laboratories
Adelphi, MD 20783-1197

The findings in this report are not to be construed as an official Department of the Army position unless so designated by other authorized documents.

Citation of manufacturers' or trade names does not constitute an official indorsement or approval of the use thereof.

Destroy this report when it is no longer needed. Do not return it to the originator.

REPORT DOCUMENTATION PAGE

Form Approved
OMB No 0704-0188
Exp Date Jun 30 1986

1a. REPORT SECURITY CLASSIFICATION Unclassified		1b. RESTRICTIVE MARKINGS	
2a. SECURITY CLASSIFICATION AUTHORITY		3. DISTRIBUTION / AVAILABILITY OF REPORT Approved for public release; distribution unlimited.	
2b. DECLASSIFICATION / DOWNGRADING SCHEDULE		5. MONITORING ORGANIZATION REPORT NUMBER(S) HDL-CR-86-146-1	
4. PERFORMING ORGANIZATION REPORT NUMBER(S)		7a. NAME OF MONITORING ORGANIZATION Harry Diamond Laboratories	
6a. NAME OF PERFORMING ORGANIZATION Motorola Tactical Elec. Div. CDRL A004	6b. OFFICE SYMBOL (If applicable) PF650	7b. ADDRESS (City, State, and ZIP Code)	
6c. ADDRESS (City, State, and ZIP Code) 8220 E. Roosevelt St. Scottsdale, AZ 85252		9. PROCUREMENT INSTRUMENT IDENTIFICATION NUMBER	
8a. NAME OF FUNDING / SPONSORING ORGANIZATION	8b. OFFICE SYMBOL (If applicable) SLCHD-DE-OM	10. SOURCE OF FUNDING NUMBERS	
8c. ADDRESS (City, State, and ZIP Code)		PROGRAM ELEMENT NO. 61101A	PROJECT NO. 1L161101A91A
		TASK NO.	WORK UNIT ACCESSION NO.
11. TITLE (Include Security Classification) Solid - State Threshold Accelerometer Chip - Final Report			
12. PERSONAL AUTHOR(S) Lou Farace, Al Meyer HDL contact: Keith Warner			
13a. TYPE OF REPORT Final	13b. TIME COVERED FROM 9/85 TO 3/87	14. DATE OF REPORT (Year, Month, Day) 87/3/28	15. PAGE COUNT 97
16. SUPPLEMENTARY NOTATION			
17. COSATI CODES		18. SUBJECT TERMS (Continue on reverse if necessary and identify by block number)	
FIELD	GROUP	SUB-GROUP	
19. ABSTRACT (Continue on reverse if necessary and identify by block number) Micromechanical cantilever beam structures having a maximum length of 0.16 in. were designed, fabricated, and tested in six configurations for use as threshold acceleration sensors for projectile fuzes. Their small size and ability to be produced using monolithic fabrication techniques commonly used to make integrated circuits provides the possibility of incorporating multiswitch arrays into a single die surface area one-hundredth of a square inch. Design, fabrication, and test details are provided for two triple-beam arrays of cantilever structures made from 3-um-thick silicon dioxide.			
20. DISTRIBUTION / AVAILABILITY OF ABSTRACT <input checked="" type="checkbox"/> UNCLASSIFIED/UNLIMITED <input type="checkbox"/> SAME AS RPT. <input type="checkbox"/> DTIC USERS		21. ABSTRACT SECURITY CLASSIFICATION	
22a. NAME OF RESPONSIBLE INDIVIDUAL Robert Keith Warner		22b. TELEPHONE (Include Area Code) (202)394-3420	22c. OFFICE SYMBOL SLCHD-DE-OM


SOLID STATE THRESHOLD ACCELEROMETER
CHIP
FINAL REPORT

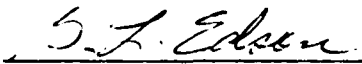
A004
MARCH 1987

Submitted to:

U.S. ARMY LABORATORY COMMAND
ISA/LABCOM
2800 Powder Mill Road
Adelphi, MD 20783-1145

Approved by:


M.A. Fried, Manager
Projectile Fuze Section


G. Edson, Chief Engineer
Fuze Systems Engineering

Microscale G-Switch

CONTENTS

	Page
1. INTRODUCTION	12
2. DEVICE DESCRIPTION	12
3. REQUIREMENTS	17
3.1 Threshold Acceleration Response	18
3.2 Maximum Length	19
3.3 Shock Survivability	19
3.4 Open Circuit Voltage	20
3.5 Closed Circuit Voltage	20
4. BEAM DESIGN CALCULATION	20
4.1 Microbeam Design Program	20
4.2 Electrostatic Effects	23
5. BEAM ANALYSIS	24
5.1 Launch Stiffening Effects	24
5.2 Setback Response	30
5.3 Spin Response	34
5.4 Balloting Sensitivity	43
5.5 Rough Handling Response	47
6. BEAM PACKAGING	53
7. BEAM PERFORMANCE/TESTING	55
7.1 Electrostatic Closure Testing	55
7.2 Test Configuration and Results	57
7.3 Post-Test Analysis	61
7.4 Contact-Weld Phenomenon	65
8. BEAM FABRICATION	67
9. COST MODEL	69
10.0 SUMMARY	70
11.0 CONCLUSIONS	70
12.0 RECOMMENDATIONS	71

DISTRIBUTION



Microscale G-Switch

APPENDICES

- | | |
|-------------------|---|
| Appendix A | Microbeam Design BASIC Program |
| Appendix B | Torsional Versus Bending Stiffness Effects |
| Appendix C | Modal Analysis Methods |

FIGURES

		Page
2-1	Microbeam sensor array	13
2-2	Microbeam gull wing--close-up view	14
2-3	Microbeam array with bridgewire	15
2-4	Microbeam device with reduced-width cross section	15
2-5	Microbeam /bridgewire illustration	16
4-1	Microbeam configuration	22
4-2	Polarization at microbeam contacts	23
5-1	Setback acceleration stiffening effects	27
5-2	Effect of setback acceleration on beam natural frequency	28
5-3	Effect of setback acceleration on spin sensor tip deflection	29
5-4	Effect of spin rate on setback sensor tip deflection	29
5-5	Effect of spin rate on setback sensor first natural frequency	29
5-6	Acceleration-time history at S&A for zone 8 launch from 105-mm howitzer	32
5-7	Tip deflection response of 217- μ m beam--contact and damper bar removed	32
5-8	Tip deflection response of 217- μ m beam--contact and damper bar included	32
5-9	Tip deflection response of 170- μ m beam--contact and damper bar included	33
5-10	Tip deflection response of 149- μ m beam--contact and damper bar included	33
5-11	105-mm Heppner data--zone 1 launch	35
5-12	105-mm Heppner data--zone 8 launch	36
5-13	Centrifugal force versus time--105 mm,zone 1	40

FIGURES (CONT)

		Page
5-14	Tip deflection response--434- μ m beam--105-mm zone 1 launch	41
5-15	Tip deflection response--268- μ m beam--105-mm zone 1 launch	41
5-16	Tip deflection response--214- μ m beam--105-mm zone 1 launch	41
5-17	Centrifugal force versus time--105-mm zone 8 launch	41
5-18	Tip deflection response--434- μ m beam--105-mm zone 8 launch	42
5-19	Tip deflection response--268- μ m beam--105-mm zone 8 launch	42
5-20	Tip deflection response--214- μ m beam--105-mm zone 8 launch	42
5-21	Tip deflection response--214- μ m beam--105-mm zone 8 launch	42
5-22	Balloting load application and beam sensor location for instrumentation projectile--155 mm	44
5-23	Acceleration-time history at S&A location	45
5-24	Tip deflection response of 214- μ m microbeam to closing acceleration	45
5-25	Tip deflection response of 214- μ m microbeam to opening acceleration	
5-26	Tip Deflection Response of 268-Micrometer Microbeam to Closing Acceleration	46
5-27	Tip Deflection Response of 268-Micrometer Microbeam to Opening Acceleration Load	46

FIGURES (CONT)

PAGE

5-28	Tip Deflection Response of 434-Micrometer Microbeam to Closing Acceleration	46
5-29	Tip Deflection Response of 434-Micrometer Microbeam to Opening Acceleration Load	46
5-30	Tip Deflection Versus Time; Damper Bar and Contact Removed; Forcing Frequency 2000 HZ And 224 g's	48
5-31	Root Stress Versus Time--Damper Bar And Contact Removed; Forcing Frequency 2 kHz and 224 g's	48
5-32	Tip Deflection Versus Time; Damper Bar And Contact Added; 2-kHz Forcing Frequency and 224 g's	
5-33	Root Stress Versus Time--Damper Bar and Contact Added	48
5-34	Tip Deflection Versus Time; Damper Bar Flush with Top of Beam; 2-kHz Forcing Frequency and 224 g's	48
5-35	Tip Deflection Versus Time; Damper Bar Preloads Beam; Forcing Frequency 2 kHz And 224 g's	50
5-36	Root Stress Versus Time; Damper Bar Preloads Beam; Forcing Frequency 2 kHz And 224 g's	50

	FIGURES (CONT)	Page
5-37	Tip Deflection Versus Time; Contacts And Damper Bars Included; Forcing Function 5 kHz and 224 g's	50
5-38	Root Stress Versus Time; Contacts and Damper Bars Included; Forcing Function 5 kHz and 224 g's	
5-39	Tip Deflection Versus Time; Contacts and Damper Bar Included; Forcing Function 9706 Hz and 224 g's	51
5-40	Root Stress Versus Time; Contacts and Damper Bar Included; Forcing Function 9706 Hz and 224 g's	51
5-41	Tip Deflection Versus Time; Damper Bar Removed; Forcing Frequency 9706 Hz and 224 g's	52
5-42	Root Stress Versus Time; Damper Bar Removed; Forcing Frequency 9706 Hz and 224 g's	
5-43	Tip Deflection Versus Time; Damper Bar Removed; Forcing Frequency 9706 Hz; Q = 20 Assumed; 11.2 g's Input	54
5-44	Root Stress Versus Time; Damper Bar Removed; Q = 20 Assumed; Forcing Frequency 9706 Hz And 11.2 g's	54
5-45	Tip Deflection Versus Time; Contacts and Damper Bar Included; Q = 20 Assumed; Forcing Frequency 9706 Hz and 11.2 g's	54
5-46	Root Stress Versus Time; Contacts and Damper Bar Included; Q = 20 Assumed; Forcing Frequency 9706 Hz and 11.2 g's	54
6-1	J-Pak Exploded View	53
7-1	Test Circuit Schematic For Electro-Static Closure Testing	55
7-2	Motorola Spin Pit Facility	57
7-3	J-Pak Mounting Illustration	57
7-4.1	Multiplex Circuit--Board A	58
7-4.2	Multiplex Circuit--Board B	59
7-5	Typical Oscilloscope Trace	60
7-6	Microbeam Switch Operative In Centrifuge--434-Micrometers Long	62

Microscale G-Switch

	FIGURES (CONT)	PAGE
7-7	Microbeam Switch Operative In Centrifuge--268-Micrometers Long	62
7-8	Undistorted Microbeam with 1-Micrometer Gap	63
7-9	Microbeam Exhibiting Gold Cohesion Problem	64
7-10	Close-up View of Contact Gap	66
7-11	Microbeam Contact with Insufficient Step Coverage	66
8-1	Cross Section After Bottom Contact Formation	68
8-2	Cross Section After Top Metal Patterning	68
8-3	Cross Section After Silicon Etch	69
12-1	Recommended Two-Substrate Approach	72

TABLES

	Page
TABLE 1. Microbeam Design Requirements	17
TABLE 2. Stiffening Effects of Longitudinal Loading	26
TABLE 3. Setback Sensor Nominal G-Levels and Resonant Frequencies	30
TABLE 4. Velocity and Spin Rate: 105-mm, Zone 1	37
TABLE 5. Velocity and Spin Rate: 105-mm, Zone 8	37
TABLE 6. Generalized Coordinate Characteristics	39
TABLE 7. Measured Electrostatic Closure Levels	56

Microscale G-Switch

(THIS PAGE INTENTIONALLY LEFT BLANK)

1.0 INTRODUCTION

This is the final report summarizing test results and program accomplishment under Contract DAAL02-85-C-0146 for a microscale threshold accelerometer(g-switch). The report is submitted as part of CDRL Sequence No. A004.

2.0 DEVICE DESCRIPTION

The microscale g-switch was first developed in two triple-beam arrays, one to sense setback and one to sense spin. Each sensor consists of three cantilever beams and is illustrated in Figure 2-1. Each beam is a normally open switch and is configured with a pair of metallized contacts at the end of each beam. When viewed under a plain microscope, the contacts appear in a "T" configuration. Under the action of the applied acceleration the beam deflects until the right- and left-hand tips of the top of the "T" touch metallized trace patterns located beneath. When viewed under high magnification, the contact at the end of each beam can be seen to have a gull-wing configuration which moves down through a 1 μm gap to bridge across a span of about 70 μm between the fixed contacts. Figure 2-2 shows a closeup view of one edge of the gull wing and the switch gap.

One of the key features of the beam configuration is the gold damper bar, which forms a bridge spaced 0.25 μm above the beam's top surface. This limits deflection in the direction opposite the sensing direction and prevents the beam from going into resonance should it be exposed to its resonant frequency for some extended duration. While it is unlikely that an environmental shock would be induced at exactly the resonant frequency of the beam, an elastic response of the projectile structure induced by a step input could be rich in a frequency range approaching that of the microbeams.

While there are many ways to implement a micromachined cantilever structure, the approach described here was chosen because it represented what potentially should be the lowest cost approach to fabricating such a switch. Our approach was tailored to require a minimum number of process steps, etching from only a single side, and employing a dielectric beam material not requiring a conductor on its top surface for the beam's full length. This final feature avoids potential distortion of the beam from thermal expansion characteristics. The ability to micromachine switch structures onto a silicon substrate also makes it possible to incorporate decision processing and signal analysis circuitry on the same substrate without resorting to "chip and wire" packaging approaches or similar interconnect schemes.

Microscale G-Switch

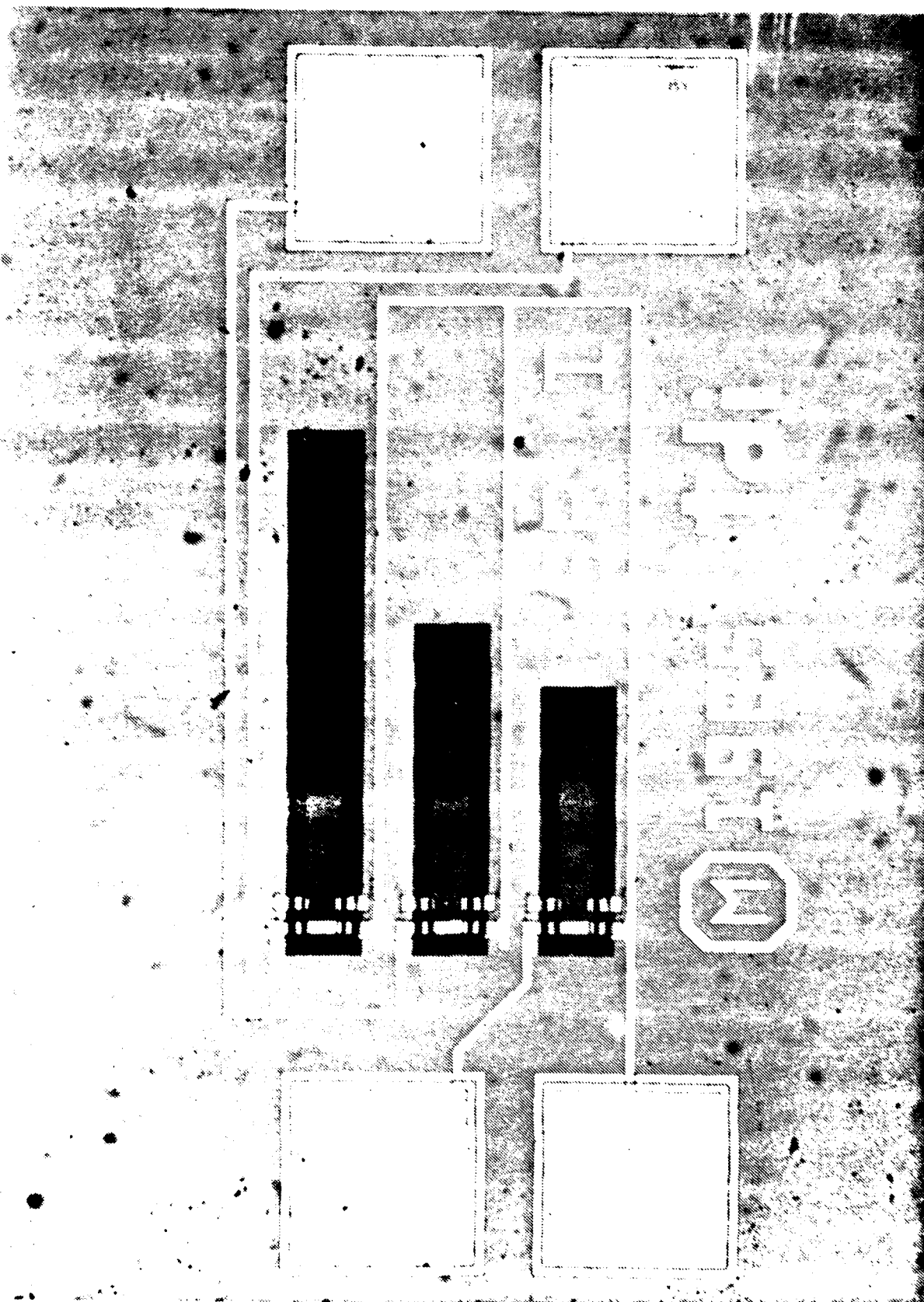


Figure 2-1. Microbeam sensor array.

Microscale G-Switch

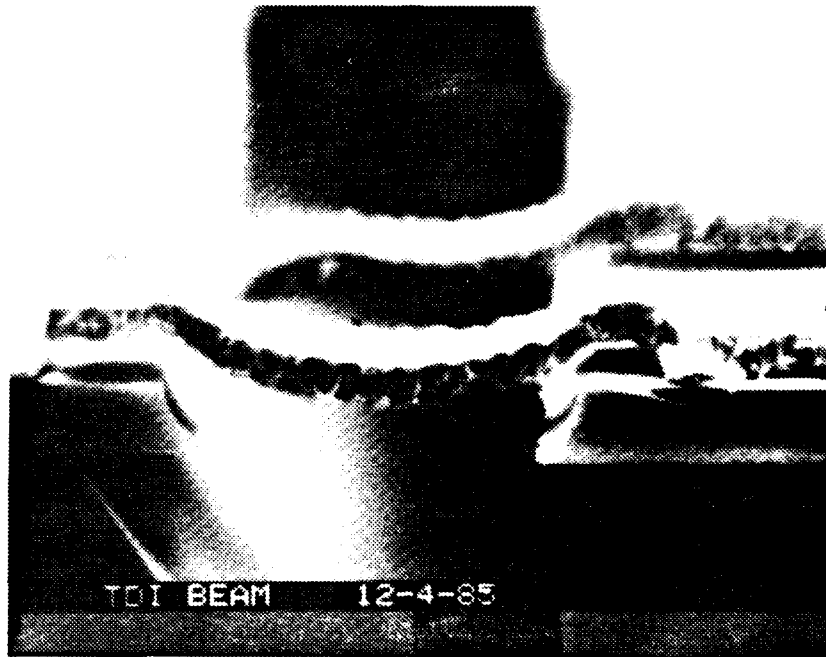


Figure 2-2. Microbeam gull-wing contact (close-up of one side).

The beams are fabricated with the use of well-controlled thin film layers and precision photolithographic techniques. The beam itself is silicon dioxide (glass), which is commonly used as a passivation material on standard large-scale integrated circuits. The glass is "grown" on a silicon substrate, patterned and etched, and finally subjected to an ethylene diamine pyrocatechol (EDP) etch which removes the silicon from beneath the glass structure. This leaves a cantilevered projection of glass which we have demonstrated to be well-controlled in shape.

The beams were fabricated under subcontract to Motorola by Transensory Devices Inc. (TDI), in Fremont, California. TDI specializes in silicon micromachining and high-rate production of microstructure components such as tactile sensors, hotwire anemometer-type flow sensors, and microtubular silicon configurations.

Several design modifications to the structure were later made in an attempt to introduce additional torsional compliance into the device and minimize sensitivity to nonuniform contact gaps on each side of the beam. The two structures resulting from these modifications are shown in Figures 2-3 and 2-4. One incorporates a zig-zag shaped bridgewire connection to the beam tip, which to a great extent is mechanically decoupled from the beam due to the shape. The second structure makes use of a reduced-width root section for additional torsional compliance. A line drawing of the beam with bridgewire is shown in Figures 2-5.

Microscale G-Switch

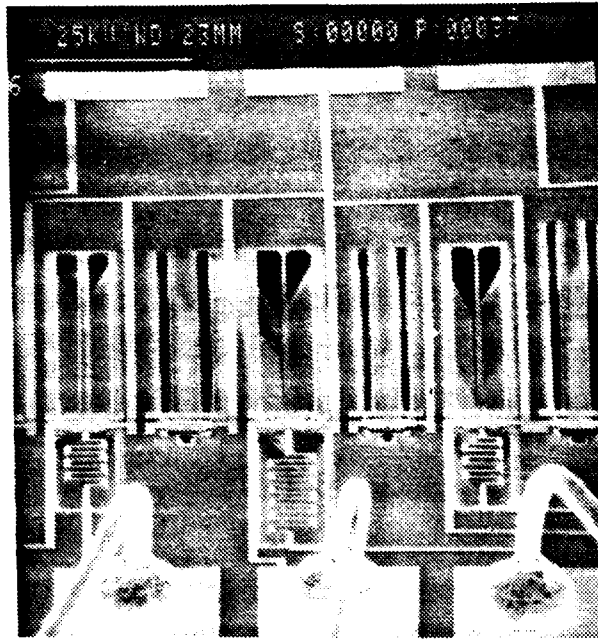


Figure 2-3. Microbeam array with bridgewire.

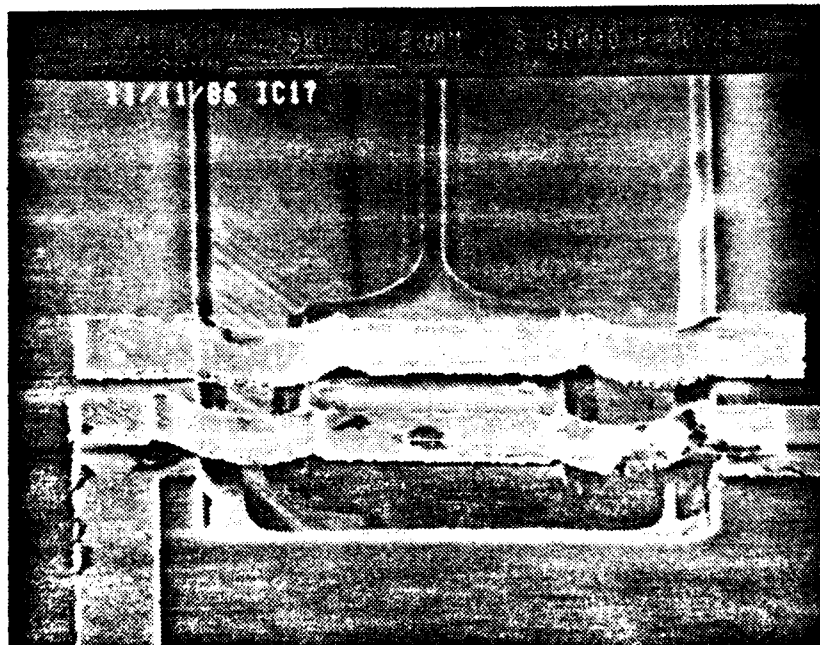


Figure 2-4. Microbeam device with reduced-width cross section.

Microscale G-Switch

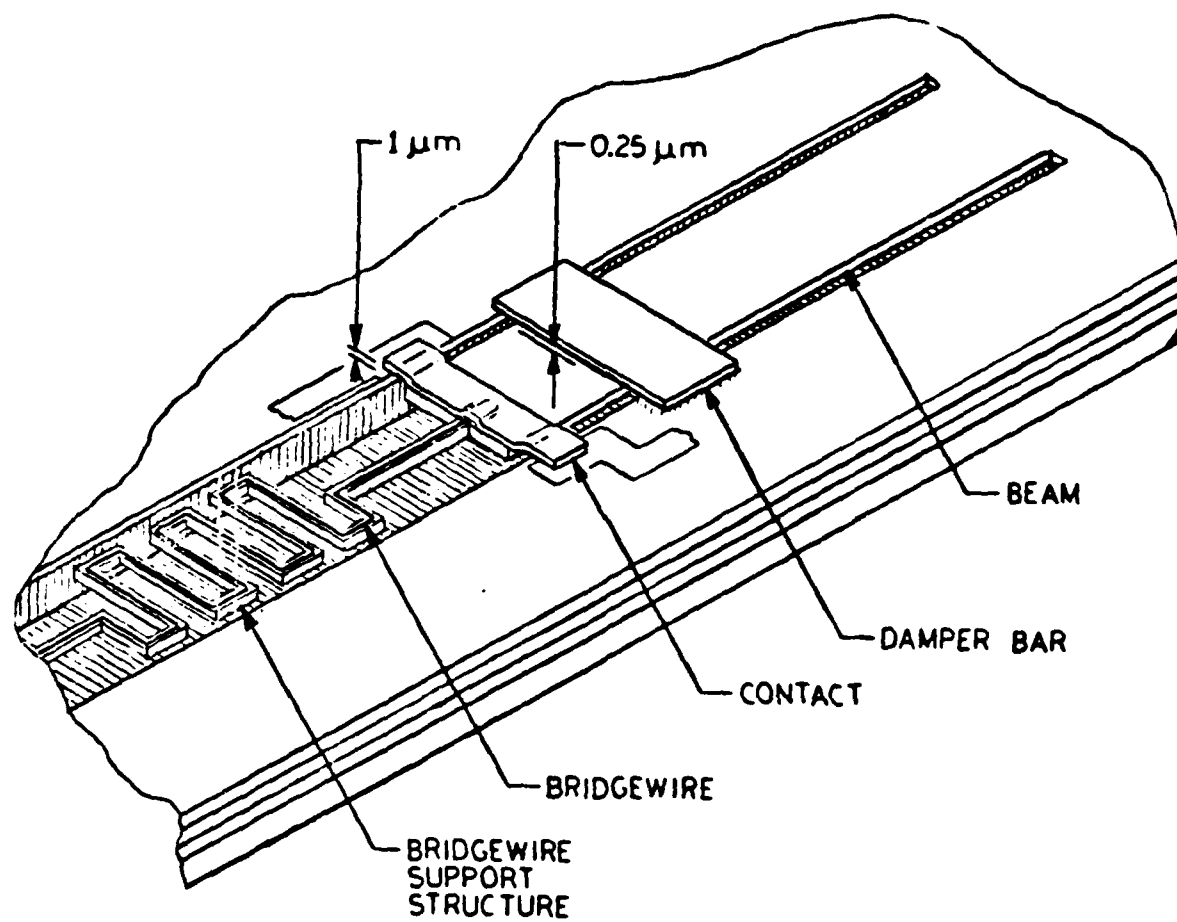


Figure 2-5. Microbeam /bridgewire Illustration

3.0 REQUIREMENTS

Table 1 lists the design requirements of the microbeams for this contract. While all requirements were not met with the present devices, the test results indicate that successful devices can be fabricated but would require further development. A sensitivity to high operating voltages was also experienced. High potential differences (40 to 100 V) across the switch contacts were found to either partially or fully close the switch with no applied acceleration. Consequently all acceleration sensitivity tests were done using a 3-V potential across the switch contacts. The following paragraphs discuss each of the individual requirements along with comments and observations relative to sensor performance for each.

Table 1. Technical Requirements

Parameter	Requirement
Cantilever beams for sensing spin rates	3 beams for spin rates of (1)4000 \pm 700rpm; (2)10,000 \pm 1800rpm; (3)15,000 \pm 2400rpm
Cantilever beams for sensing setback g's	3 beams for setback g's of 3000 \pm 600 g's; (2)7000 \pm 1,200g's; (3)11,000 \pm 1,800g's.
Maximum Beam Length	0.016 in.
Survivability	30,000 g's; 30,000 rpm.
Switch type	Normally open single-pole ohmic
Open Circuit Voltage	3 V to 35 V with 1- μ amp leakage.
Closed Circuit Voltage	<500 mV @ 5 to 500 μ amp.
Initial Bias	60 \pm 15g if feasible economically.
Shelf Life	20 years.

3.1 *Threshold Acceleration Response*

The microbeams are designed to be responsive to applied accelerations normal to the top surface of the beam. The deflection produced at the beam tip is assumed to be induced by three factors: (1) the continuously applied acceleration load on the beam itself, (2) the bending moment produced by the tip mass responding to the acceleration field; and (3) electrostatic attraction forces generated by the potential difference between the contacts. This last factor is only significant for low g beams and is predicted to account for 23 percent of the deflection of the lowest g beam when biased at 3 V. The following two subsections discuss the spin and setback response requirements and contrasts results obtained with a centrifuge to monitor threshold performance.

3.1.1 *Spin Induced Accelerations*

Requirements in the contract specify that the spin sensor must respond to:

- (A) 4,000 +/- 700 rpm
- (B) 10,000 +/- 1800 rpm
- (C) 15,000 +/- 2400 rpm

Offset distance from the spin center is specified to be 0.5 +/- 0.075 inch. If one assumes that the centrifugal force field acts perpendicular to the top surface of the beam the above figures translate to the following g- range:

- (A) 154 to 314 g's
- (B) 955 to 1978 g's
- (C) 2255 to 4301 g's

The following target threshold accelerations were utilized for the design of each of the beams:

- (A) 224 g's
- (B) 1394 g's
- (C) 3121 g's

The following response range, measured with a centrifuge, will be described in detail in a later section. As can be seen the beams performed as though much stiffer than expected.

- (A) 1100 g's
- (B) 11000 g's
- (C) Not Measured

3.1.2 *Setback Induced Accelerations*

Contract requirements for the three beams in the setback sensor are:

- (A) 3000 +/- 600 g's
- (B) 7000 +/-1200 g's
- (C) 11000 +/-1800 g's

No response was measured from setback switches tested. Possible explanations are discussed in a later section.

3.2 *Maximum Length*

A "target" of 0.016 in. maximum beam length was stated in the contract. The 224g beam in the spin sensor has a nominal length of 434 μm (0.017 inch). We could comply with this requirement exactly by using a heavier tip mass, but it was not deemed essential to overall program goals. The die on which the beams reside would be the same size in either case.

3.3 *Shock Survivability*

A minimum strength so as to withstand 30,000 g's in any direction is imperative to assure compatibility with large-caliber cannon launch applications. The contract specifies a 2000- to 5000-Hz frequency range as a relevant baseline for projectile rough handling. Since the beam frequencies are roughly from 2 to 12 times higher than the 5000 Hz band edge, the beams respond to loads induced by these frequencies as a slowly applied load. Finite element analysis performed prior to contract award demonstrated that induced stresses in the glass beam material were relatively low due to the low inertial loading inherent with the configuration chosen.

Spin centrifuge testing at 12,400 g's conducted to test the g- response range on the microbeams showed they were not damaged as a result of this loading. Future airgun and ballistic testing at higher g- levels are recommended during follow-on development.

3.4 *Open -Circuit Voltage*

While the contract called for a 3 to 35-V operation range, it was discovered after preliminary analysis that the effects of electrostatic force attraction became significant at the higher voltages. Consequently the beams were designed to operate in the range of complimentary metal-oxide semiconductor (CMOS) logic voltage levels-- 3 to 5 V. This is discussed in a later section. While it would be relatively easy to design the switches to withstand 35-V operation, the use of voltages at this level would heighten the sensitivity to operating voltage variation leaving the acceleration sensitivity diminished. This was deemed undesirable.

3.5 *Closed-Circuit Voltage*

A maximum voltage drop of 500 mV was specified in the contract with 5- to 500- μ amp current flow. Closed-circuit resistance on the order of 10 ohms was measured, indicating this requirement is easily met.

4.0 BEAM DESIGN CALCULATIONS

The following paragraphs discuss the fundamental design equations for the cantilever structures using standard closed form solutions in addition to an iterative algorithm to adjust for electrostatic effects.

4.1 *Microbeam Design Program*

A BASIC program was developed to aid in the computation of dimension required to achieve the particular acceleration thresholds desired of the microbeams. A copy of the program is attached as appendix A. The design equation is the superposition of the closed form solutions for a point-loaded cantilever and a distributed-loaded cantilever. The point-load force was converted to a mass times acceleration, and the distributed load was converted to the cantilever's own density times acceleration times its cross-sectional area. The initial form of the equation is as follows:

$$d = \frac{(3/2) \rho a l^4}{E h^2} + \frac{4 m a l^4}{E b h^3} \quad (1)$$

Where:

ρ = mass density of SiO_2
 a = acceleration field (units of length/s^2)
 l = length of cantilever
 E = Young's modulus of cantilever
 h = thickness of cantilever
 b = width of cantilever
 m = mass of concentrated gold contacts
 d = distance to make contact

Rather than solving this equation for the four roots of "l," a simple BASIC program was written to find the value of "l" using a high-low iterative technique. The deflection can be thought of as force divided by the spring constant of the cantilever. Therefore, to make the terms in the equation easier to distinguish, and to be able to quantify the effect of each term, the spring constant, K, was divided out of each term, and calculated based on an estimate of "l":

$$K = \frac{E b h^3}{4 l^3} \quad (2)$$

The incremental deflection due to the concentrated load is then calculated for the acceleration level desired:

$$d_m = \frac{ma}{K} \quad (3)$$

as is the incremental deflection due to the body forces:

$$d_b = \frac{(3/8)\rho a b l}{K} = \frac{(3/2)\rho a l^4}{E h^2} \quad (4)$$

These incremental deflections are then added. If the total deflection exceeds the switch gap, a shorter estimate of "l" is used and the program reiterates. If the total deflection is less than the switch gap, the program adds in the deflection due to the electrostatic deflection. The total deflection is then compared to the original switch gap, the length estimate is updated accordingly, and the iteration continues until the correct length is found within a certain error limit entered by the operator.

Since the electrostatic attraction is highly sensitive to gap, the effect is not considered until after the deflection due to both the body forces and concentrated load are calculated. Only then is the electrostatic attraction calculated using the following form of the equation developed in section 4.2:

$$d_e = \frac{V^2 A \epsilon_0}{4 (d_r)^2 K} \quad (5)$$

where

V = Potential across the device

A = Area of one side of switch contact

ϵ_0 = permittivity of the gap

d_r = the switch gap remaining after the body

force and concentrated loads are accounted for
 $[d - (d_m + d_b)]$

It should be noted that what is actually calculated is the equilibrium position at which the electrostatic attraction would cause the switch to snap shut. Because the attraction is inversely proportional to distance, once the switch moves past this position, the attraction increases asymptotically to infinity. In the program, the point at which the electrostatic attraction takes over and closes the switch is referred to as the "instability point."

Finally, the program included a calculation to determine what voltage could be applied to close the switch without any acceleration field. This was done by using the above equation, setting d equal to one micrometer, and solving for the voltage. Figure 4-1 illustrates the final configuration selected for all beams. Acceleration levels were "designed" into the beams by varying their length dimension.

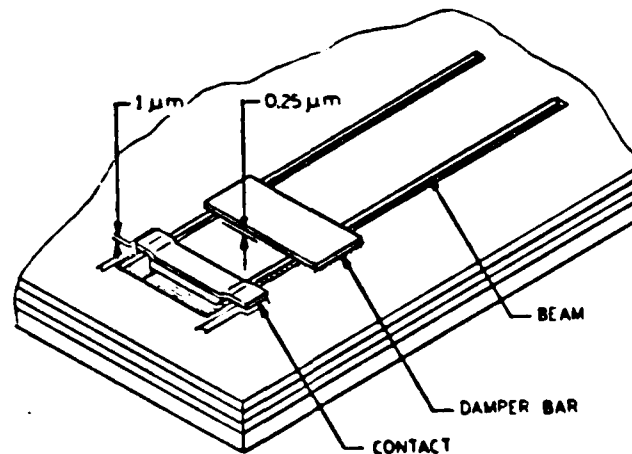
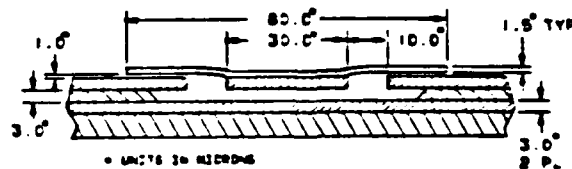


Figure 4-1. Microbeam configuration

4.2 Electrostatic Effect

Early in the program, it was discovered that the microbeam switches were likely to be sensitive to electrostatic attraction between the gull wing contacts and the stationary contact pads. The force between two parallel finite plates of a capacitor is

$$F = \frac{V^2 A \epsilon_0}{2 X^2} \quad (6)$$

where

- V is the voltage potential
- A is the area of the plates
- ϵ_0 is the permittivity of the space between the plates
- X is the gap between the plates

A typical value for ϵ_0 is $8.85 \times 10^{-12} \text{ coulomb}^2/\text{nt-m}^2$

The above equation is not in a usable form because it assumes both plates are charged. In the microbeam configuration, the gull wings are electrically floating. While one contact pad is grounded, the other is held to a fixed potential. The floating gull wing is then polarized by the electric field of the two contact pads, so that in effect half the voltage applied to the device appears across each contact. See figure 4-2.

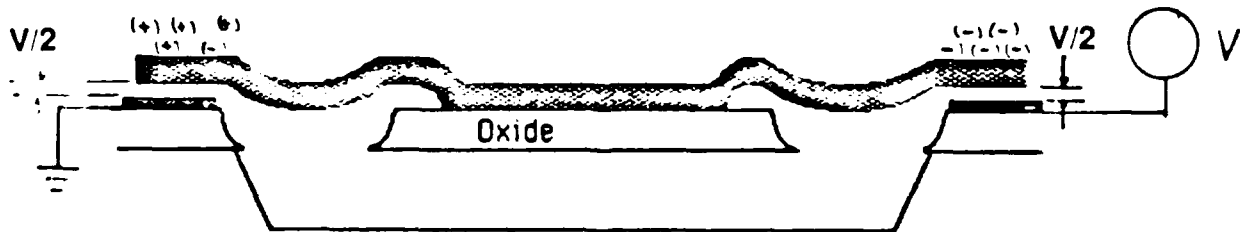


Figure 4-2 Polarization at contact tip.

If "A" is defined to be the area of each contact pad, (i.e., half the total contact area), then the total force pulling the microbeams closed is

$$F = \frac{(V/2)^2 A \epsilon_0 + (V/2)^2 A \epsilon_0}{2 X^2} \quad (7)$$

$$= V^2 A \epsilon_0 / (4 X^2) \quad (7a)$$

This effect was incorporated into the BASIC microbeam design program (attached as app A). The beam lengths were adjusted to compensate for the electrostatic attraction accordingly. For operation at the 3- to 5-V range of CMOS circuitry, the effect is second order (never more than 11 percent). But because the force is proportional to the square of the voltage, it is actually possible to close the switches by applying a higher voltage. This effect was used to test switches for continuity. During these experiments it was observed that the voltage required to close the switches was always higher than the value calculated. For example, a 228 g beam, predicted to close at 28-V, actually required 90-V to close. Section 7.1 further discusses test results on this characteristic of the switches.

It was also discovered that beam switches exercised by this method had a tendency to weld shut. Therefore this method of testing the switches was abandoned in favor of spin testing with a low voltage bias.

5.0 BEAM ANALYSIS

Extensive theoretical analysis was performed on the microbeam design and is summarized in the following paragraphs.

5.1 *Launch Stiffening Effects Analysis*

Since the setback-sensing array was designed so that the beams' length axes are normal to the spin axis, a stiffening effect arises due to centrifugal force. This effect was long noted with balance springs used in mechanical artillery fuzes. The escapements beat faster in a spin field because the spring wire tension increases, effectively stiffening the spring. The spin array is likewise affected by setback forces. Here the stiffening effect is much more pronounced. However, sensing of spin while under setback was not a requirement for the design.

A specialized program developed at Motorola to characterize effects from both gyroscopic and externally induced accelerations, ANTBETA, was used to analyze the beam configuration for the setback orientation. All the microbeams studied are assumed to be made of silicon dioxide with a density of 0.0903 lb/in.³ and a Young's modulus of 10 million psi. The tip of the microbeams is assumed to have a gold mass attached weighing 232 micrograms. The lengths of the beams were varied such that their tips would deflect a specified amount under a given steady acceleration. A deflection of 1 μm is assumed to cause switch closure.

Table 2 lists six of the beam lengths that were studied. The first three sense spin rate and the second set senses setback. The lengths are given along with the nominal acceleration level that will close the switch. The effect on the first two beam-bending frequencies are given for each of four different setback acceleration levels and spin rates. In addition, the tip deflection under the applied acceleration load is given. This calculation was made using the modal data for the first mode from ANTBETA. It is assumed that this is sufficiently accurate since the second mode occurs at a much higher frequency and therefore contributes very little to the deflection response of the beam tip.

The table should be interpreted along with figure 5-1 to determine the deflections of the beam sensors when they are stiffened ballistically by an acceleration field applied along the length of the beam, in addition to that applied normal to the beam. Recall that the beam is designed to "just close" when deflected at the tip by one micrometer. The disparity between the deflection values noted in the last column (see table 2) and this 1- μm gap exists because the beam is designed to deflect the remaining amount by electrostatic attraction. For example, the first spin beam listed on the table is predicted to deflect by 0.770 μm from the combined centrifugal and acceleration forces. At this deflection point, the electrostatic attraction between the beam's gull-wing contacts and the contact pads directly beneath them will cause the beam to further deflect by 0.230 μm and produce the 1- μm total deflection.

Cases 1 to 3 represent the spin sensors which were designed to be oriented parallel to the spin axis. As such, setback acceleration tends to slightly stretch the beams elastically, thus increasing tension within the beam and stiffening it slightly. Effects were noticeable only for the 230g beam, which has a nominal natural frequency of 9706 Hz. The natural frequency increased by 13 percent to 10,976 Hz. Since the launch acceleration was assumed to be a constant value, this result applies only near the gun breech for a 30,000-g launch. This effect is significant only if one expects the low-level spin sensor to respond shortly after initial motion begins. Motion will be biased on the slow side since the beam acts slightly stiffer, delaying closure by some small amount. The effect can also be viewed from a standpoint of diminished deflection by comparing the higher number of g's required to close the switch due to the cross-axis acceleration. The most sensitive beam, the 228-g structure, would deflect 0.596 μm rather than 0.770 μm requiring 29 percent more g's (18 percent higher spin) to close in the presence of a uniform 30,000-g longitudinal acceleration field. Note that sensing spin in the presence of setback acceleration was not a requirement of the device.

Microscale G-Switch

TABLE 2. STIFFENING EFFECT OF LONGITUDINAL LOADING

MICROBEAM DEFLECTION						
SPIN SENSOR CASE	\bar{L} (\bar{U})	G_0 (g's)	G_A (1000g's)	f_1 (μz)	f_2 (μz)	x (μm)
1	434	224	0	9706	69950	0.770
			10	10243	72652	0.684
			20	10616	73049	0.637
			30	10976	73445	0.596
2	268	1394	0	22316	176667	0.860
			10	23009	183368	0.803
			20	23276	183665	0.765
			30	23539	183963	0.767
3	214	3121	0	32585	272656	0.862
			10	33483	283123	0.830
			20	33711	283327	0.819
			30	33937	283652	0.808

MICROBEAM DEFLECTION						
SETBACK SENSOR CASE	\bar{L} (\bar{U})	G_0 (g's)	Ω 1000(RPM)	f_1 (μz)	f_2 (μz)	x (μm)
4	217	3000	0	31830	265365	0.2895
			10	32520	275377	0.847
			20	32620	275493	0.842
			30	32787	275665	0.833
5	170	7000	0	47114	425742	0.901
			10	46793	442119	0.257
			20	46877	442221	0.854
			30	49017	442392	0.849
6	149	11000	0	59220	550037	0.907
			10	60996	571437	0.863
			20	60675	571534	0.861
			30	60603	571696	0.859

Microscale G-Switch

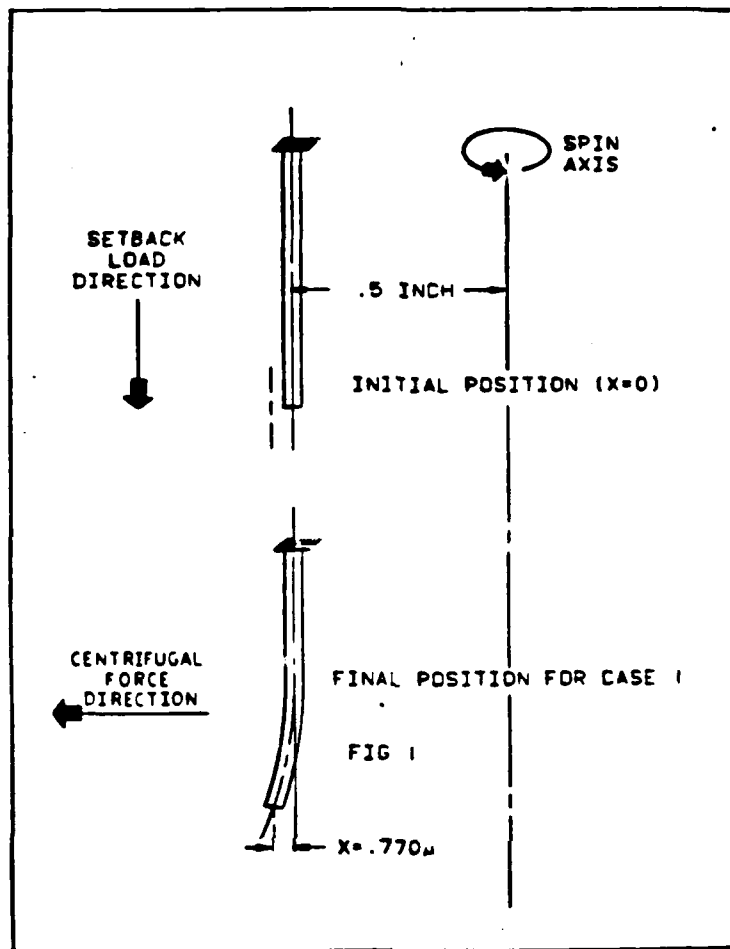


Figure 5-1. Spin sensor deflection - influences of setback acceleration.

Since large-caliber 30,000 g weapons do not presently exist, consider the case of the 105-mm Howitzer at zone 8. One achieves 4000 rpm in the gun tube approximately 2.5 ms. after initial motion of the projectile (T-Zero). Heppner's curves predict a setback acceleration level of 18,000 g-s at this point. One can approximate the error in beam response by using Table 2 which indicates that a deflection error of approximately $0.14 \mu\text{m}$ would result at 20,000 g's (0.770 minus 0.637). Consequently it can be seen that 21 percent higher spin-g's (9.9 percent higher rpm) would be necessary to obtain closure. This will be achieved approximately 0.5 ms. later. Consequently, these results do not influence the design of the spin sensors, but they have been quantified.

Cases 4 thru 6 address stiffening effects on the setback sensors which also appear to be only minimally affected with the largest change occurring with the 3,000 g beam which indicated a natural frequency shift from 31,830 to 32,787 Hz at 30,000 rpm. Since the centrifugal acceleration was assumed to be a constant value, this result only applies near muzzle

exit for a 30,000-rpm gun launch. It is anticipated that a high-g gun launch would activate the low-level threshold switch well before significant centrifugal acceleration is present.

Figure 5-2 shows a plot of the effect of setback acceleration on the first resonant frequency of the spin sensor microbeams. As indicated, the setback acceleration which puts the beams in tension increases their resonant frequency. As a result of this increase, the tip deflection response to a given constant acceleration decreases as shown in figure 5-3.

Similarly, figures 5-4 and 5-5 show the effects of spin rate on the microbeams sensing setback acceleration. As shown in figure 5-4, the spin rate increases the resonant frequencies of the beams and thereby decreases the tip deflection response. The beams are assumed to be offset 0.5 in. from the centerline in these cases.

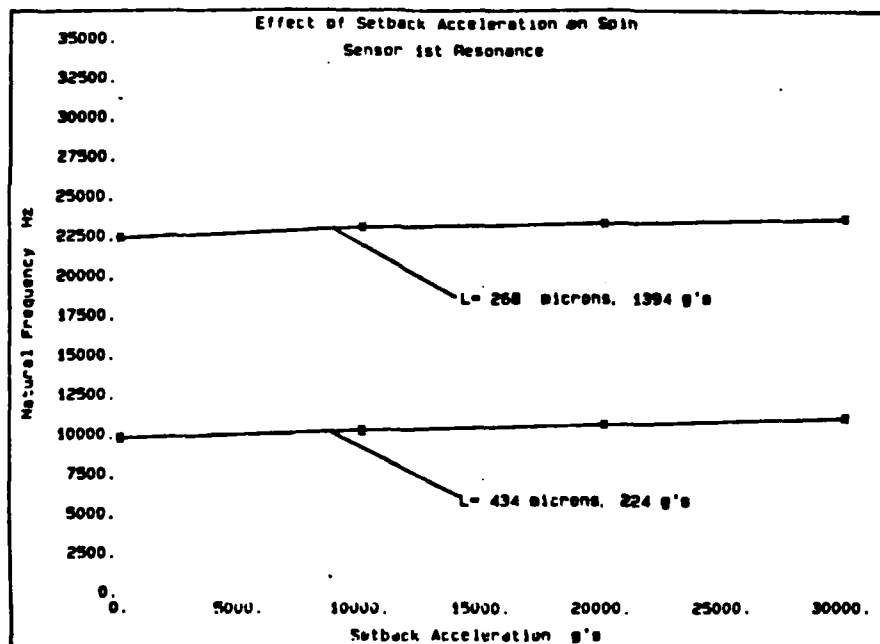


Figure 5-2. Effect of setback acceleration on spin sensor natural frequency.

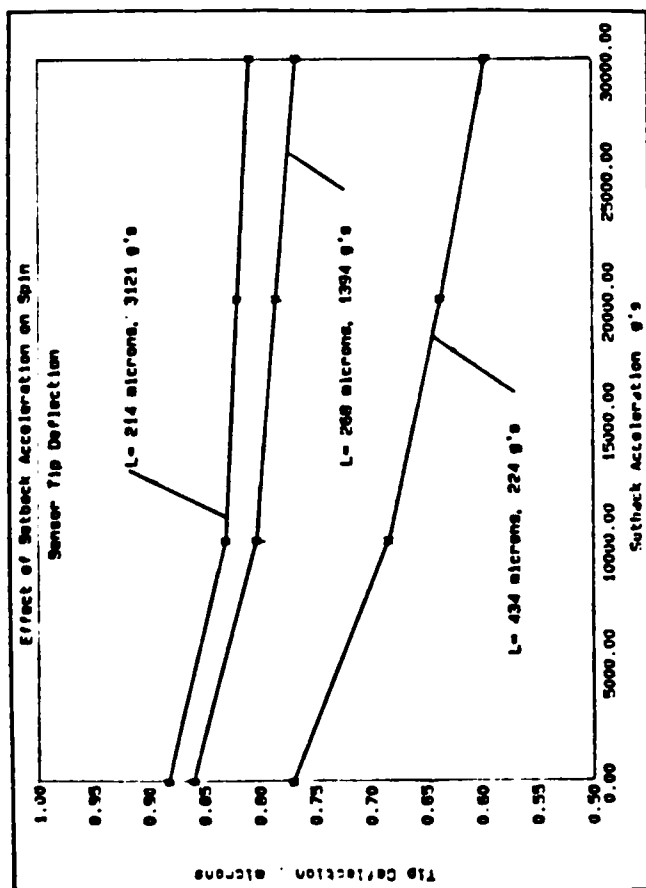


Figure 5-3. Effect of setback acceleration on spin sensor tip deflection.

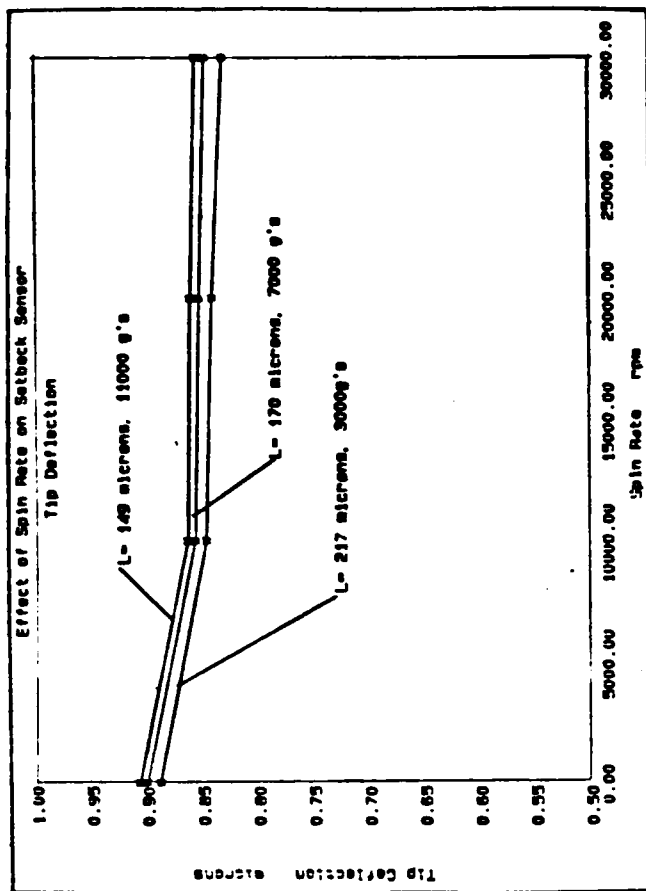


Figure 5-4. Effect of spin rate on setback sensor tip deflection.

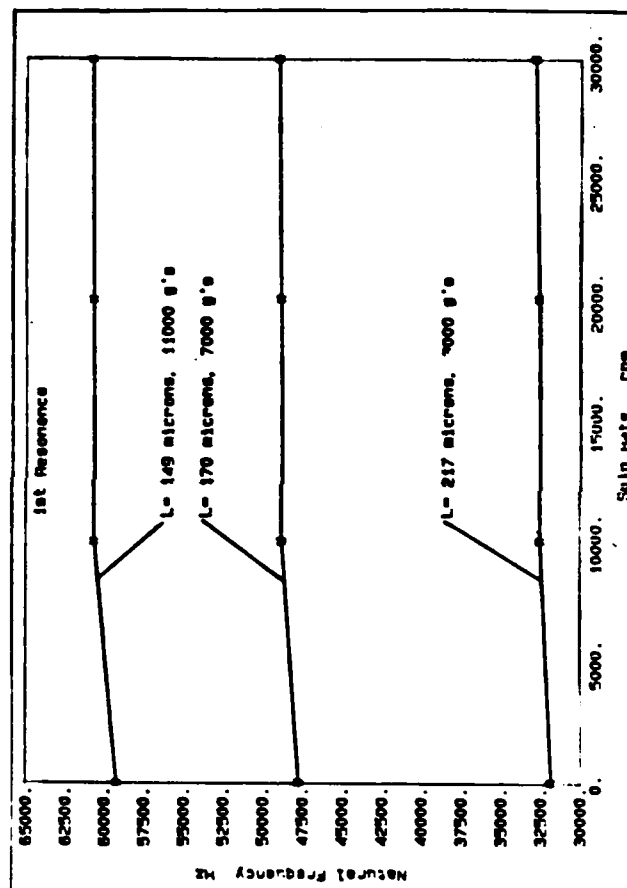


Figure 5-5. Effect of spin rate on setback sensor first natural frequency.

5.2 *Dynamic Response In a 105-mm Setback Environment*

A Multi-Degree of Freedom (MDOF) model of the XM762 fuze on a 105-mm projectile was used to predict the acceleration, velocity, and displacement of each of the three setback beams during a zone 7 gun launch. This scenario was selected because of the large accelerations characteristic of this zone. Because of its complexity, the model is able to characterize the elastic response of the fuze/projectile system superimposed on the rigid body motion of the projectile's center of gravity. Ground motion acceleration at the S&A location was used as an input to a Generalized Coordinate Response (GCR) model of the three beams. The stiffness of the gull wing contacts, contact pads, and damper bar was accounted for in the analysis in an attempt to characterize any contact bounce which might occur. This characterization would be important in defining any additional debounce circuitry requirements that may be necessary to properly interface with the setback sensors.

In Table 3 the beam lengths studied are given along with design g level and the first two resonant frequencies. These properties were determined with the use of the program ANTBETA, described previously. Only the first mode response was considered in this analysis.

TABLE 3. Setback Sensor Beam Frequencies

Length (μm)	Nominal g Level	f_1 (Hz)	f_2 (Hz)
217	3000	31,830	265,400
170	7000	47,714	425,700
149	11,000	59,220	550,000

Figure 5-6 shows the predicted acceleration time history at the location of the safing and arming (S&A) device in a model of the 105-mm projectile characterized using MDOF. These results were used as a ground acceleration forcing function for the microbeams. In this analysis it is assumed that the gap between the tip of the beam and the contact is 1 μm and the gap between the beam and the damper bar is 0.25 μm . To obtain the response of these beams to the applied ground acceleration, a generalized coordinate response program (GCR) was used. The additional capability of analyzing impact springs (contacts and damper bars) at positions both above and below the beam was added to GCR for this analysis. Figure 5-6 shows the predicted tip deflection response of the 217- μm long beam to the ground acceleration input of figure 5-7 when neither the damper bar nor contact exists. As shown, the beam deflects a maximum of approximately 0.21 mils under this loading, following the ground acceleration curve closely since its resonant frequency is much greater than the ground acceleration loading.

Figure 5-8 shows the tip deflection response of the same beam with the effects of the contact and damper bar included. As indicated, the beam impacts the contact in about 0.7 ms at 0.0394 mils (1 micrometer). The beam stays in touch with the contact until 7.1 ms. At this instant the beam tip separates from the contact and continues to follow the ground acceleration input curve until 9.2 ms. At this point in time the input ground acceleration rapidly drops causing the microbeam to oscillate in a transient fashion at its resonant frequency. The oscillations are then hampered by the damper bar set at 0.25- μ (0.01 mils).

Figure 5-9 shows the tip deflection response of the 170- μ long microbeam to the loading of figure 5-6 with the contact and damper bar in place. In this case the beam makes contact in about 1 ms and remains closed until 4.8 ms. As in the previous case, the shape of the response curve follows the ground acceleration loading until 9.2 ms at which time the load drops off suddenly allowing the beam to vibrate at its resonant frequency. Impact is made with the damper bar during this time.

Finally, figure 5-10 shows the tip deflection response of the 149 - μ long microbeam to the acceleration loading of figure 5-6. This beam reaches the contact in about 1.3 ms and stays in touch with it until about 3.3 ms, whereupon it again follows the input acceleration curve waveform until 9.2 ms, when the loading is suddenly reduced. As in the previous cases the beam then vibrates at its resonant frequency impacting the damper bar several times.

As indicated in table 3 the three beams with lengths of 217 μm , 170 μm , and 149 μm were designed to close at 3,000, 7,000, and 11,000 g's. The results show that during gun launch, the beams are mainly influenced by the rigid body motion of the projectile and close when the projectile acquires the g level designated to close the switch. However, at muzzle exit, the beams attempt to ring violently from the elastic response of the projectile/fuze system in addition to their own resonant response. In addition to the motion characterization, the effect of

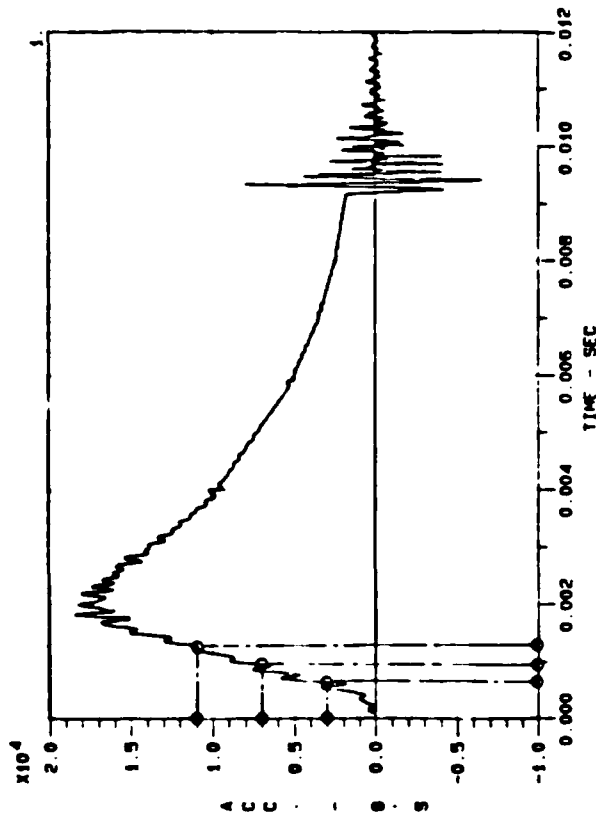


Figure 5-6. Acceleration-time history at S&A for zone 8 launch from 105-mm howitzer.

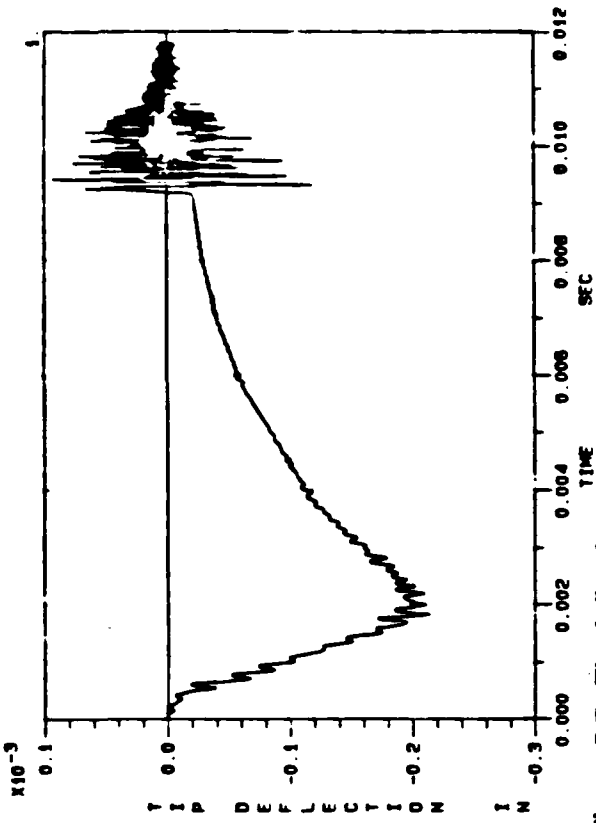


Figure 5-7. Tip deflection response of 217- μ m beam-contact and damper bar removed.

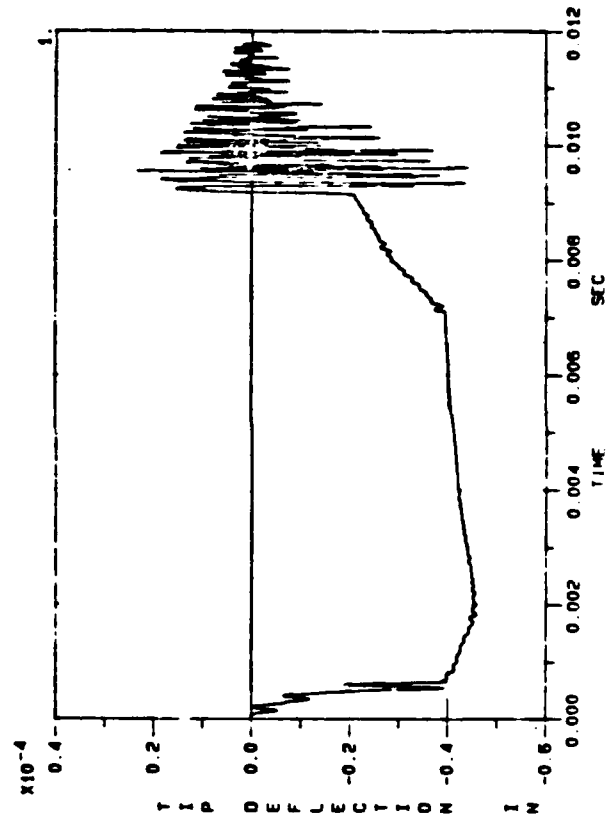


Figure 5-8. Tip deflection response of 217- μ m beam-contact and damper bar included.

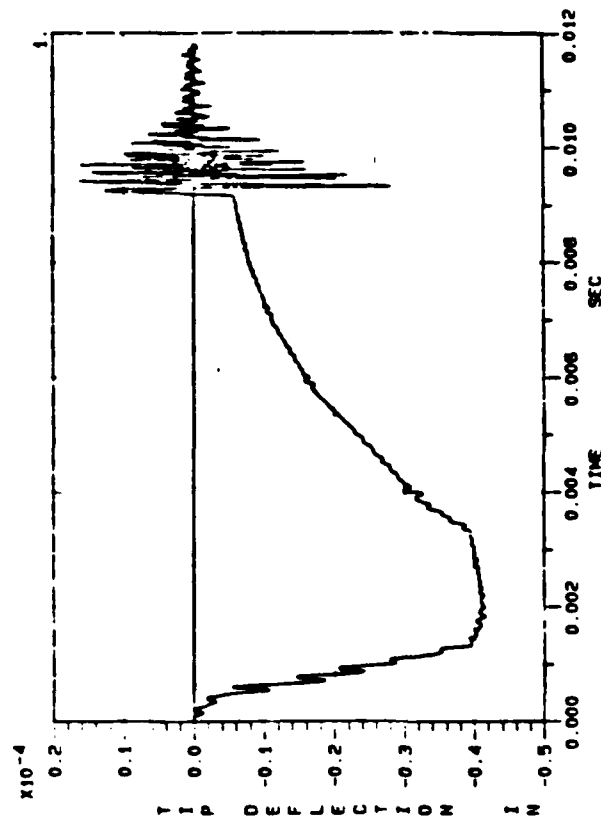


Figure 5-10. Tip deflection response of 149- μ m beam—contact and damper bar included.

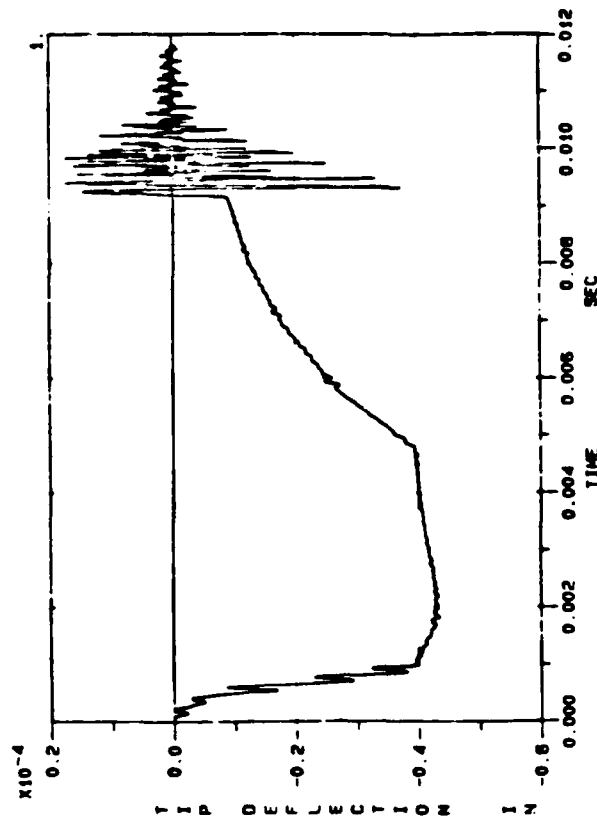


Figure 5-9. Tip deflection response of 170- μ m beam—contact and damper bar included.

the damper bar was determined by removing it from the model for one run sequence. Oscillation amplitudes were significantly increased as expected. It can be concluded from the response of the beams that onboard power would be required either before or within the first several milliseconds of initial projectile motion. Significant bouncing of the contacts during the beams' duty cycles are not predicted, indicating that sophisticated debounce circuitry is not required.

5.3 *Dynamic Response In a Spin Environment*

For this analysis, the progressive twist of the 105-mm howitzer was characterized as a linear progression from 1 in 35 calibers to 1 in 18 along the length of the barrel. This case was chosen since it was identified in the contract as a possible environment for future test vehicle firing. Angular velocity and resulting centrifugal forces were used to compute the response of the spin sensors to both a high and low zone launch scenario.

When placed in the fuze with the length of the beam along the longitudinal axis of the projectile, the sensor will experience acceleration loading due to spin of the projectile if the sensor is offset from the spin axis. In this study an offset of 0.5 in. was assumed and spin-rate time histories of a 105-mm projectile for zone 1 and zone 8 charges were used.

A progressive twist is used in this gun. Initially it is 1/35 and decreases to 1/18. While it is true that the last 12.4 inches of rifling do in fact have a constant twist, this last foot of travel was assumed to be rifled such that the 1/18 twist occurred at 9.25 feet--the full barrel length. This was done for ease of approximation and is not estimated to change the results shown here significantly. Assuming the twist varies linearly along the length of the barrel the twist at any position x is,

$$T(X) = 0.5211 + 0.053206 X$$

where the units for $T(X)$ and X are radians/ft. and feet, respectively.

The total rotation in radians at location x is then,

$$\theta(X) = 0.5211X + 0.026603 X^2$$

Consequently the coefficient 0.5211 has units of radians /foot; similarly the coefficient 0.026603 has units of radians/ft².

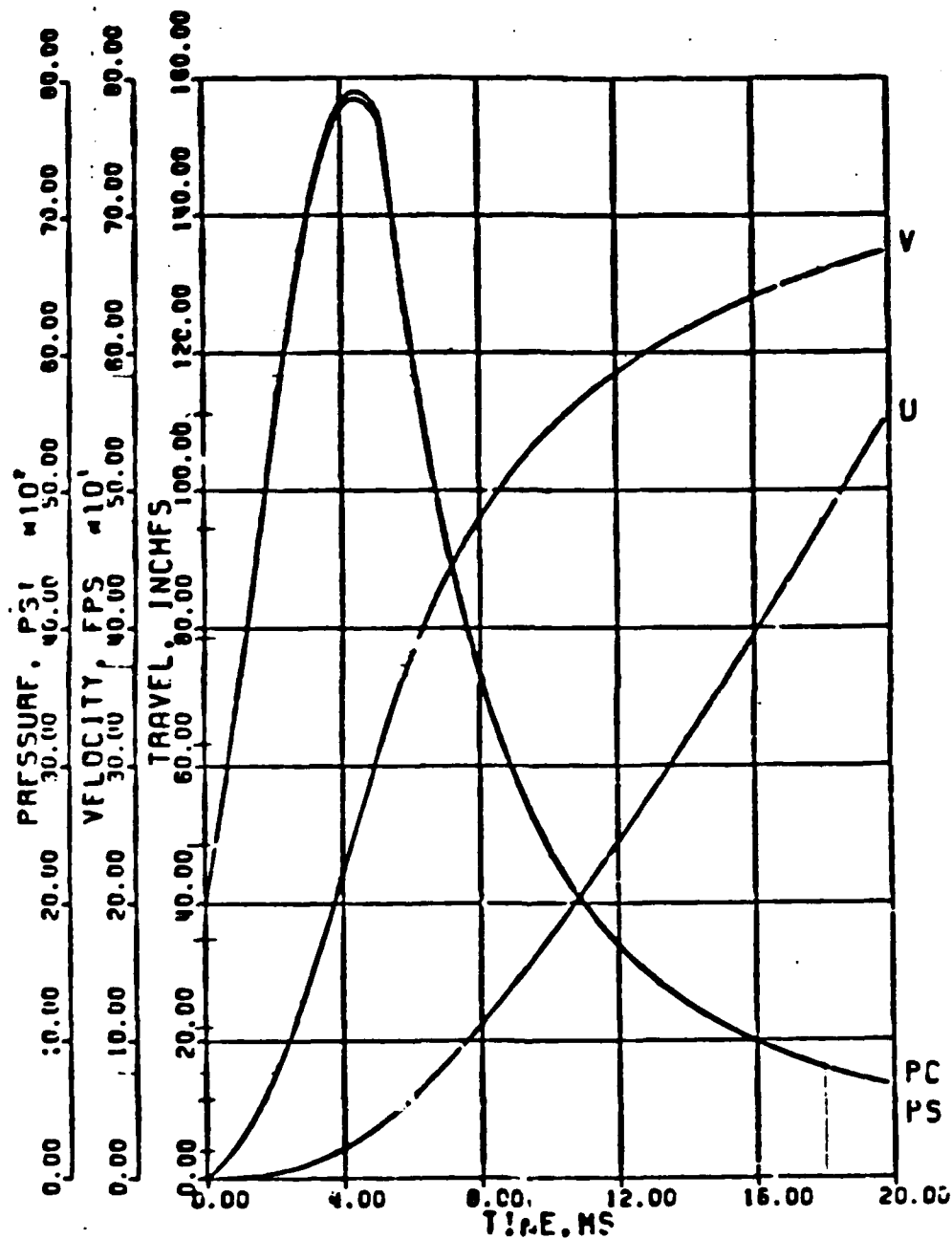
The rotational velocity in rpm, determined by taking the time derivative and adjusting the units appropriately is,

$$\dot{\theta}(X) = (4.97614 + 0.508075X) \dot{X}$$

where the units for \dot{X} are ft/sec.

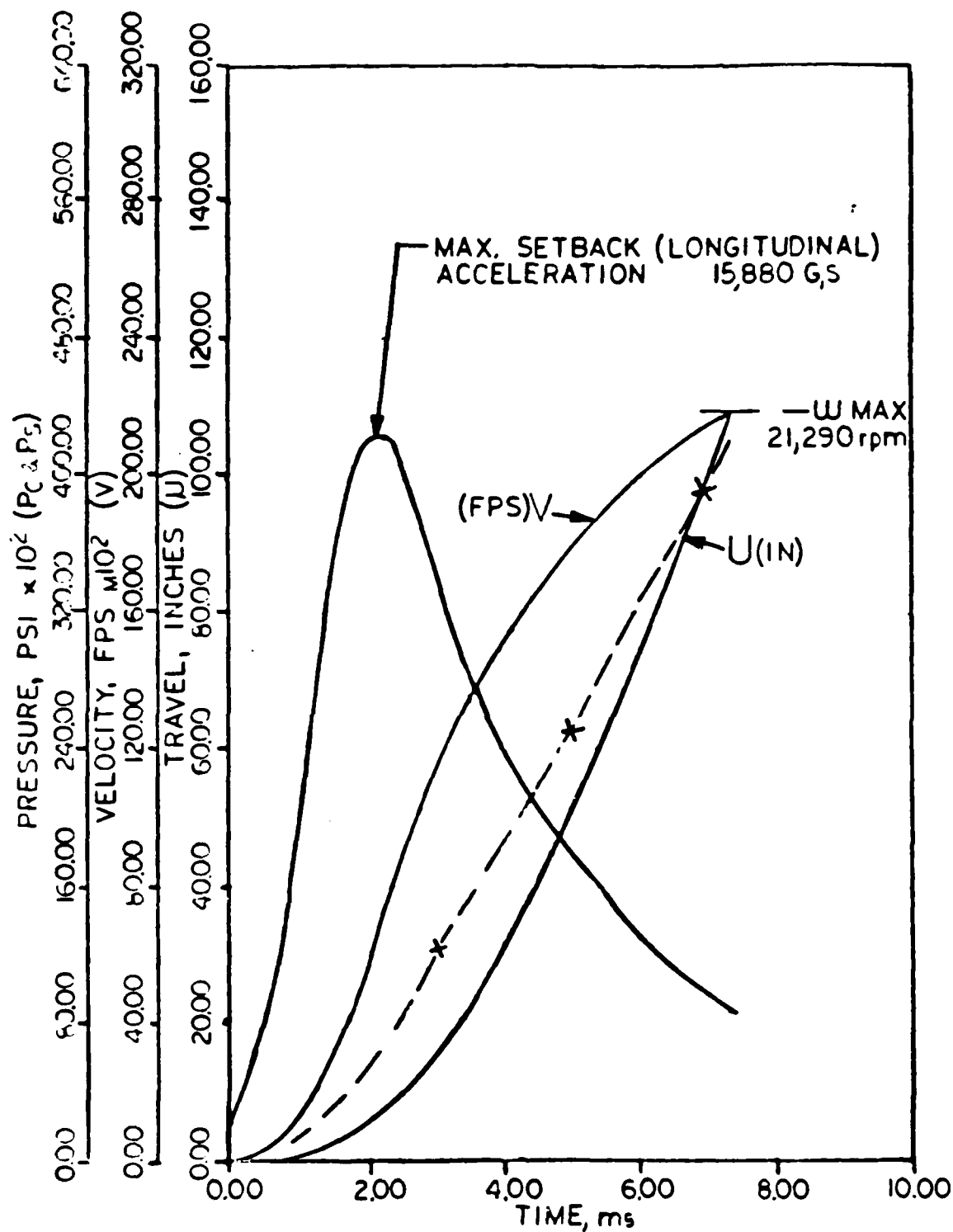
Using this equation and the Heppner curves shown in figures 5-11 and 5-12 for zone 1 and zone 8 charges, respectively, the data in tables 4 and 5 were derived.

Microscale G-Switch



192. CANNON: 105.0" M34.M103.M137.M165 PROJ: HE.11 CM2: M67. ZONE 1

Figure 5-11. 105-mm Heppner data--zone 1 launch.



100. CANNON: 105mm HOW. M103. M137. M165 PROJ: HE. XM606 CHG: M85.

ZONE 8

Figure 5-12. 105-mm Heppner data--zone 8 launch.

Microscale G-Switch

TABLE 4. 105MM CANNON ZONE 1 CHARGE

t	x	x	e	CF at
ms	ft	ft/s	rpm	1/2" (g's)
0	0	0		
2	0.08	76.1	382	2.072
4	0.32	213.3	1117	17.72
6	0.95	371	2025	58.24
8	1.85	477	2822	113.1
10	2.89	542	3493	173.3
12	4.05	583	4101	238.8
14	5.25	616	4708	314.8
16	6.53	639	5300	398.9
18	7.87	656	5887	492.2
20	9.25	671	6492	598.5

TABLE 5. 105MM CANNON ZONE 8 CHARGE

t	x	x	e	CF at
ms	ft	ft/s	rpm	1/2" (g's)
0	0	0	0	
1	0.01	104	518	3.81
2	0.30	586	3005	128.2
3	1.21	1128	6307	564.9
4	2.59	1521	9570	1301
5	4.32	1795	12872	2353
6	6.18	2003	16256	3753
7	8.31	2146	19739	5533
7.4	9.25	2193	21219	6394

These tables show the predicted centrifugal acceleration in g's acting on the beams during gun launch. This data was input into GCR to predict the tip deflection of each of the microbeams considered. Table 6 shows the beam lengths considered and their design g levels along with their resonant frequencies, generalized mass, modal participation factors, and other modal properties which were determined with the use of ANTBETA .

Figure 5-13 shows a plot of the centrifugal force versus time for the zone 1 charge plotted from data in table 4. The tip deflections of the microbeams under this loading are shown in figures 5-14, 5-15, and 5-16 for the 434-, 268- and 214- micrometer beams, respectively. Note that any stiffening effects from the cross-axis acceleration are not included in this analysis. As indicated by these figures only the 434- μ m long beam impacts the contact located 1 μ m (39.37×10^{-6} in.) from the unloaded position of the beam tip. It reaches the contact in 13.5 ms which corresponds to an acceleration level from figure 5-13 of approximately 290 g's. According to table 4 this is not within the desired specification of 224 \pm 40 g's. This discrepancy will however be accounted for by the electrostatic force generated as the beam tip approaches the contact.

The centrifugal force versus time for the zone 8 charge, which is listed in table 5, is plotted in figure 5-17. As shown in figure 5-18, the 434- μ m long beam reaches the contact in 2.37 ms. This corresponds to approximately 290 g's -- the same as for the zone 1 charge.

Figure 5-19 shows the tip deflection response of the 268- μ m long beam vs time to the centrifugal loading. In this case the beam reaches the contact in 4.29 ms, which corresponds to a g level of 1,620 g's. This is just within the desired specification of 1,394 \pm 291 g's. The shortest beam's response (214- μ m) is shown in figure 5-20. It reaches the contact in 5.82 ms, which corresponds to 3,541 g's , which is also just within the required specification of 3,278 \pm 530 g's. The effect of the electrostatic force will cause the contacts to close at acceleration levels that are closer to those required by the design specification. Figure 5-21 shows the response of this beam with the contact tip removed for comparison.

Overall, the responses of the beams were those expected from rigid body theory indicating almost no resonance effects. This is due to the relatively slow risetime of the centrifugal force field within the spinning projectile. Since the spin rate decays slowly subsequent to muzzle exit, it is apparent that onboard power is not required before launch or muzzle exit. No resonant response of the beam is expected as long as the beams are oriented parallel to the spin axis of the projectile.

TABLE 6. MODAL PROPERTIES AND DESIGN G LEVEL

	LENGTH (μm)		
	434	268	214
f_1	9706	22316	32585
f_2	69950	176667	272656
m_1	0.2643E-12	0.2118E-12	0.19485E-12
m_2	0.66722E-12	0.72059E-12	0.76813E-12
v_1	0.34453E-12	0.262E-12	0.23528E-12
v_2	-0.28463E-12	-0.23702E-12	-0.22058E-12
c_1	8.059E-10	1.485E-12	1.995E-9
c_2	1.466E-8	4.0E-8	6.58E-8
k_1	9.83E-4	0.004164	0.008168
k_2	0.1289	0.8879	2.2544
σ_{root_1}	-6.606E8	-1.701E+7	-2.646E7
M_{root_2}	+0.2174E-3	0.7283E-3	0.1301E-2
σ_{root_2}	7.917E+7	2.652E8	4.738E-8
Design g level	224+40	1394+291	3151+530

f_1, f_2 = first and second natural frequencies.

m_1, m_2 = generalized masses for first and second mode shape.

v_1, v_2 = modal participation factors for first and second mode.

c_1, c_2 = damping coefficients for modes 1 and 2.

k_1, k_2 = spring rates for modes 1 and 2.

M_{root_1} = bending moment at root due to first mode deflection.

M_{root_2} = bending moment at root due to second mode deflection.

σ_{root_1} = stress at root due to first mode bending.

σ_{root_2} = stress at root due to second mode bending.

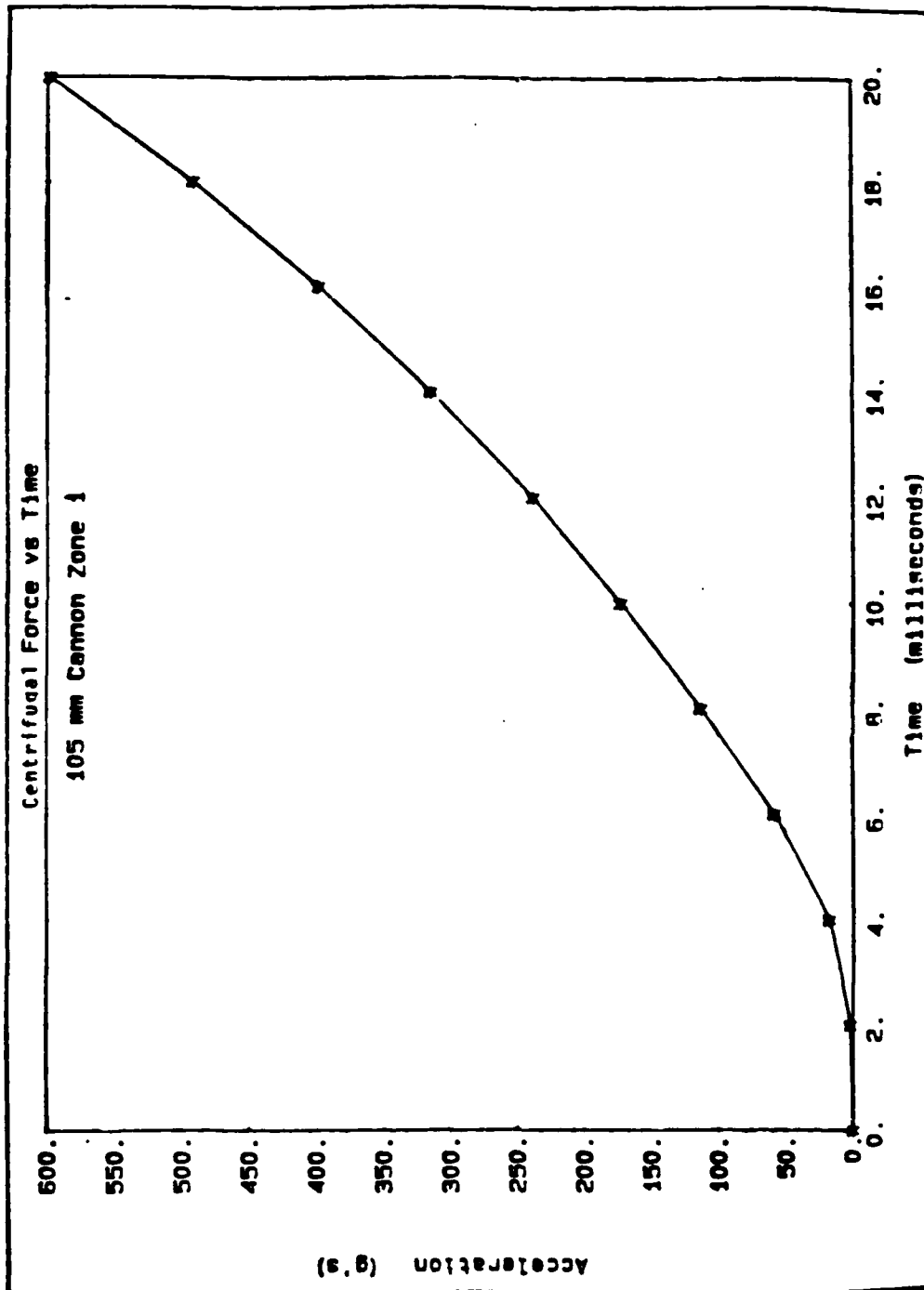


Figure 5-13. Centrifugal force versus time--105 mm, zone 1.

Microscale G-Switch

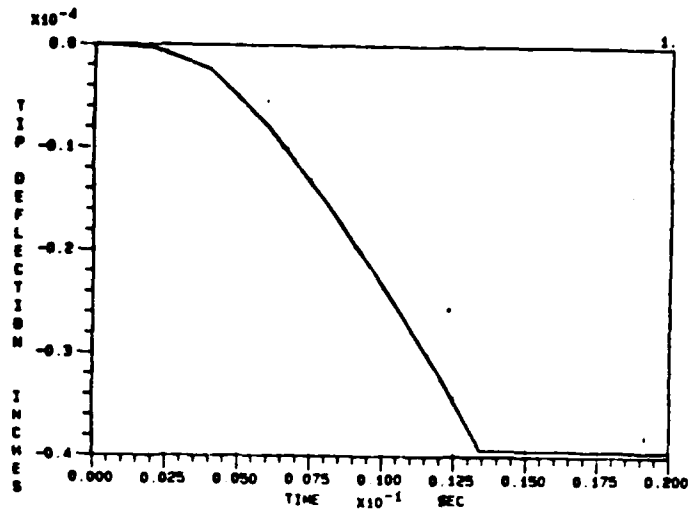


Figure 5-14. Tip deflection response--434- μ m beam--105-mm, zone 1 launch.

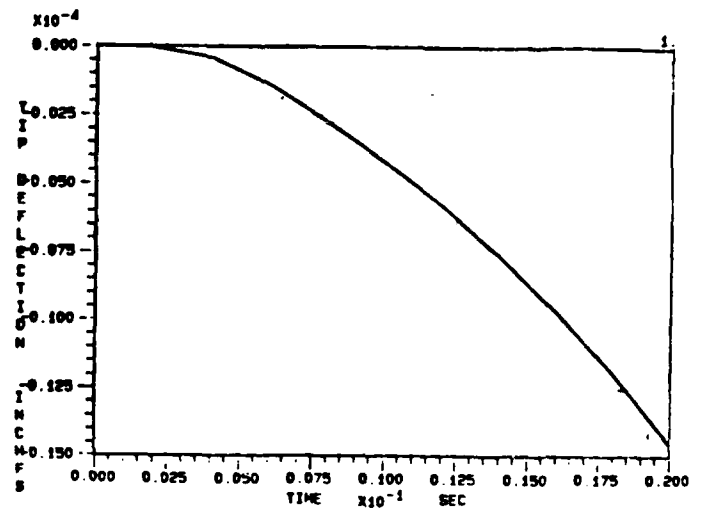


Figure 5-15. Tip deflection response--268- μ m beam--105-mm, zone 1 launch.

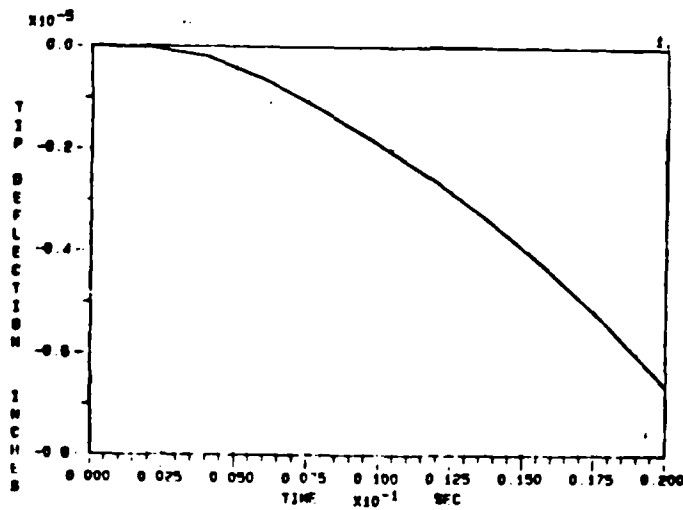


Figure 5-16. Tip deflection response--214- μ m beam--105-mm, zone 1 launch.

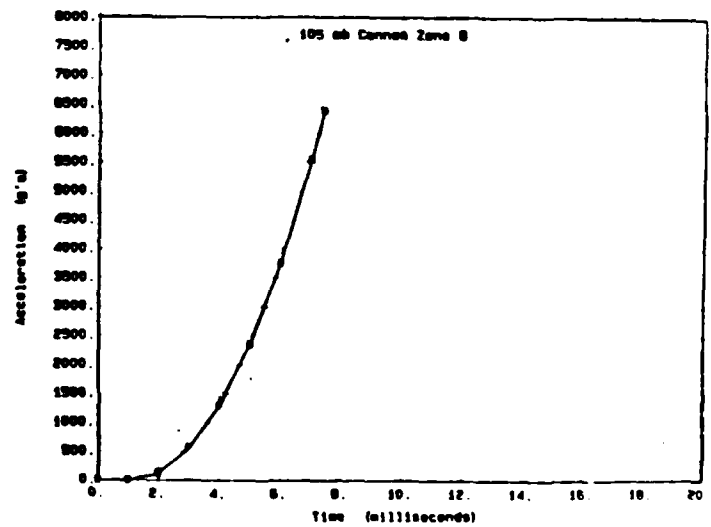


Figure 5-17. Centrifugal force versus time--105-mm, zone 8 launch.

Microscale G-Switch

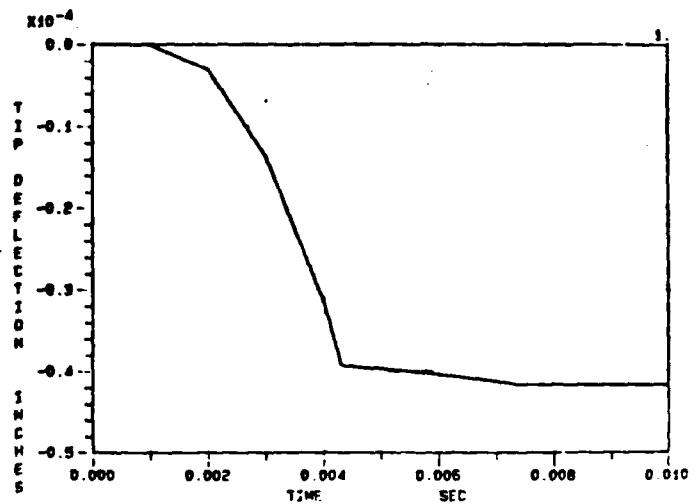
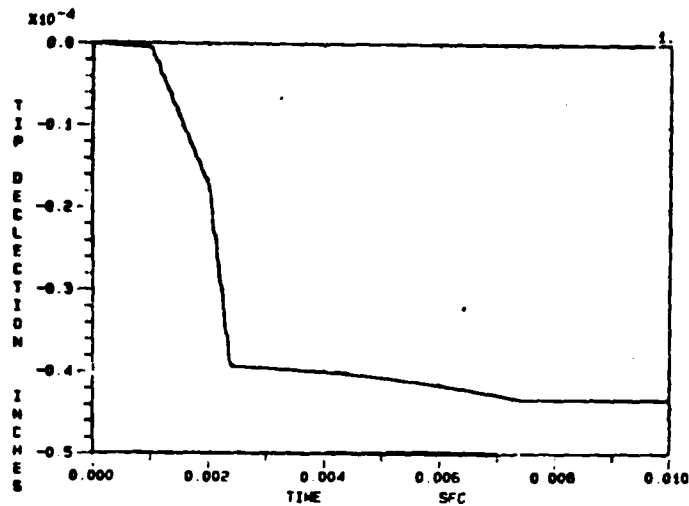


Figure 5-18. Tip deflection response--434-μm beam--105-mm, zone 8 launch.

Figure 5-19. Tip deflection response--268-μm beam--105-mm, zone 8 launch.

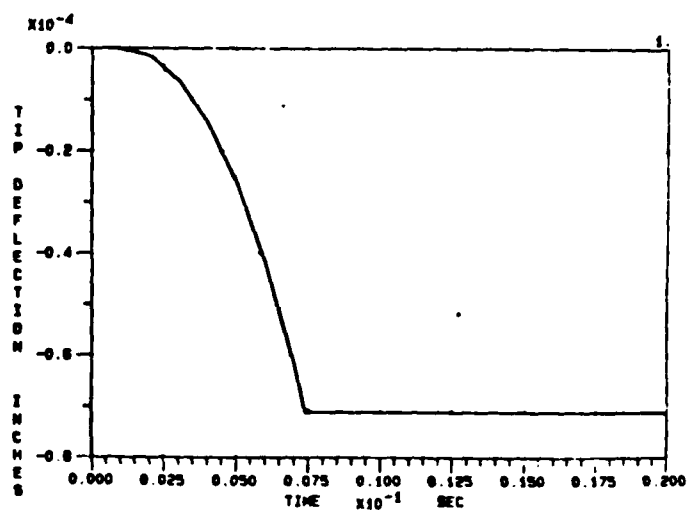
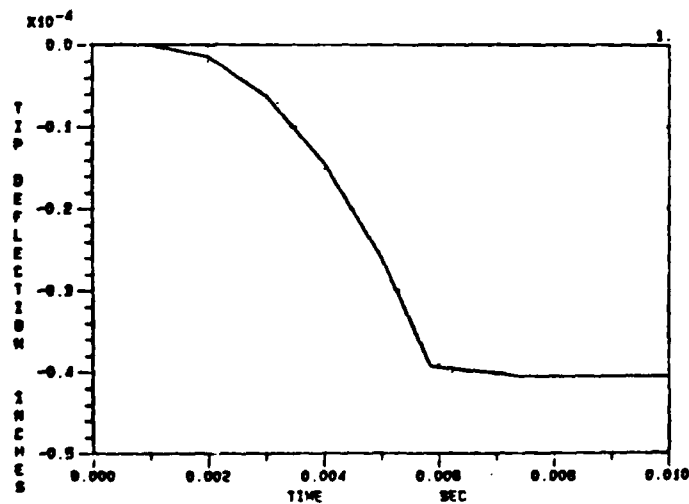


Figure 5-20. Tip deflection response--214-μm beam--105-mm, zone 8 launch.

Figure 5-21. Tip deflection response--214-μm beam--105-mm, zone 8 launch

5.4 *Balloting Sensitivity*

The sensitivity of the spin sensor array to typical balloting levels were studied by mathematically subjecting the beams to a response input "measured" with the use of an instrumented 155-mm projectile. Forcing functions were estimated from strain gage data taken with an instrumented cantilever beam on the centerline of the projectile. Strain gage data were transmitted through a telemetry link utilizing an FM-FM transmitter and voltage controlled oscillator (VCO) array having frequency responses in the 10-kHz range. The launch environment was that resulting from a zone 8 firing from guntube PT08 (NATO) M199 during a wear test at Yuma Proving Grounds.

Force-time half-sine inputs were applied to a lateral stiffness model of the projectile as illustrated in figure 5-22. This procedure was continued until the response actually measured reasonably agreed with that predicted. The projectile motion at what would typically be the S&A location in the fuze was then used as an input to the microbeam model developed for this purpose. The load applied was a half -sine force pulse of 50,000 lb lasting 1.5 ms. The acceleration-time history at a position 32 inches (approximate S&A position) from the base of the projectile is shown in figure 5-23.

Each beam model was run twice with the balloting load applied in "worst case" directions -- each 180 degrees opposite. The gold contact damper bar was assumed to limit deflection of the beam when the model predicted induced deflections to "open" the switch.

Figures 5-24 shows the deflection response of the 214- μ m long (3100-g) microbeam for the orientation where the balloting load tends to close the switch. As mentioned previously, the closure contact is located at a distance of 1 μ m (39.37×10^{-6} in.) and the damper bar is 0.25 μ m (9.8425×10^{-6} in.) above the beam. Figure 5-24 shows that the beam tip will not close; neither will it impact the damper bar on its excursions in the reverse direction. For loading in the opposite direction, figure 5-25 shows the tip deflection predicted. Impact of the damper bar takes place but not the contact.

Figures 5-26 and 5-27 show the response of the 268- μ m long microbeam to the same acceleration loading. Figure 5-26 shows that a closing acceleration loading will cause closure of the switch. Figure 5-27 shows that an opening acceleration load will not cause switch closure; however impact with the damper bar does occur.

Figures 5-28 and 5-29 considers the response of the 434- μ m long microbeam (234-g). Figure 5-28 shows the tip deflection response to a closing acceleration; as indicated, this figure shows that closure will occur several times. Figure 5-29 shows that an opening acceleration loading will also cause switch closure several times.

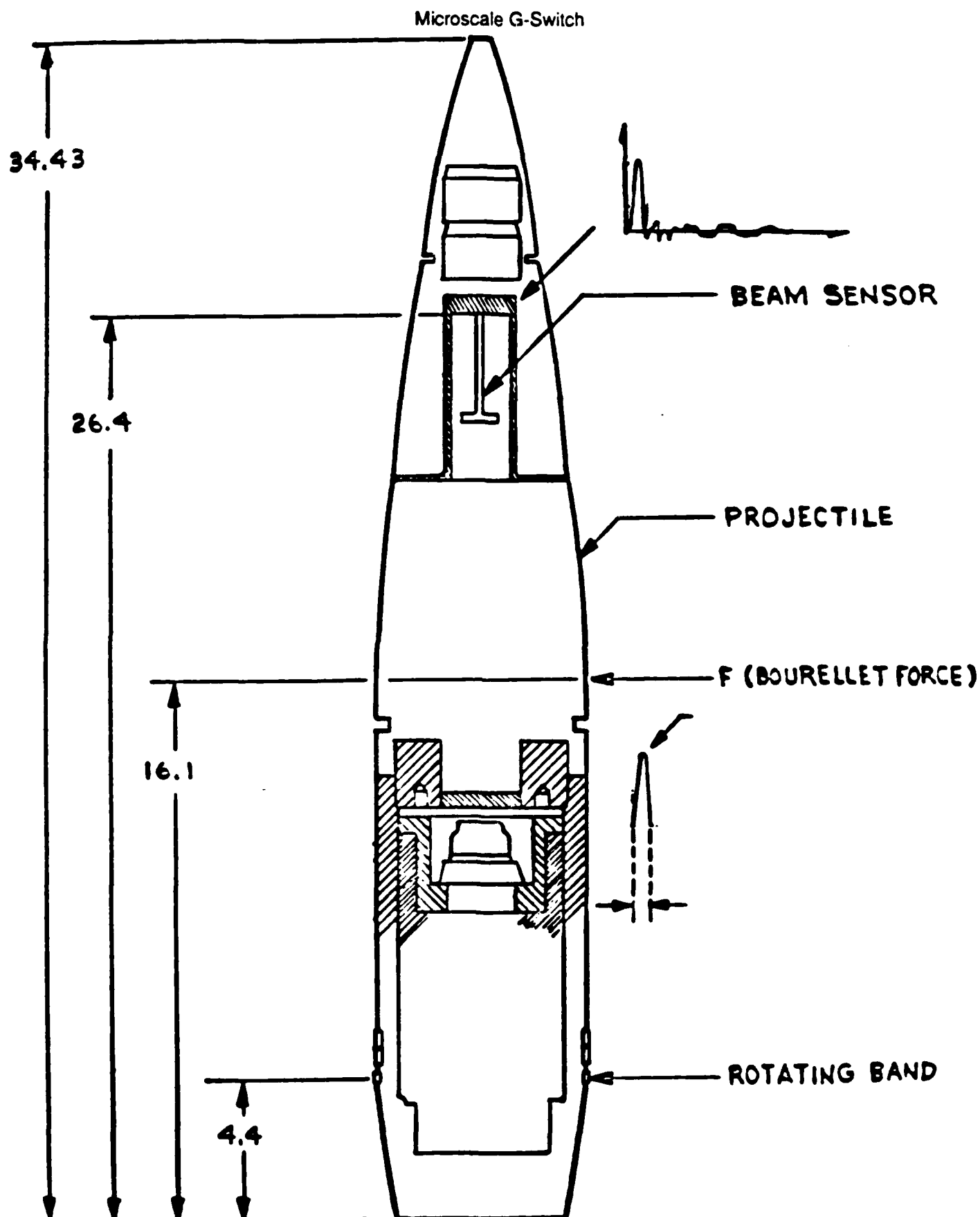


Figure 5-22. Balloting load application and beam sensor location for instrumentation projectile-155 mm.

Microscale G-Switch

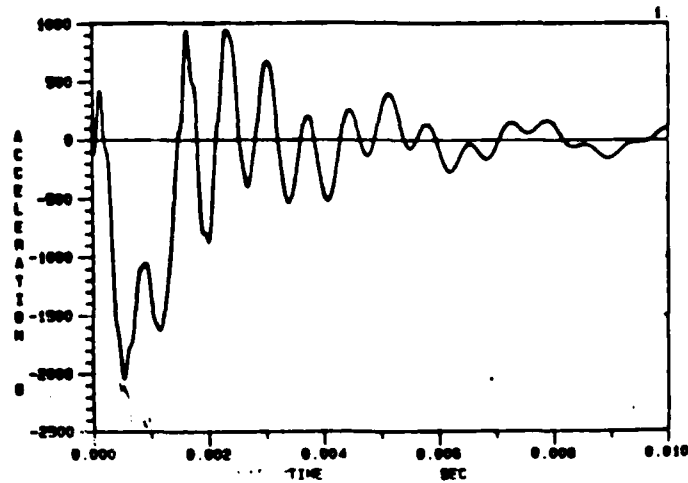


Figure 5-23. Acceleration-time history at S&A location.

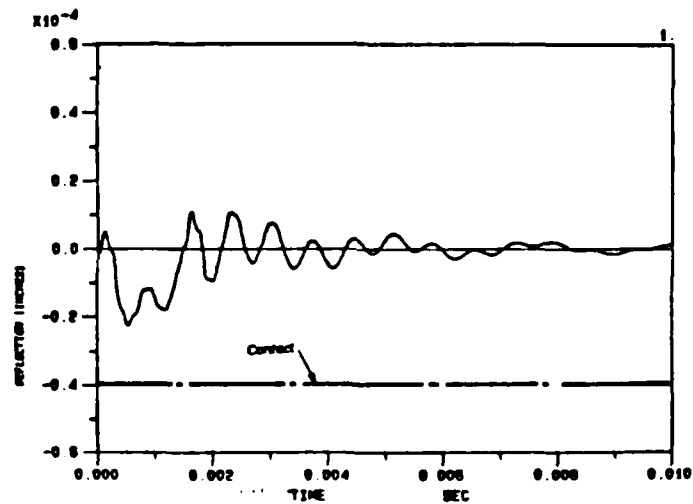


Figure 5-24. Tip deflection response of 214- μ m microbeam to closing acceleration.

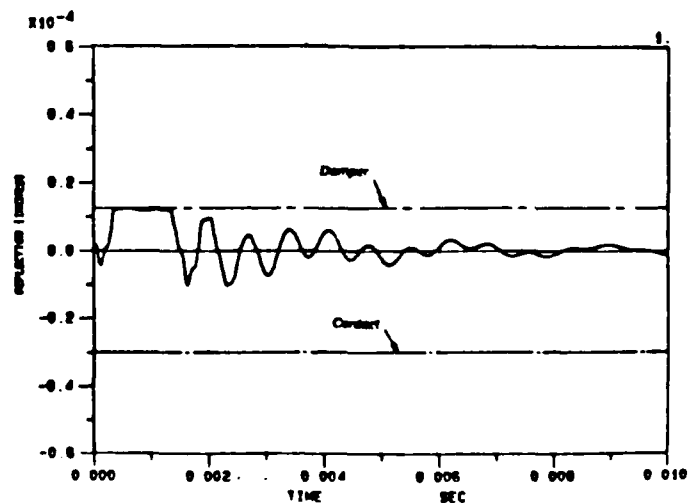


Figure 5-25. Tip deflection response of 214- μ m microbeam to opening acceleration.

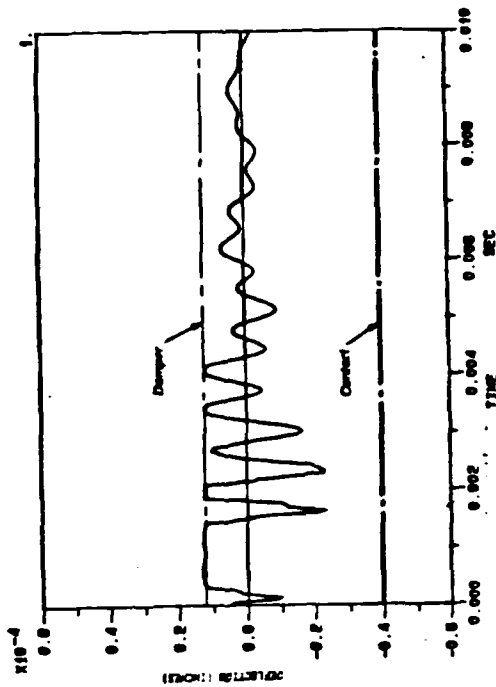


Figure 5-27. Tip Deflection Response of 268-Micrometer Microbeam to Opening Acceleration Load

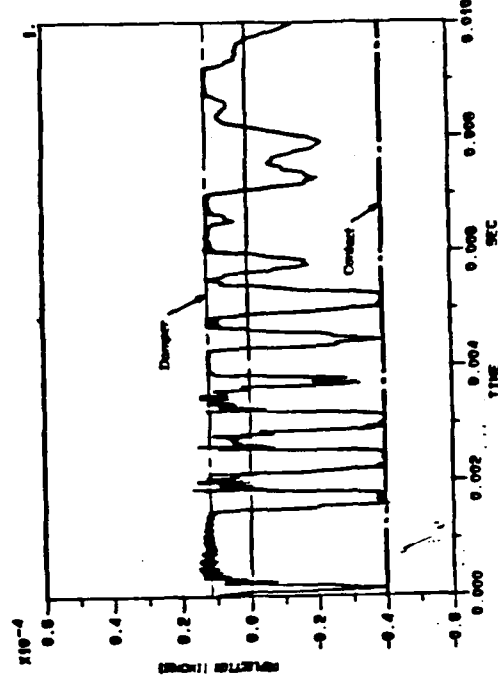


Figure 5-29. Tip Deflection Response of 434-Micrometer Microbeam to Opening Acceleration Load.

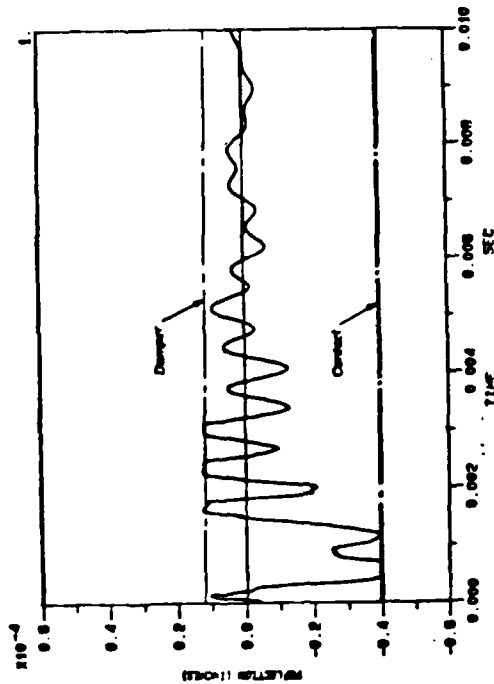


Figure 5-26. Tip Deflection Response of 268-Micrometer Microbeam to Closing Acceleration

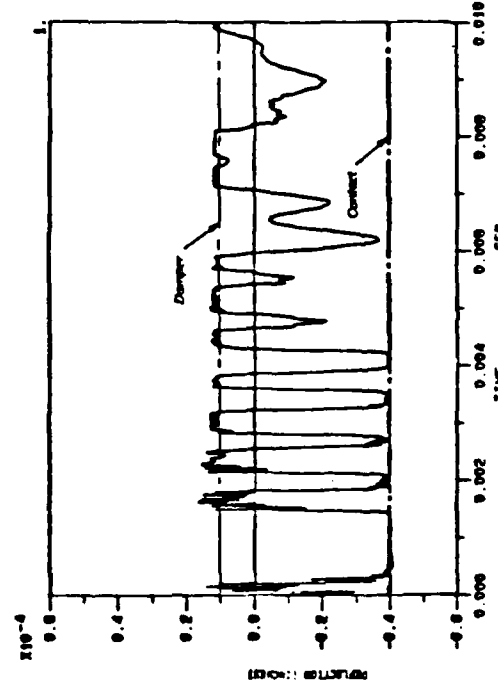


Figure 5-28. Tip Deflection Response of 434-Micrometer Microbeam to Closing Acceleration.

The overall implication from this analysis is that the spin array is sensitive to the effects of balloting should it occur in precisely the right direction. Switch closure could be induced well before appreciable spin rates were encountered. This implies that any logic system utilizing switch closure as a launch-level indicator would best be applied after muzzle exit when balloting accelerations are absent. One distinguishing characteristic noted is that the switches are predicted to close for approximately the same length of time that the balloting load is applied. This hints that electronic logic that detects some minimum length of closure might be suitable to differentiate between these ambiguous environments.

5.5 *Rough Handling Response*

Since the switch gap employed with the microbeam design is only 1 μm , one would expect a high-Q spring-mass system to be easily excited by rough handling--especially at resonance. A worst-case scenario of sustained sinusoidal vibration was hypothesized for analysis and used as an input to test the beam's sensitivity to rough handling and gauge the effect of the contact damping bar on the beam's response in this situation.

The analytical study performed predicted the response of the lowest frequency microbeam to sinusoidal excitation (beam length = 434 μm). In this study the tip deflection and effects of the damper bar on these responses is evaluated at 2000, 5000 and 9706 Hz (the first resonant frequency of the beam). The input level of excitation was 224 g's for all cases except for the case at the beam's first resonant frequency. In that case the response to both 224 g's and 11.2 g's (224 g's divided by 20, the assumed amplification factor "Q" of the beam) was predicted. The method of analysis used was generalized coordinate theory (modal analysis). The first two beam bending modes of the microbeam were included in these calculations.

Figure 5-30 shows the response of the beam with no contact and no damper bar to 224 g's of sinusoidal excitation at a frequency of 2000 Hz. Notice that the tip deflection has a steady-state response of about 31.5 microinches. The contact which would have been at 39.37 microinches would not have been reached. The root stress for this case shown in figure 5-31 has a steady-state value of about 21,000 psi.

The second case studied is a 224 g sinusoidal excitation at 2000 Hz with the damper bar and contact in place. Figures 5-32 and 5-33 show the tip deflection and root stress, respectively, for this excitation. As expected from the previous case, the damper bar located at 9.84 microinches above the beam was impacted as indicated by the amplitude limiting at approximately 100 microinches in figure 5-32. This corresponds to contact with the damper bar which is spaced 0.25 μm above the beam's top surface at a location 25 μm from the end of the beam. Figure 5-34 shows the effect of the damper bar positioned flush with the top surface

Microscale G-Switch

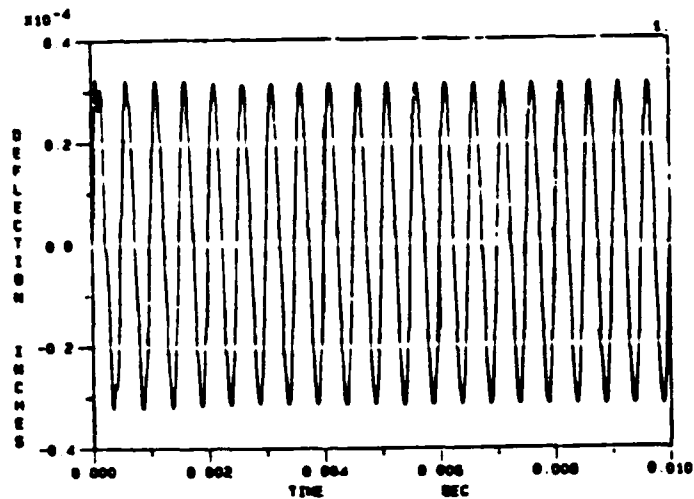


Figure 5-30. Tip Deflection Versus Time; Damper Bar and Contact Removed; Forcing Frequency 2000 HZ And 224 g's.

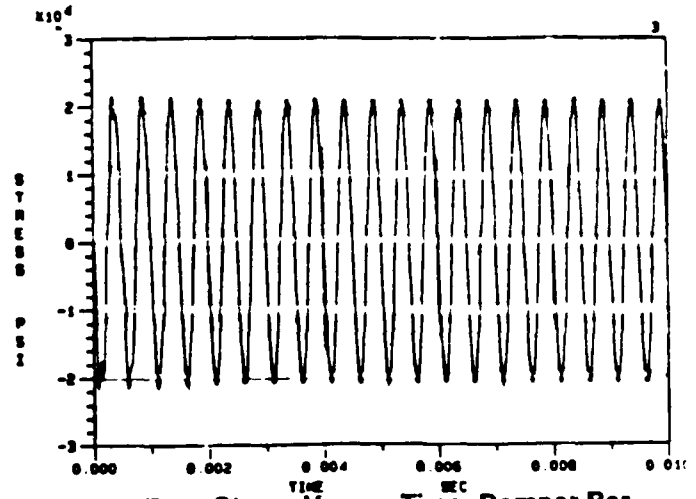


Figure 5-31. Root Stress Versus Time; Damper Bar And Contact Removed; Forcing Frequency 2 kHz at 224 g's.

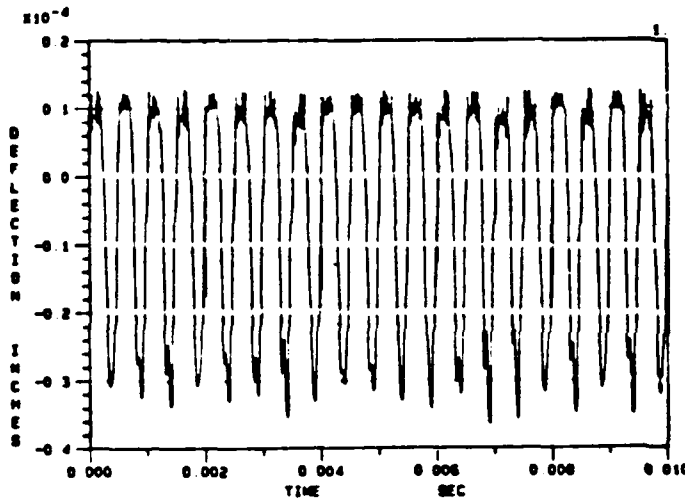


Figure 5-32. Tip Deflection Versus Time; Damper Bar And Contact Added; 2-kHz Forcing Frequency and 224 g's.

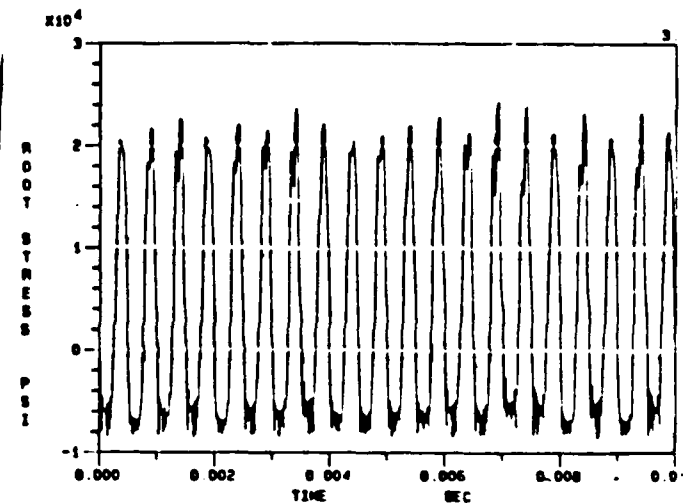


Figure 5-33. Root Stress Versus Time--Damper Bar and Contact Added.

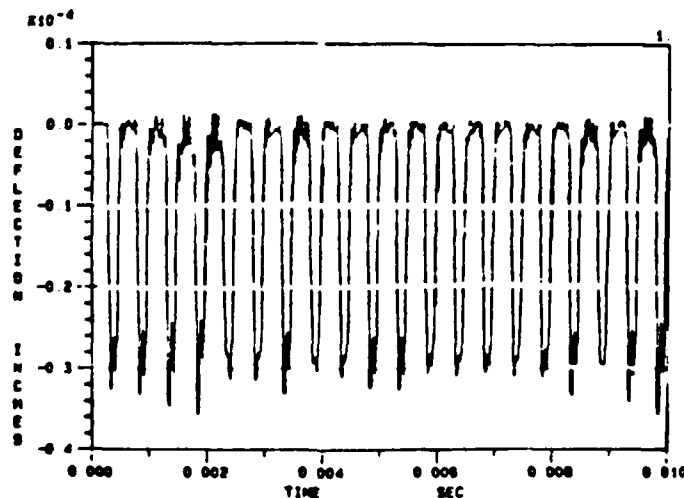


Figure 5-34. Tip Deflection Versus Time; Damper Bar Flush with Top of Beam; 2-kHz Forcing Frequency and 224 g's

of the beam for contrast. Comparing figure 5-30 with figure 5-32 shows that the beam tip deflects towards the contact (negative direction) as far as it would have had the damper bar not been there. This is expected at forcing frequencies far below resonance since the loading is effectively a statically applied loading in each direction; therefore, the damper bar has little influence on the response of the beam when it approaches the contact. Positioning of the damper bar closer to the beams's top surface also has little effect for this situation.

Figures 5-35 and 5-36 show the beam deflection at the tip along with the root stress due to 224-g sinusoidal excitation at 2000 Hz. In this case, the damper bar is preloaded against the beam so that the deflection of the beam at the damper bar location is 10 microinches. The maximum tip deflection toward the contact is 37 microinches, which is greater than any of the previous cases. This implies that a preload type of set-up is not as effective as the use of a damper bar in reducing the response of the beam when it is driven at high levels. Forcing excitations at levels below 60-g would of course be eliminated by the bias mechanism.

The next parameter evaluated was a higher input forcing frequency. Figures 5-37 and 5-38 show the tip deflection and root stress response of the beam due to 224-g's sinusoidal excitation at 5000 Hz. In this case the damper bar is 9.84 microinches above the beam, and the contact is 39.37 microinches below the beam tip. As shown in figure 5-47 the tip of the beam barely reaches the contact. Since the resonant frequency is 9706 Hz and the forcing frequency is 5000 Hz, the amplification factor would be $Q = 1.36$. This is greater than the amplifications at a forcing frequency of 2,000 Hz ($Q = 1.04$), and therefore the response would be expected to be greater at the higher forcing frequency, which was the case. The amplifications quoted above, namely 1.36 and 1.04, are not exactly correct but the trend of increasing amplification as resonance is approached is expected. Maximum root stress is 23 KSI.

Figures 5-39 and 5-40 show the tip deflection and root stress due to 224 g's sinusoidal excitation at the beams first resonant frequency (9,706 Hz). In this case the damper bar is located 9.84×10^{-6} inches above the beam and the contact is 39.37×10^{-6} inches below the beam tip. As shown in Figure 5-39, the contact is barely reached. If the damper bar were not in place, the contact would have been strongly impacted. Therefore it is shown that the damper bar significantly affects the beam response at the beam's resonant frequency since it does not allow a free resonant condition to occur.

Figures 5-41 and 5-42 show the response of the beam for the same conditions of the previous case except that the damper bar is removed. Figure 5-41 shows the beam tip impacting the contact. The impact load calculated was 1.006×10^{-6} lb. compared to 0.249×10^{-6} lb. for the previous case with the damper bar in place. It might have been expected that the difference should have been even greater; however, it should be remembered that the contact itself also prevents the full amplification of the beam response from developing. Maximum root stress predicted was 40KSI compression.

Microscale G-Switch

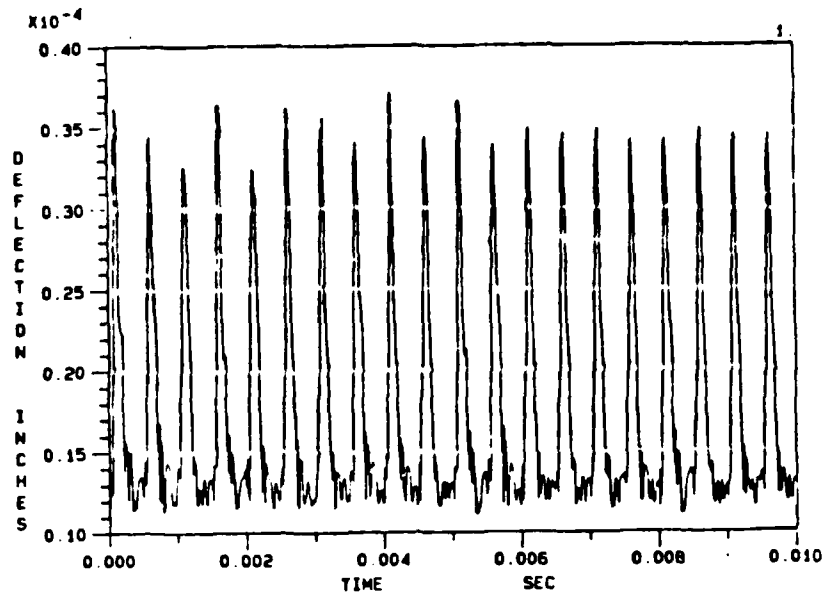


Figure 5-35. Tip Deflection Versus Time; Damper Bar Preloads Beam; Forcing Frequency 2 kHz And 224 g's.

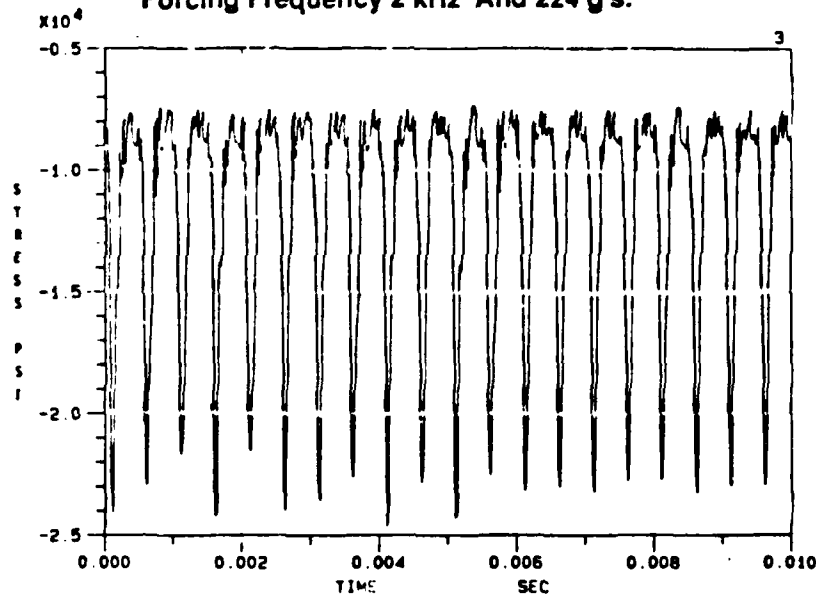


Figure 5-36. Root Stress Versus Time; Damper Bar Preloads Beam; Forcing Frequency 2 kHz And 224 g's.

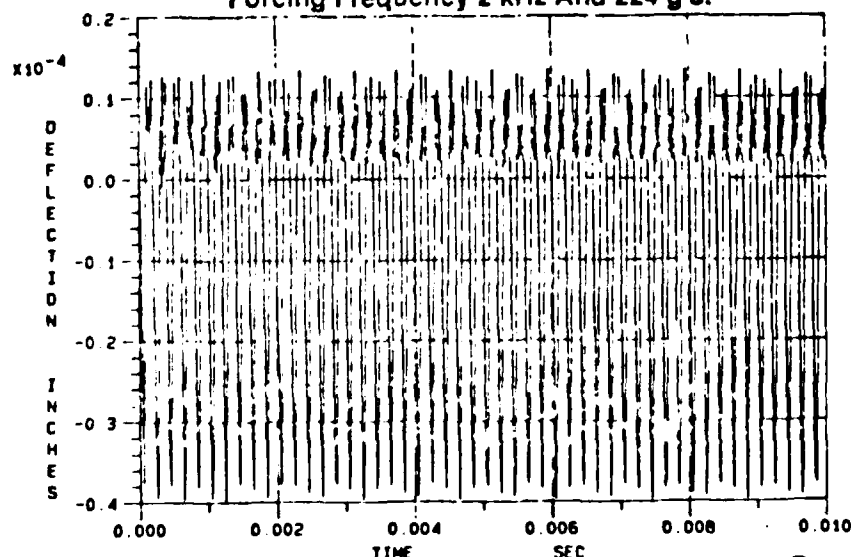


Figure 5-37. Tip Deflection Versus Time; Contacts And Damper Bars Included; Forcing Function 5 kHz and 224 g's. 50

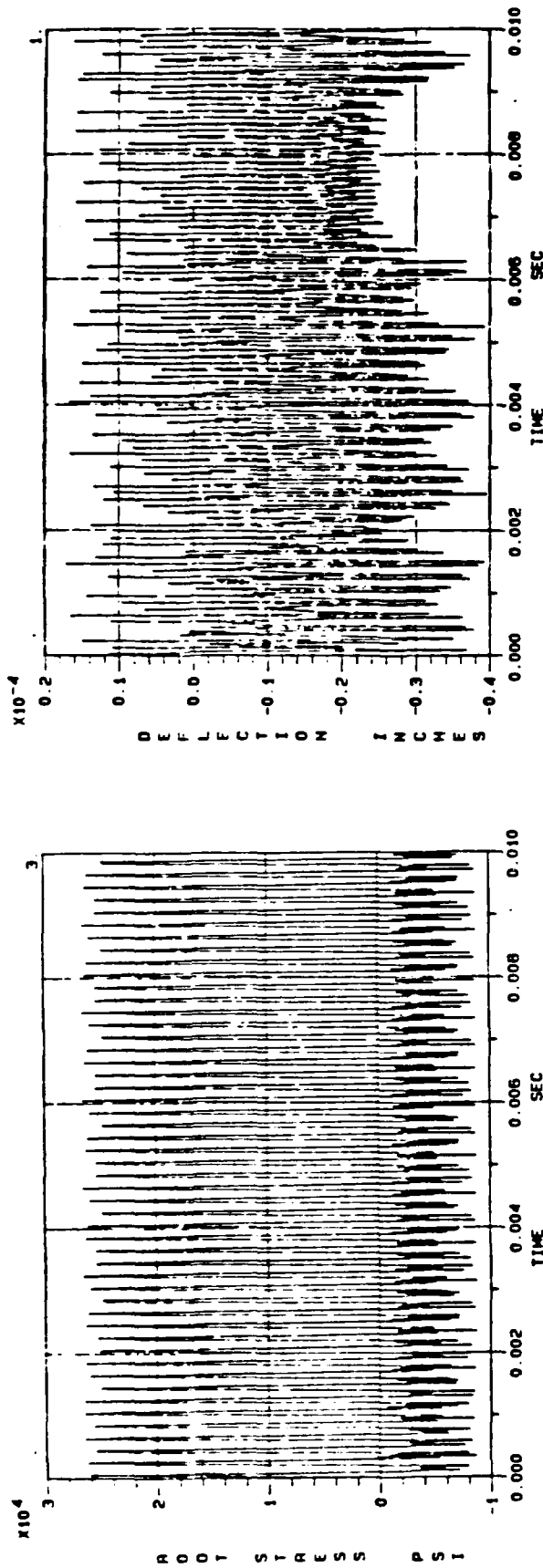


Figure 5-38. Root Stress Versus Time; Contacts and Damper Bars Included; Forcing Function 5 kHz and 224 g's.

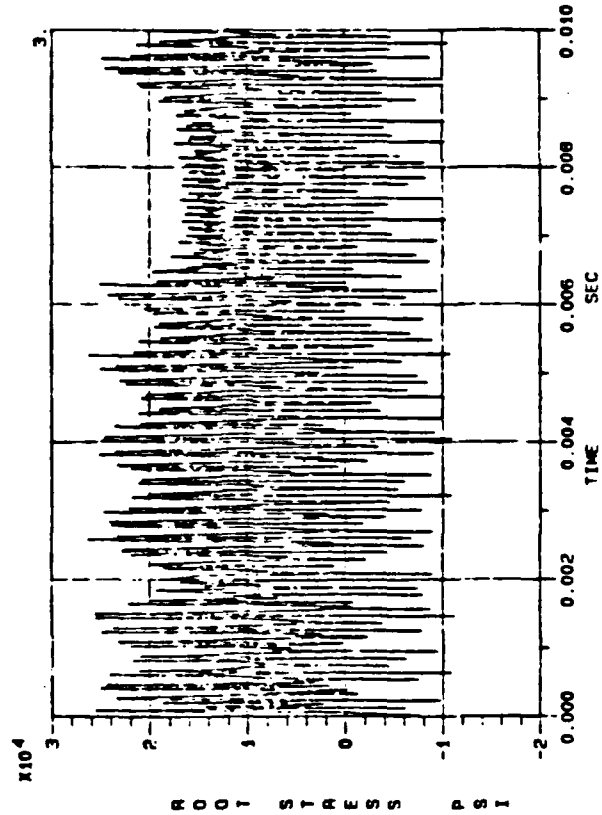


Figure 5-39. Tip Deflection Versus Time; Contacts and Damper Bar Included; Forcing Function 9706 Hz and 224 g's.

Microscale G-Switch

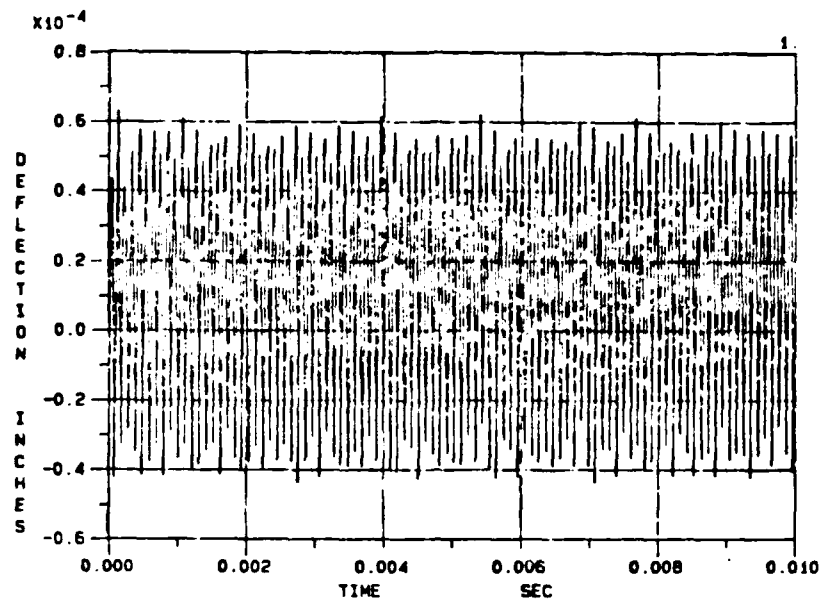


Figure 5-41. Tip Deflection Versus Time; Damper Bar Removed;
Forcing Frequency 9706 Hz and 224 g's.

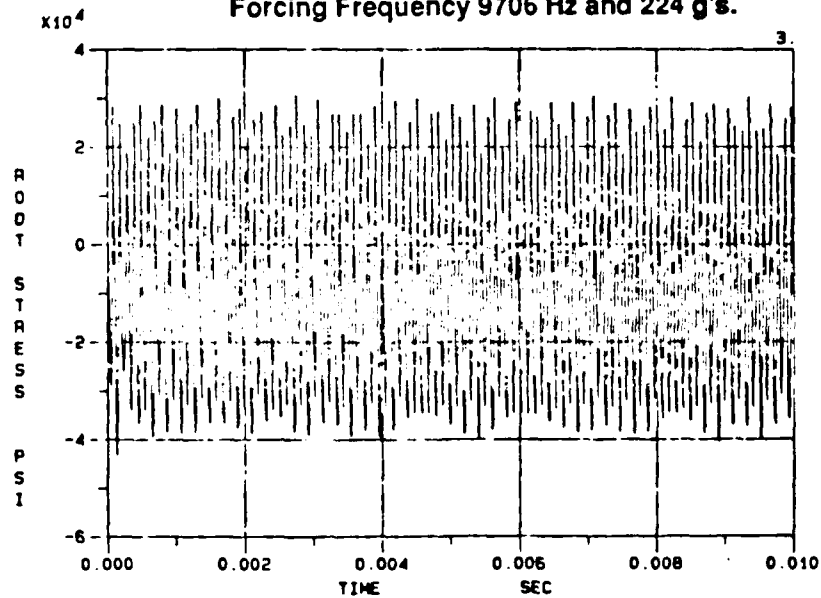


Figure 5-42. Root Stress Versus Time; Damper Bar Removed;
Forcing Frequency 9706 Hz and 224 g's

For the cases shown in figures 5-43 and 5-44, the sinusoidal input load was reduced by the assumed amplification "Q" of the beam ($Q = 20$). The ground acceleration was therefore 11.2 g's and the forcing frequency remained at 9,706 Hz. Figures 5-45 and 5-46 show the responses when no damper bar is used. The tip deflection therefore builds up to a steady-state value of approximately 30 microinches as shown in figure 5-43. As indicated by comparison with figure 5-45 it is approximately half the response attained by the beam when the damper bar is not used. Again the damper bar is shown to be effective in reducing the response of the microbeam at its resonant frequency.

6.0 BEAM PACKAGING

Difficulty obtaining T05 packages prompted the review of several alternative methods for mounting and testing the microbeams on a vertical board within a fuze structure. The test package subsequently chosen was the "J-Pak" shown in figure 6-1. This component has beam leads that extend from a lead frame which is sandwiched between several layers of ceramic. The multilayer construction is then thermally fused in a furnace. A Kovar lid is reflow sealed to complete the package after the die is attached and wire-bonded. The package generically is a surface mount device and has been used successfully in large-caliber nuclear fuzing able to withstand 16,000 g's and 16,000 rpm gunlaunch environments produced by a 155-mm gun.

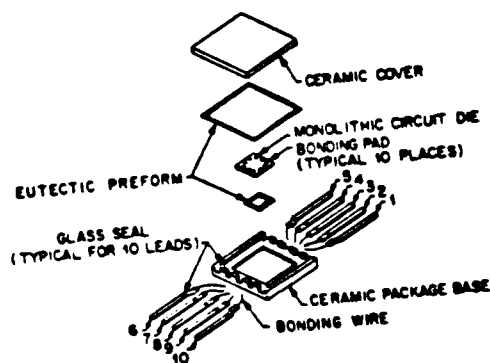


FIGURE 6-1

J-PAK EXPLODED VIEW

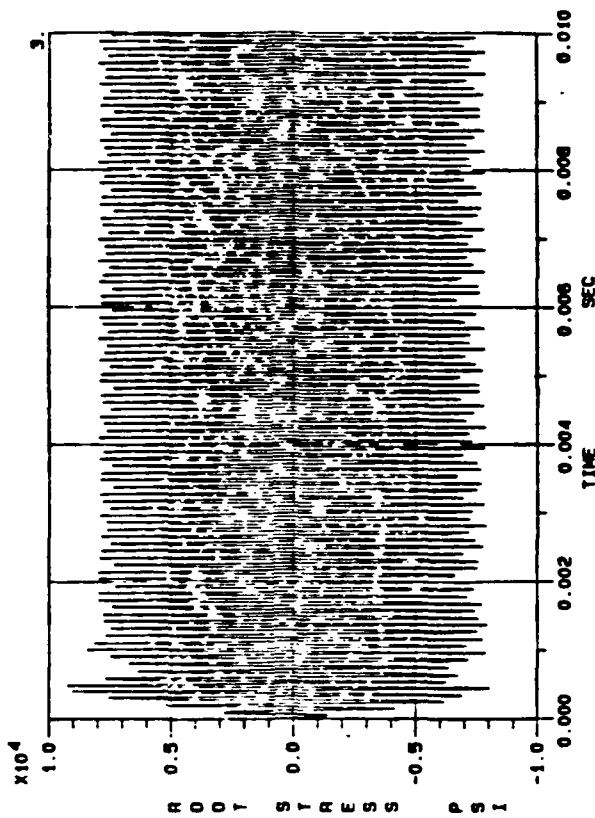


Figure 5-43. Tip Deflection Versus Time; Damper Bar Removed; Forcing Frequency 9706 Hz; Q = 20 Assumed; 11.2 g's Input

Figure 5-44. Root Stress Versus Time; Damper Bar Removed; Q = 20 Assumed; Forcing Frequency 9706 Hz And 11.2 g's.

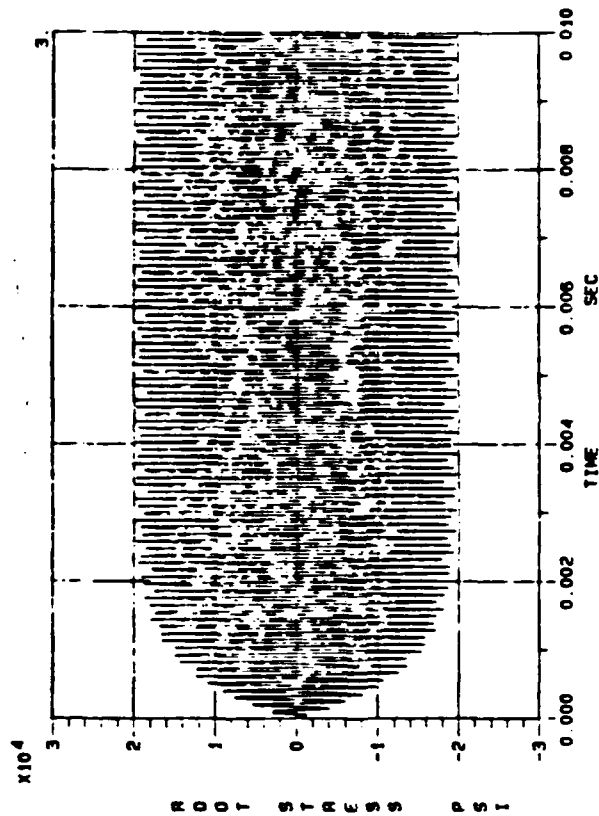


Figure 5-45. Tip Deflection Versus Time; Contacts and Damper Bar Included; Q = 20 Assumed; Forcing Frequency 9706 Hz and 11.2 g's

Figure 5-46. Root Stress Versus Time; Contacts and Damper Bar Included; Q = 20 Assumed; Forcing Frequency 9706 Hz and 11.2 g's

Packages were generally left unsealed for the centrifuge evaluation to facilitate scanning electron microscope (SEM) examination. While this risked contamination of the devices it was felt that careful handling and application of a thick adhesive mylar tape between tests was sufficient to prevent dust, dirt, etc. from contaminating the unit.

7.0 BEAM PERFORMANCE TESTING

The test device, actual testing, and post-test analysis are discussed in the following paragraphs following a review of preliminary electrostatic testing performed on several devices.

7.1 *Electrostatic Closure Testing*

A preliminary screening was performed in an attempt to close the switches with electrostatic attraction. A test circuit as shown in figure 7-1 with typical current levels of 0.1 microamps was used. Voltage was gradually increased until the switch closed. Four of the switches tested closed at the voltage indicated in table 7 and are contrasted with voltages predicted by appendix A. All switches which closed electrostatically would not reopen once they were disconnected from the circuit. This test was subsequently discontinued since it rendered the test device nonusable for later centrifuge analysis.

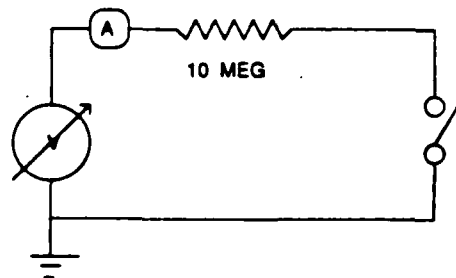


FIGURE 7-1. Test circuit schematic for electrostatic closure voltage determination.

TABLE 7. Measured Electrostatic Closure Voltages

Device No.	Design Threshold (g's)	Closure Voltage (V)	
		Predicted	Measured
1	3120	80	108
3	1390	57	72
4	228	28	90
5	3120	80	87

The fact that even one switch did close near the predicted voltage level indicates that the electrostatic effect must be considered in overall beam operation. In no cases were closure voltages lower than anticipated--always higher. However, closure voltages 9 to 225 percent higher than predicted were measured. This can be caused by several factors:

(1) Excessive gap: Since the closure forces vary inversely as the square of the contact separation distance, a closure voltage two times higher could indicate a gap twice as large in the switch. Larger than normal gaps were observed with several devices later inspected with SEM photography as will be discussed later.

(2) Nonuniform gap: Since the beam would be required to twist to close should a different gap exist on either side, the 69:1 ratio of torsional to bending stiffness cited in Appendix B would require significant excess voltage to be applied. Since the force varies as the square of the voltage, the over-voltage for switch 4, for example, might be indicative of a 3.25- μm variation in gap distance between each of the two contact points. Note that nine of the switches tested could not be closed at the max test voltage of 125 V.

The use of electrostatic force to screen this type of microbeam structure would be extremely attractive as a substitute for applied acceleration were it not for the contact weld phenomena exhibited. Note that closure voltages are easily in the range of I^2L operating voltages.

The ability to "program" a switch closed permanently by applying an encoding voltage may be useful in many applications as a nonchattering latch--albeit an irreversible one. The "contact weld" phenomena observed is discussed in more detail in Section 7.4

7.2 Test Configuration and Test Results

Thirty three microbeam switches were spin tested with the use of Motorola's spin pit facility shown in figure 7-2. The microbeams were packaged in 14-leaded J-paks and mounted as shown in figure 7-3. Two custom-designed multilayer printed wiring boards were utilized. These provide the capability to test 16 three-beam arrays simultaneously--eight on each board. The boards are positioned at the output board location of the XM749 proximity fuze for the XM785 nuclear projectile. The boards are symmetrically located with respect to the spin center and offset at a radius of 1.3 in. The switches lay flat on the board. All switch outputs were monitored through a 10-channel telemetry link utilizing the instrumentation used to support the XM749 power supply structural telemeter. This system uses an onboard VCO assembly in conjunction with a Microcom FM transmitter. The signal is received by a stationary antenna and decoded by an array of rack-mounted demodulator units. An oscillograph was used to record all 10-channel outputs. Since only 10 channels are used to monitor 48 switches, it is necessary to multiplex switch outputs. Figure 7-4 shows the multiplex circuit. A typical oscillograph trace is shown in figure 7-5.

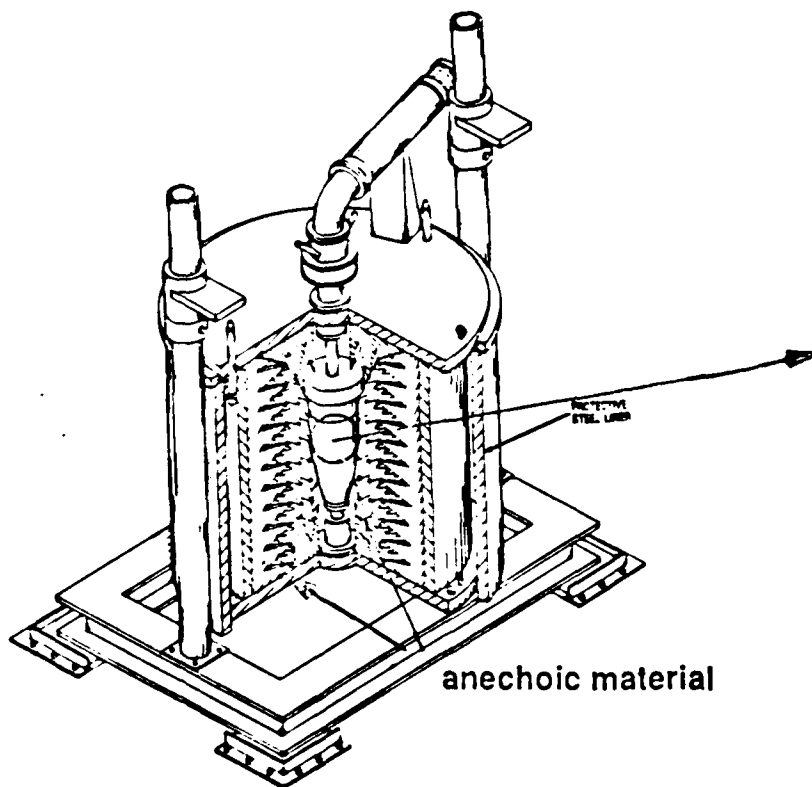


FIGURE 7-2
MOTOROLA SPIN PIT FACILITY

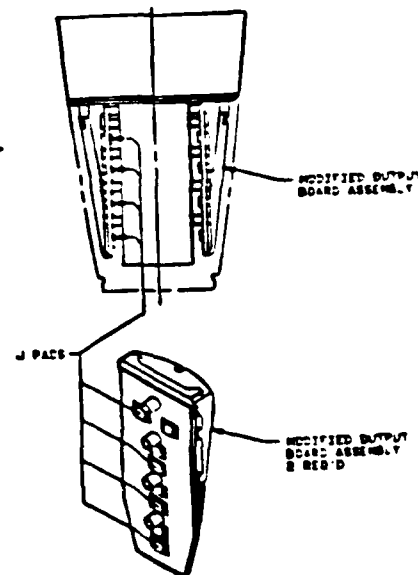


FIGURE 7-3
J-PAK MOUNTING ILLUSTRATION

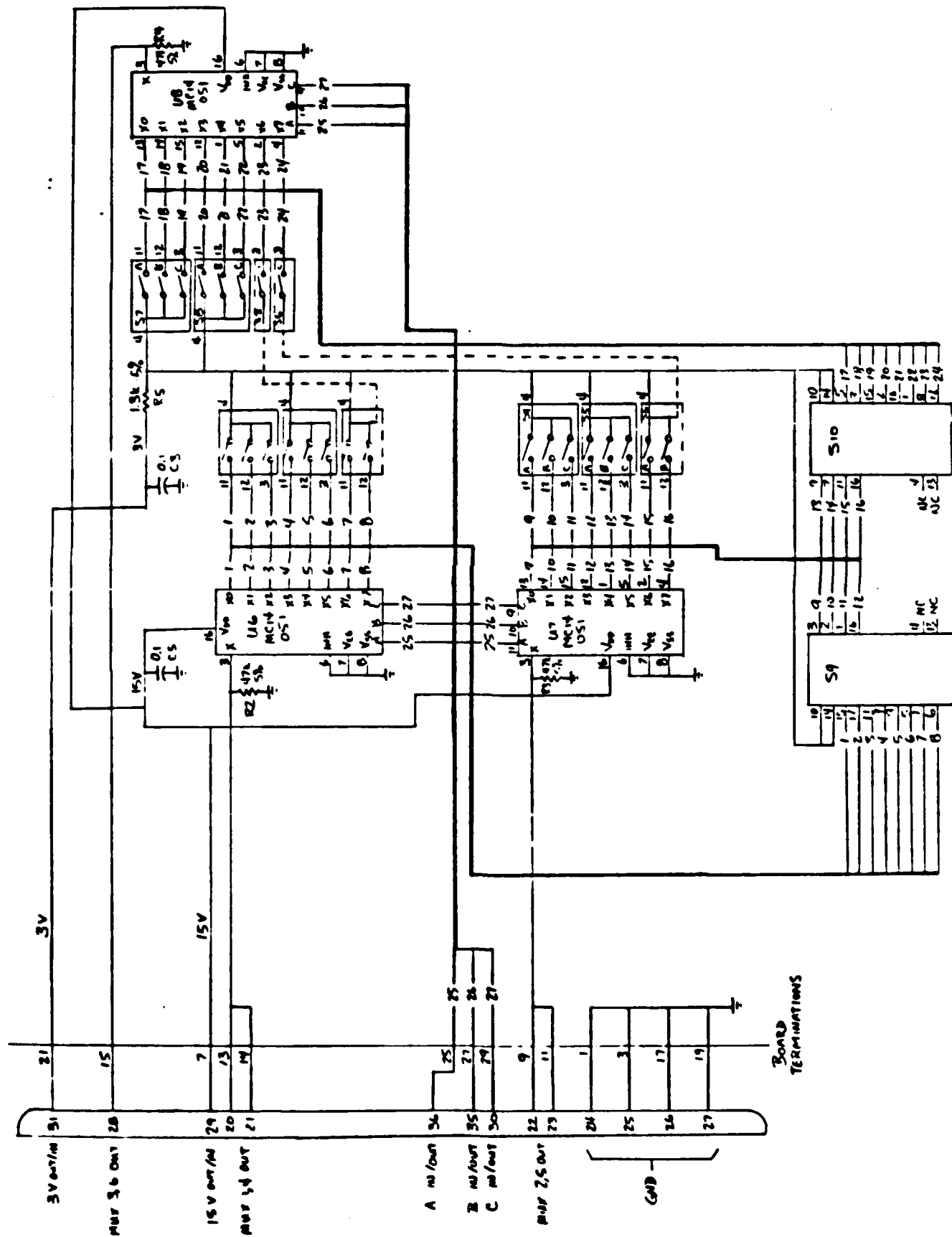


Figure 7-4.2. Multiplex Circuit--Board B.

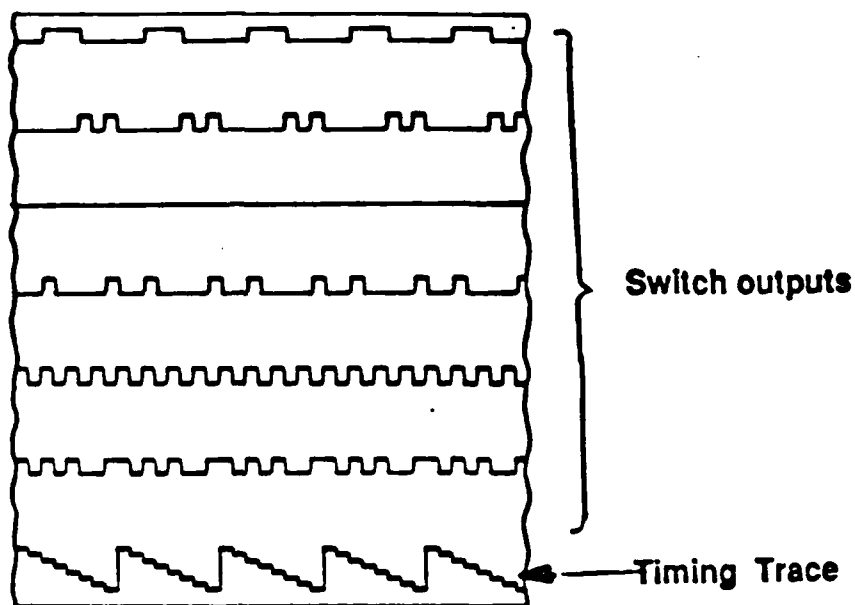


Figure 7-5. Typical oscillograph trace format.

Twenty four of the switches were positioned on the centerline of the board such that centrifugal force is applied normally to each beam's top surface. Four were positioned at a 15-degree angle.

Sixteen devices were screened electrically before the spin tests to determine if any switches were welded closed before the test. At least one switch of each array was found closed, with the exception of device No. 14 in which all switches were open. This screening was performed using a 0.6-V source to eliminate the possibility of electrostatic closure.

Centrifuge testing was conducted wherein the rpm was gradually increased to 18,000 rpm over a 7-minute period. Two switches were found to open and close consistently at some threshold rpm level. The first switch, nominally designed to close at 230 g's closed at 1,000 g's and the second switch designed to close at 1,400 G's closed at 12,000 g's. Each switch opened and closed twice demonstrating that the gold to gold contact weld was successfully avoided. Note that no intentional surface plating was used with these contacts; however, the possibility that titanium alloys present from one of the processing steps existed on the surfaces cannot be ruled out. It is estimated that the test circuit previously shown in figure 7-4 results in approximately 62 microamps of current flow through the microbeam switch contacts when the

switch is shut.

A second series of spin tests was conducted on the devices shown in Figures 2-3 and 2-4 but the devices failed to operate because of a process problem experienced during manufacture. SEM examination indicated that a gold crust had formed adjacent to the beam tip pinning the beam in an open position. Attempts to make the beam a single contact device by using a bridgewire electrically connected to the beam tip but mechanically decoupled were thwarted by a mask error resulting in an open-circuit between bridgewire and beam tip.

7.3 *Post-Test Analysis*

Eight of the 16 arrays tested were subjected to SEM analysis. Figures 7-6 and 7-7 show the functional beams which opened and closed successfully. Switch TG11 in figure 7-6 can be seen to contain tip contacts which have taken on a "Y" configuration exaggerating the contact gap. An undistorted beam is shown in figure 7-8 for contrast. This gap (an estimated five microns) can easily explain the performance of this particular switch since the threshold activation g level varies linearly with the contact gap.

Switch TG9, however, is not deformed but still required nearly nine times the g level anticipated to induce closure. It is conjectured that variation in the contact gap between each contact pad can account for this variation.

Of the remaining 31 switches, 12 were found to be half-closed so that contact was observed on the right side of the contact pair. Since the switches were not photographed before test, it was not possible to determine whether half closure resulted from the centrifugal force field. The calculation shown in appendix B indicated that the g field required to obtain deflection by twisting the beam can be as much as 69 times higher than that required to deflect it linearly. Consequently it is conjectured that the condition induced by a half-closed beam would result in the beam behaving much stiffer than designed.

Figure 7-9 shows one additional anomaly noted. One switch, TB10, was first photographed and shown to be closed. However a subsequent electrical measurement indicated it to be electrically open. SEM re-examination showed the switch had mechanically reopened from handling, indicating the gold-to-gold weld to be marginal and potentially able to be eliminated entirely.

Microscale G-Switch

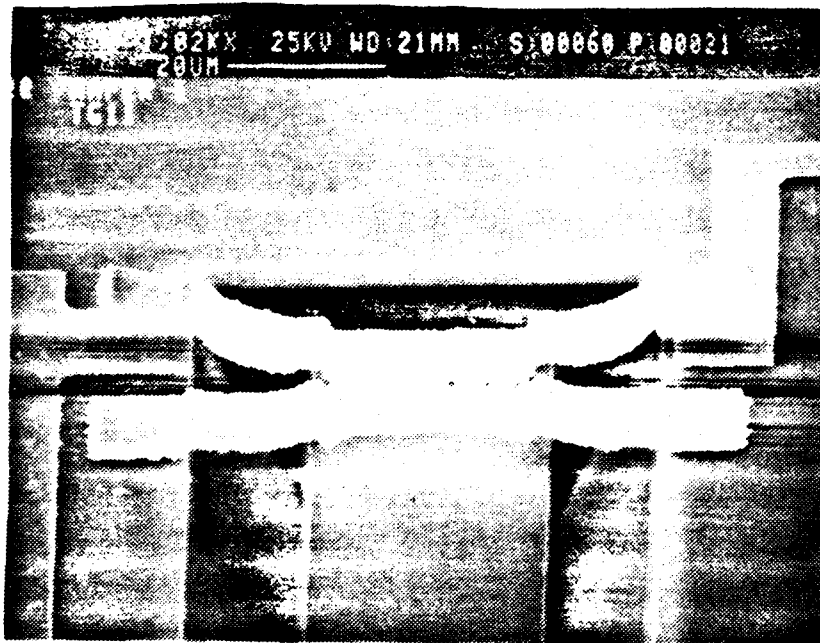


Figure 7-6. Microbeam Switch Operative In Centrifuge--434-Micrometers Long.



Figure 7-7. Microbeam Switch Operative In Centrifuge--268-Micrometers Long.

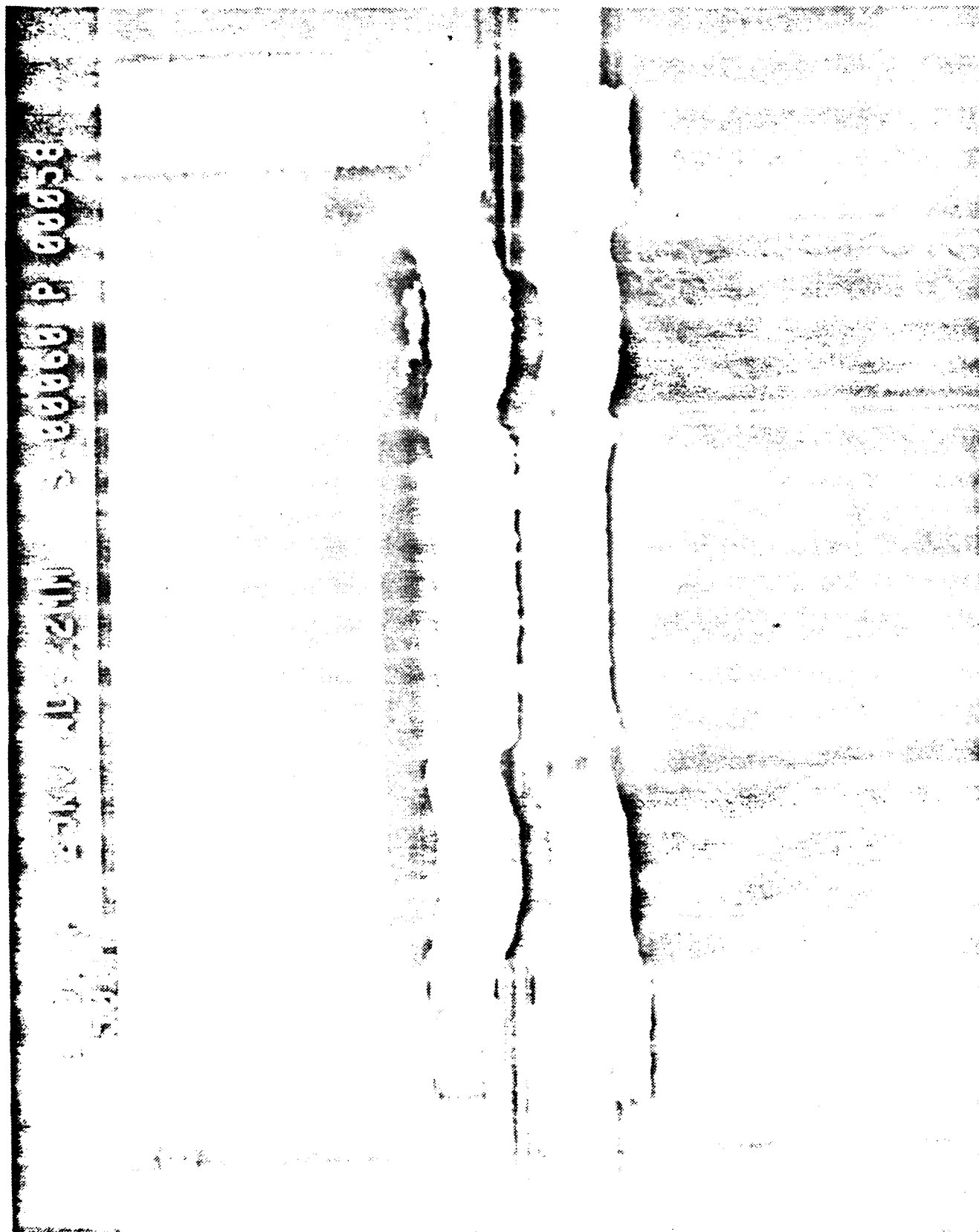
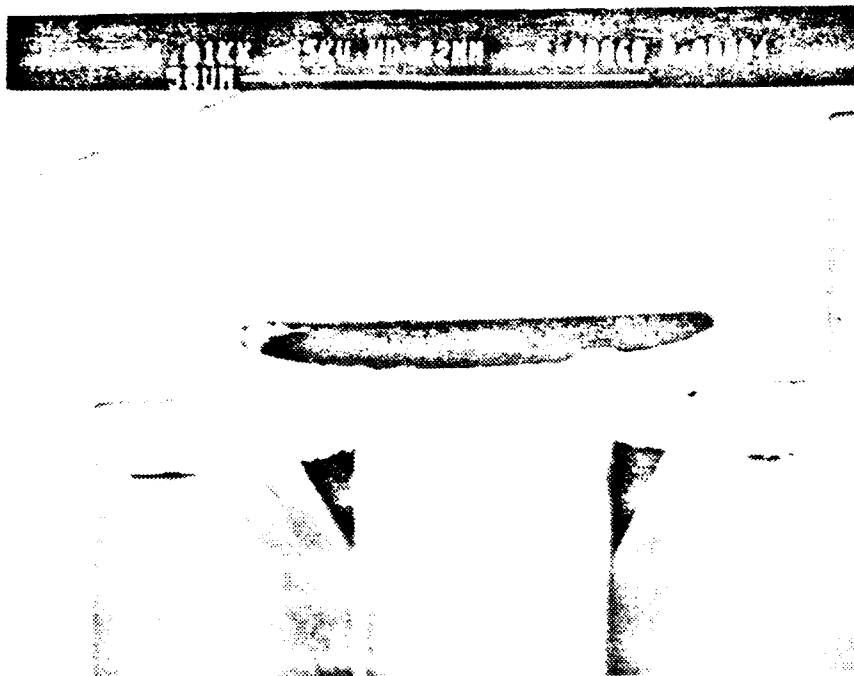
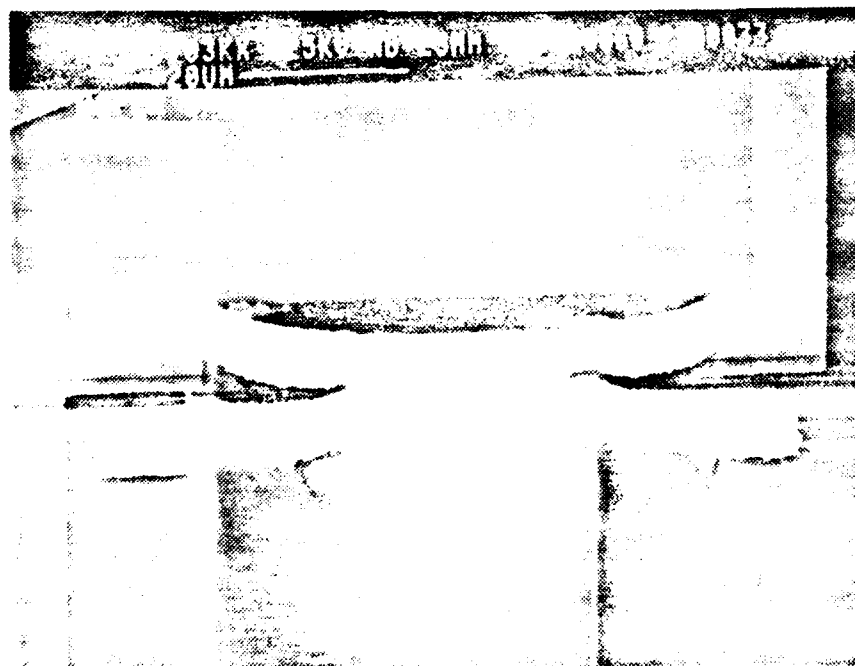


FIGURE 7-8
UNDISTORTED MICROBEAM WITH 1 MICRON GAP



(a) Closed initially.



(b) Later opened.

Figure 7-9. Microbeam Exhibiting Gold Cohesion Problem.

One other possibility for the lack of beam response offered by TDI, the fabricators, was the possibility of microdirt in the beam contact area. Figure 7-10 shows the texture of the gold contact tip. It can be seen to contain many flake-like projections at the edges. These could, if dislodged, become positioned in the contact gap resulting in a beam which effectively contains nonparallel contacts. TDI indicated that the die sawing operation is prone to generate microdust which is typically washed from the wafer with distilled water and then centrifuged away. An oven bake operation was substituted for the residue/wash centrifuge spin due to the fact that the force of the radially moving water could exert relatively large forces on these microscale devices. It is conjectured that the capillary attraction of the parallel gaps in the beam forms a collection site for residue which remains after the distilled water evaporates. Note that switch TG11 which worked had a "y" configuration less likely to include capillary attraction.

One chronic problem which was in evidence at various times on several wafers was "step coverage." Since the gull wing shape is formed by gold metallization at two distinct levels above the plane of the silicon dioxide, it becomes necessary to "connect" the two levels across an open gap. This entails forming a "step". While very good step coverage is apparent in the photograph shown as figure 2-2, difficulty was experienced at other times during the development resulting in very thin sections as illustrated in figure 7-11.

It was observed that this variation was apparent at times on the right contact but not on the left, absent on some wafers but not on others, and in general more a result of the processing and mask alignment than a characteristic of the design itself. Unfortunately this "step" exists at that point in the contact projection where the maximum bending moment exists on the gold projection. This stress concentration makes the contact many times more flexible than desired and results in contact yield such as the "Y" configuration illustrated by figure 7-6. The net result is a variation in the contact gap which decreases the sensitivity of the switch. This effectively makes the switch appear much stiffer.

TDI later demonstrated several ways to correct this problem. One involved the formation of short stubby gull wings with step rises closer to the contact pad as shown in figure 2-3. No deformation has been observed with this "shorter wingspan" approach. Another corrective measure attempted unsuccessfully involved mask corrections affecting the position of one photoresist layer. Results proved variable. In summary, this step appears to be inherent in the use of a monolithic approach to forming the beams and contacts on one die rather than utilizing a laminated configuration.

7.4 *Contact Weld Phenomenon*

A review of the usage of gold surfaces in contact switches revealed that this phenomenon was not limited to microscopic devices. Several instances were readily identified where cohesion between gold surfaces were apparent. It was found that low-g retard switches used in the FMU-139 bomb fuze once used gold contacts but abandoned this surface metallurgy because the switch would "stick" closed. Particle Impact Noise Detection (PIND) experiments

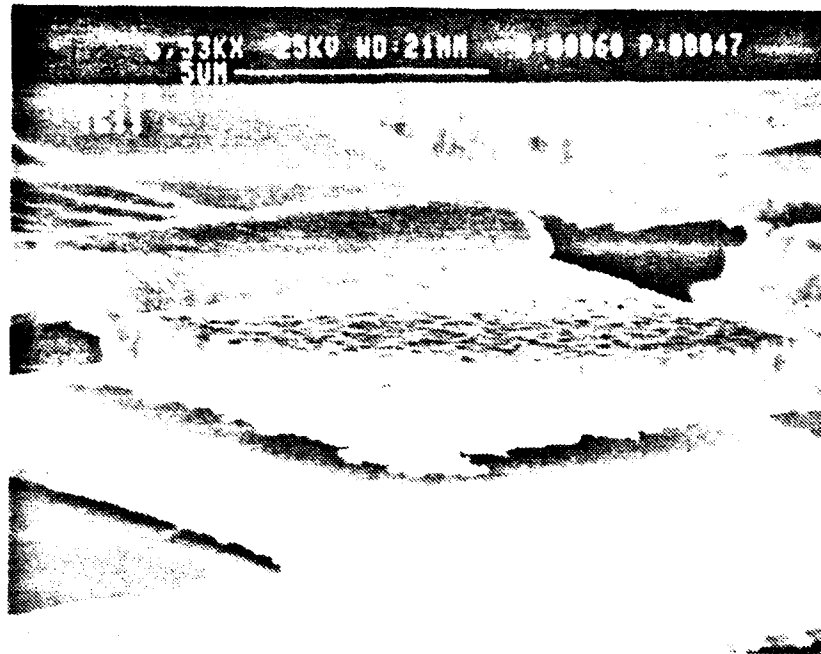


Figure 7-10. Close-up View of Contact Gap

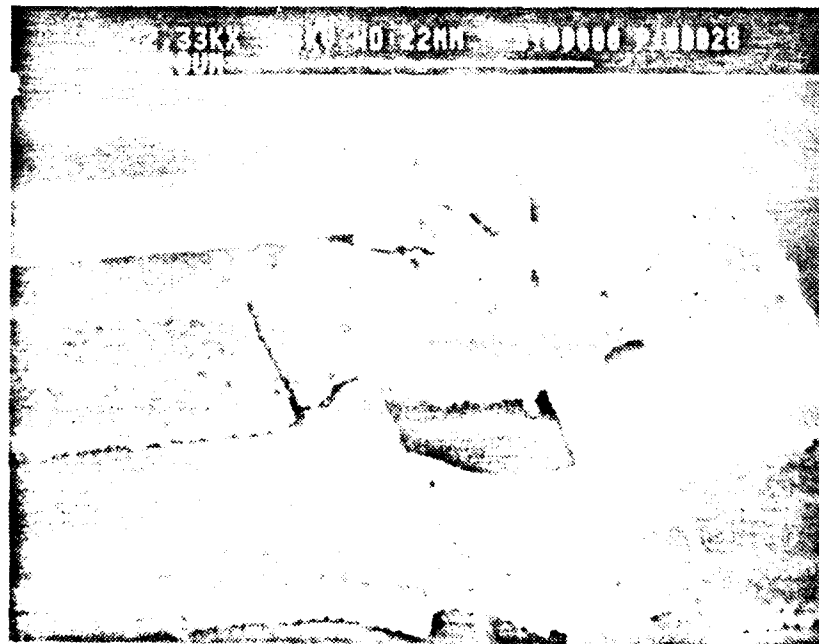


Figure 7-11. Microbeam Contact with Insufficient Step Coverage.

conducted in Motorola's Hybrid Integrated Circuit facility with gold plated slivers of ribbon purposely introduced into an IC cavity to identify its acoustic signature during PIND testing found that the gold quickly adhered to another gold surface and "welded." Literature on surface wear and friction effects with various surface treatments often show that gold-on-gold surfaces exhibit remarkably high coefficients of sliding friction (values between 3.0 and 5.0 are typical).

It is the opinion of the author that gold surfaces exhibit this effect because of two factors: (1) the absence of oxide build-up on the surface; and (2) the low yield point of the material which permits adjacent surfaces to experience differential motion when squeezed together. While this factor affects all gold-on-gold contact interactions, it is most apparent when the stored energy available to pull the surfaces apart is minimal. When the microbeams are viewed to be springs which store energy as they are deflected towards the closed position, it is apparent that because of the microscopic size, they possess only minimal ability to overcome this bonding action when the mechanism that induces the switch closure is later removed. This argues for increasing the stored energy in the cantilever portion of the structure for a given deflection.

The fact that this weld is always apparent when the switches are closed from electrostatic attraction forces may also be explained by the fact that the contacts act as microcapacitors which store charge continuously until the gold surfaces come in contact when the switches close-- discharging almost immediately. This results in a current density that is extremely large at the split second of final discharge which produces localized melting of the material and a subsequent bond when cooled.

We feel that correction of this problem can be implemented by utilizing either different contact metallurgies or adjusting the ratio of the stored energy in the switch to the bonding energy of the gold. We prefer the first option but feel it would most easily be implemented by using a double-substrate approach to the switch design. The fact that this phenomena is not apparent at low voltage operation when the switches are exercised by centrifuge motion hints at the fact that small corrections in switch geometry might neutralize this problem for most operational environments.

8.0 BEAM FABRICATION

Before a device like the beam array can be designed, a fabrication sequence must be considered. Often initial tests must be performed to investigate the feasibility of one or more approaches. In this case it was not known what residual stress might be incorporated in the oxide beams. The desired beam thickness was 3.0 μm , which is relatively thick by integrated-circuit standards. Before the devices were designed, test beams were fabricated to

try to measure the bow in the beam after it is freed from the underlying silicon. For beams on the order of 100 μm long, the residual bow was below the resolution of an optical microscope, and the initial fabrication sequence was designed.

The fabrication starts with the thermal oxidation of standard, $\langle 100 \rangle$ oriented silicon, to produce 3.0 μm of silicon dioxide. Next, this oxide layer is patterned with the mask which defines the beams. The bottom contact metal, usually gold, is then deposited and patterned to form the bottom contacts. A cross section of the device at this stage is shown in figure 8-1.

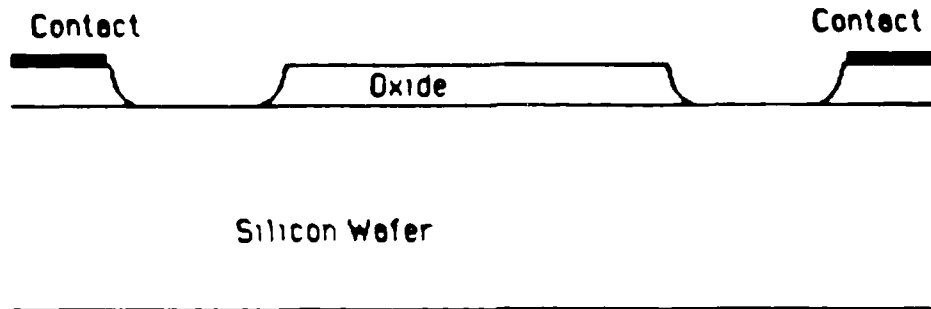


Figure 8-1. Cross section after bottom contact formation

Next, the spacer is formed which will set the eventual separation of the top and bottom contacts, and the spacing between the damper bars and the beam. The damper is an additional strap which spans the beam directly behind the gull wing contacts. The damper is designed to be about 0.25 μm above the beam top surface, so as to damp out vibrations of the beam during handling, and to support the beam during firing. The damper spacing is also formed at this time.

The top metal is then deposited, which has been a 1.5 μm thick gold layer, to achieve the desired proof mass of about 2.3×10^{-8} gm. After the top contacts and damper bars have been patterned, the cross section looks something like that shown in figure 8-2.

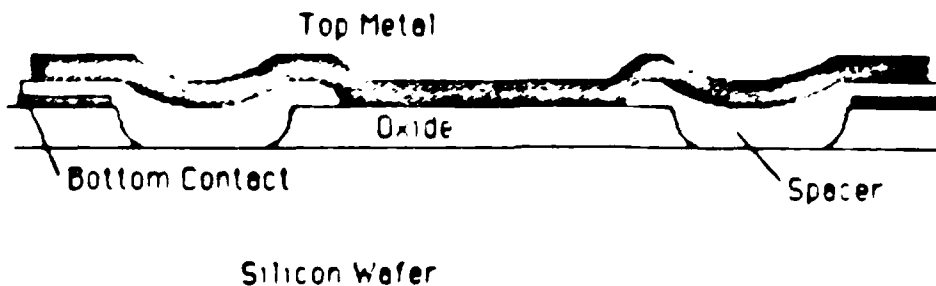


Figure 8-2. Cross section after top-metal patterning.

Microscale G-Switch

Finally, the spacer is removed and the silicon is etched. The oxide beams are undercut by the anisotropic silicon etch, and the supporting silicon is etched away. This leaves the beams supported at the back end.

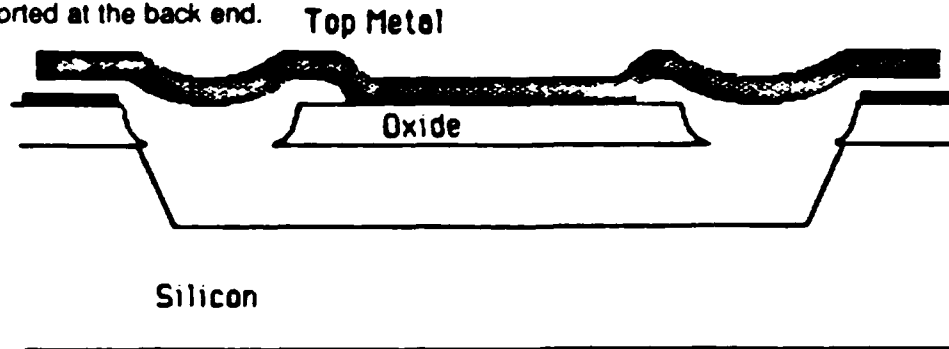


Figure 8-3. Cross section after silicon etch
(VERTICAL DIMENSIONS NOT TO SCALE)

9.0 COST ANALYSIS FOR BEAM ARRAY DIE

A detailed cost analysis was carried out assuming a process schedule similar to the present devices, with the addition of a glass cap to facilitate sawing. The costs were calculated assuming lots of 25, 4-in. wafers. The process requires a total of seven masking and major processing steps, along with the time required to bond and saw the wafers. These estimates are through die fabrication only, and do not include packaging or testing costs. It is assumed that a simple electrical test can be made on the final die, perhaps sensing capacitance of the contacts as a function of applied voltage, to allow for inexpensive testing.

The die cost is found by taking the cost to fabricate the 25-wafer lot through dicing, which is about \$11,400, assuming a mature production process. This includes the fully loaded costs of the starting material, 7 major masking and processing levels, and the 5 deposition steps for the contacts and spacers.

The final die size for a 5-beam array is about 1.05 by 1.4 mm, or about 1.5 square mm. There are about 4300 possible die on a 100 mm diameter wafer, or about 107,500 total die in the 25 wafer lot. If the final yield is assumed to be about 60 percent, then there will be about 64,500 good die from a lot. Thus the loaded die cost is less than 20 cents. The major cost of the finished device is in packaging and testing, and therefore the cost estimates must at this point be a bit speculative. Assuming inexpensive surface mounted packaging, and a simple electrical test for performance, it seems likely that the final unit cost could easily be between \$1.00 and \$4.00.

10. SUMMARY

Monolithic microstructures fabricated from SiO_2 were fabricated in configurations having multiple lengths--all variations of a cantilever structure. Centrifuge tests on the double contact version indicated performance consistent with a beam five to seven times stiffer than predicted by using classical beam equations. This was attributed to torsional stiffness and variation in switch gap between the two end contacts. A design modification introduced to enable operation with only a single contact was unsuccessful on the first try and contract funding did not permit further development. The addition of the bridgewire in this later configuration was predicted to augment the acceleration response of the microstructure because of the additional weight of the bridgewire itself and the glass structure supporting the bridgewire.

Cohesion or "cold welding" of the beam's gold contacts was evident throughout the effort and resulted initially in low test yields and the inability to reset after closing electrostatically. Two switches able to close from the acceleration field and later reopen were identified, indicating that successful operation is possible. The most notable achievement of the overall effort was the successful fabrication of 3- μm thick glass multibeam arrays without significant distortion.

11. CONCLUSIONS

Micromechanical multibeam threshold acceleration sensors for artillery fuzing are feasible but require more development to produce electrically functional switches with required mechanical integrity and acceptable yields. Successful operation with switches responding to accelerations as low as 1000 g's indicate design feasibility; however, the gold-to-gold contact metallization was found to cause difficulty in switch reset due to the low restoring force available with the microminiature structure. Successful operation of several of the switches indicate that repeatable successful operation might be possible with additional development. We feel as though we have demonstrated "proof of principle" with our results thus far. The following points are especially significant:

- (1) Microbeam silicon dioxide arrays can be successfully fabricated. A five-beam array could easily fit on a 0.1 in. square die with suitable bonding pads for each switch.

- (2) The gold-to-gold metallization combination for the switch contacts presents potential production yield problems and threshold performance variation should one contact close and the other remain open.

(3) The use of a process analogous to the "lost wax" method for casting metals is fraught with technical difficulty when used to form the switch gap for a microbeam structure. However the resulting simplicity of a monolithic suspension structure without laminates, frit bonding, etc., remains especially attractive and merits additional research.

(4) Mathematical analysis of microbeam arrays indicates that threshold acceleration sensors designed to accommodate typical large caliber artillery spin rates can withstand gunlaunch setback levels. Furthermore the beams are stiff enough to deliver rigid body response in ballistic environments, being only minimally affected by the elasticity of the fuze and projectile structure.

12. RECOMMENDATIONS

Threshold acceleration switches fabricated from silicon dioxide should be developed further for use in future munitions. The capability afforded by multiswitch arrays which can survive the extremes of ballistic environments is extensive. Solid-state safety and arming, void sensing, impact sensing, and target differentiation are typical functions which can be enhanced using these devices which can mature with further developmental effort beyond this exploratory fabrication and analysis effort.

Two areas which should be explored in more detail for future designs deal with the beam's torsional stiffness and its tendency to effect a gold "contact-weld" due to the cohesive properties of gold-on-gold surfaces and the small amount of beam opening force available.

Two torsional compliance mechanisms which were applied unsuccessfully were prone to processing problems during their implementation. The first involved a significant width reduction (see Figure 2-4). This reduces the beam's torsional stiffness by 85 percent. The second involved the addition of a zig-zag shape attachment to the end of the beam with a conductive layer on the top surface of the meander as illustrated in Figure 2-6. This transforms the beam from a cantilever structure to a simple end-supported beam with ends that have varying degrees of fixity. This later approach could only be implemented with a reduced-thickness structure which left the beam unacceptably sensitive to electrostatic closure.

Figure 12-1 shows an approach recommended by Transensory Devices utilizing a separate substrate for the stationary portion of the switch. This scheme involves a compliant stationary contact arrangement which has an increased probability of securing a two-point "landing" without requiring the beam to twist torsionally. The tip of the beam would no longer need to have a "T" configuration since the contacts would be in-line.

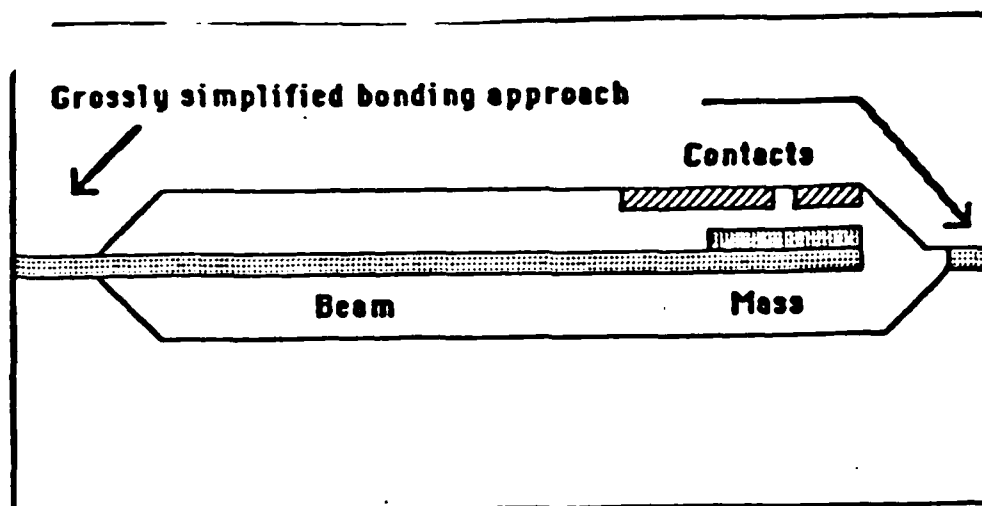


Figure 12-1. Recommended Two-Substrate Approach

A recommendation to desensitize the beam to contact-welding between the gold surfaces could also take advantage of the double substrate approach. Using different metallurgies on the contacts invariably requires that one address the compatibility between different etchants involved and the silicon dioxide material from which the beams are fabricated. Additional protective layers may be necessary to prevent exotic metallizations (e.g. titanium, rhodium) using a single substrate approach. A double substrate approach, however, permits processing of the stationary contact separately - a definite advantage. This approach also permits the contact gap to be larger. TDI estimates they could double the contact gap distance with the monolithic approach but could increase it many times when separate substrates are utilized. One can take advantage of the larger gap by increasing the stored energy in the beam which the acceleration field is removed.

The possibility of utilizing conductive polymers having inherently low elastic modulus properties should also be considered since this affords a certain degree of mechanical compliance and avoids the problem gold-to-gold surface contact.

APPENDIX A. MICROBEAM DESIGN PROGRAM

```

5 DEFSNG L
6 DEFSNG G
10 INPUT "ACCELERATION (G'S)"; ACCEL
20 INPUT "THICKNESS (MICRONS)"; THICK
30 INPUT "WIDTH (MICRONS)"; WDT
40 INPUT "GAP (MICRONS)"; GAP
50 INPUT "POTENTIAL (VOLTS)"; VDD
60 INPUT "PLATE AREA PER SIDE (MICRONS^2)"; APLATE
70 INPUT "MINIMUM LENGTH (MICRONS)"; LMIN
80 INPUT "MAXIMUM LENGTH (MICRONS)"; LMAX
90 INPUT "PRECISION FOR SOLUTION (EPSILON IN MICRONS)"; EPS
100 REM
110 REM   CONVERT INPUT TO CGS SYSTEM
120 REM
130 ACCEL=ACCEL*980.6
140 WDT=WDT/10000
150 THICK=THICK/10000
160 GAP = GAP/10000
170 VDD = VDD*1E+07
180 APLATE = APLATE/1E+08
181 LMIN = LMIN/10000
182 LMAX = LMAX/10000
183 EPS=EPS/10000
190 REM   FIXED PARAMETERS, E=ELASTIC MODULUS, RHO=MASS DENSITY
200 REM   GMASS= MASS OF GOLD CONCENTRATED AT TIP,
210 REM   EPZRO= ELECTROSTATIC CONSTANT
220   E=6.9E+11
230   RHO=2.5
240   GMASS=2.32E-08
250   EPZRO=8.85E-21
260 REM
270 REM   GUESS FIRST LENGTH
280 REM
290   LENGTH = (LMIN + LMAX)/2
300 REM
310 REM   CALCULATE BEAM STIFFNESS
320 REM
330 REM   GOSUB 1000
340 REM
350 REM   CALCULATE DEFLECTION DUE TO MASS
360 REM
370 REM   GOSUB 2000
380 REM
390 REM   CALCULATE DEFLECTION DUE TO BODY FORCES
400 REM
410 REM   GOSUB 3000
420 REM
430 REM   SUM DEFLECTIONS DUE TO ACCELERATION
440 REM
450 REM   DFLA = DFLM + DFLB
460 REM
470 REM   DETERMINE IF SWITCH CLOSURES WITHOUT VOLTAGE (GAP REMAINING)
480 REM
490 REM   GAPR = GAP - DFLA
500 REM
510 REM   IF SWITCH CLOSURES DUE TO ACCELERATION ALONE, REITERATE
520 REM
530 REM   IF GAPR < 0 THEN LMAX=LENGTH: GOTO 500
540 REM
550 REM   CALCULATE ELECTROSTATIC DEFLECTION
560 REM
570 REM   GOSUB 4000
580 REM
590 REM   CALCULATE SWITCH CLOSURE TOTAL REMAINING GAP
600 REM
610 REM   GAPR = GAPR - DFLC

```

```

840 REM
850 REM IF SWITCH DEFLECTS TO WITHIN EPSILON OF CLOSURE THEN STOP
860 REM
870 IF ABS (GAPT) < EPS THEN GOTO 10000
880 REM
890 REM OTHERWISE CALCULATE NEW MIN OR MAX LENGTH AND REITERATE
900 REM
910 IF GAPT < 0 THEN LMAX = LENGTH : GOTO 500
920 IF GAPT > 0 THEN LMIN = LENGTH : GOTO 500
930 STOP
1000 REM
1010 REM SUBROUTINE BEAM STIFFNESS
1020 REM
1030 K = (E*WDT*(THICK^3))/(4*(LENGTH^3))
1040 RETURN
1050 STOP
2000 REM
2010 REM SUBROUTINE MASS DEFLECTION
2020 REM
2030 DFLM = GMASS * ACCEL / K
2040 RETURN
2050 STOP
3000 REM
3010 REM SUBROUTINE BODY FORCE DEFLECTION
3020 REM
3030 DFLB = 1.5 * RHO * ACCEL * (LENGTH^4)
3040 DFLB = DFLB/(E*(THICK^2))
3050 RETURN
3060 STOP
4000 REM
4010 REM SUBROUTINE ELECTROSTATIC DEFLECTION
4020 REM 1/2 OF VDD ACROSS EACH PLATE
4030 REM
4040 EFORC = ((VDD^2)*EPZRO*APLATE)/(4*(GAPR^2))
4050 DFLE = EFORC / K
4060 RETURN
4070 STOP
4080 REM
4090 REM
10000 REM OUTPUT
10010 REM
10020 LPRINT "ACCELERATION ";ACCEL/980.6;" G's"
10030 LPRINT "WIDTH "; WDT*10000 " MICRONS"
10040 LPRINT "THICKNESS "; THICK*10000 " MICRONS"
10080 LPRINT "GAP "; GAP*10000; " MICRONS"
10090 LPRINT "POTENTIAL "; VDD/1E+07 ; " VOLTS"
10100 LPRINT "CONTACT AREA (EACH SIDE) "; APLATE*1E+08 ; "SQUARE MICRONS"
10110 LPRINT " "
10120 LPRINT "BEAM LENGTH "; LENGTH*10000 ; " MICRONS"
10130 LPRINT "INSTABILITY POINT "; GAPR*10000 ; " MICRONS"
10140 LPRINT "BEAM SPRING CONSTANT "; K ; " DYNES/CM"
10150 LPRINT " "
10160 LPRINT " "
10170 LPRINT " "
10180 STOP
10190 END

```

ACCELERATION 3000 G's
WIDTH 30 MICRONS
THICKNESS 3 MICRONS
GAP 1 MICRONS
POTENTIAL 3 VOLTS
CONTACT AREA (EACH SIDE) 100 SQUARE MICRONS

BEAM LENGTH 216.5642 MICRONS
INSTABILITY POINT .1131294 MICRONS
BEAM SPRING CONSTANT 1375.67 DYNES/CM
THRESHOLD VOLTAGE 76.8524932861326 VOLTS

ACCELERATION 7000 G's
WIDTH 30 MICRONS
THICKNESS 3 MICRONS
GAP 1 MICRONS
POTENTIAL 3 VOLTS
CONTACT AREA (EACH SIDE) 100 SQUARE MICRONS

BEAM LENGTH 170.2726 MICRONS
INSTABILITY POINT 8.892159E-02 MICRONS
BEAM SPRING CONSTANT 2830.336 DYNES/CM
THRESHOLD VOLTAGE 113.1038436889648 VOLTS

ACCELERATION 11000 G's
WIDTH 30 MICRONS
THICKNESS 3 MICRONS
GAP 1 MICRONS
POTENTIAL 3 VOLTS
CONTACT AREA (EACH SIDE) 100 SQUARE MICRONS

BEAM LENGTH 149.4102 MICRONS
INSTABILITY POINT 7.803755E-02 MICRONS
BEAM SPRING CONSTANT 4189.219 DYNES/CM
THRESHOLD VOLTAGE 137.60205078125 VOLTS

ACCELERATION 224 G's
WIDTH 30 MICRONS
THICKNESS 3 MICRONS
GAP 1 MICRONS
POTENTIAL 3 VOLTS
CONTACT AREA (EACH SIDE) 100 SQUARE MICRONS

BEAM LENGTH 434.6619 MICRONS
INSTABILITY POINT .2270293 MICRONS
BEAM SPRING CONSTANT 170.1451 DYNES/CM
THRESHOLD VOLTAGE 27.73116111755371 VOLTS

ACCELERATION 1394 G's
WIDTH 30 MICRONS
THICKNESS 3 MICRONS
GAP 1 MICRONS
POTENTIAL 3 VOLTS
CONTACT AREA (EACH SIDE) 100 SQUARE MICRONS

BEAM LENGTH 267.7669 MICRONS
INSTABILITY POINT .1336783 MICRONS
BEAM SPRING CONSTANT 727.7696 DYNES/CM
THRESHOLD VOLTAGE 57.35268236525391 VOLTS

ACCELERATION 3121 G's
WIDTH 30 MICRONS
THICKNESS 3 MICRONS
GAP 1 MICRONS
POTENTIAL 3 VOLTS
CONTACT AREA (EACH SIDE) 100 SQUARE MICRONS

BEAM LENGTH 214.1762 MICRONS
INSTABILITY POINT .1118806 MICRONS
BEAM SPRING CONSTANT 1422.2 DYNES/CM
THRESHOLD VOLTAGE 80.17493438720703 VOLTS

Appendix B

APPENDIX B. Microbeam Torsional Stiffness Calculations.

Appendix B

The purpose of this analysis is to examine the relative stiffness of a specific cantilever structure in torsion as compared with bending. The most torsionally compliant cantilever structure fabricated during this effort was the 430- μm beam. While other beams are shorter and consequently more stiff torsionally, they are also shorter and more stiff in their first bending mode.

Beam Length; 430 μm = 1.693E-2 inches
Beam Width; 30 μm = 1.181E-3 inches
Beam Thickness; 3 μm = 1.181E-4 inches

Elastic Modulus (SiO_2) = 0.69E12 dyne/cm² = 10,000E6 psi
Shear Modulus = 0.265E12 dyne/cm² = 3.84E6 psi

The following conversion factors are listed for convenience:

1 μm = 3.937E-5 inches
1 dyne/cm² = 1.45E-5 psi
1 dyne/cm = 5.71E-6 lb/in
1 dyne = 2.248E-6 lb.

The bending stiffness of a cantilever structure is given by:

$$K_B = \frac{Eb^3}{4L^3} \quad (1)$$

where E = Young's Modulus
b = beam width
h = beam thickness
L = beam length

$$\begin{aligned} &= (10.007\text{E}6)(1.181\text{E}-3)(1.181\text{E}-4)^3 \\ &= 1.003\text{E}-3 \text{ lb/in} \end{aligned} \quad (1a)$$

Appendix B

The torsional stiffness of the same beam is given by:

$$K_T = \frac{T}{\theta} = \frac{GJ}{L} \quad (2)$$

If θ is approximately 0, $\delta = R\theta$. Then,

$$K_T = \frac{FR}{\delta/R} = \frac{GJ}{L} \quad (3)$$

$$= \frac{F}{\delta} = \frac{GJ}{R^2L} \quad (4)$$

Since

$$J = (b/2)(h/2)^3 \left[\frac{(16/3) - (3.36) \frac{(h/2)}{(b/2)} \left(1 - \frac{(h/2)^4}{12(b/2)^4} \right) \right] \quad (5)$$

$$= 6.076E-16 \text{ in}^4$$

and contact is assumed to take place at a distance "R" from the centerline of the beam; then

$$K_B = \frac{(3.84E6)(6.076E-16)}{(37.5)^2(1.693E-2)} \quad (6)$$

$$= 6.323E-2 \text{ lb/in}$$

One can similarly compute the bending stiffness of the gull wing itself by using equation 1 and adjusting the values for b, h, and I accordingly.

$$K_G = \frac{(11.99E-6)(394E-6)(59.1E-6)^3}{(4)(394E-6)^3} = 3.99 \text{ lb/in.} \quad (7)$$

Table B-1 contrasts these ratios for comparative purposes. It can be seen the torsional stiffness greatly exceeds the bending stiffness implying proportionately greater accelerations to close a contact by torsionally rotating the beam.

Appendix B

Table B-1. Comparison of stiffness values for various modes.

Beam Type	Mode	Stiffness(lb/in)	Ratio
SiO ₂	Bending	1.003 E-3	1.0
SiO ₂	Torsion	6.32 E-2	63.04
Gull Wing (Gold)	Bending	3.99	3978

Microscale G-Switch

APPENDIX C

MODAL ANALYSIS TECHNIQUES

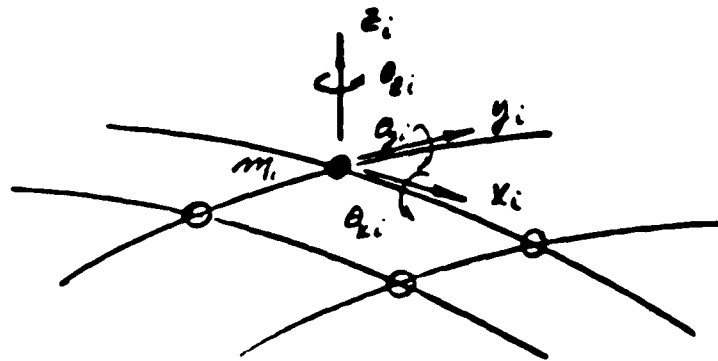
Microscale G Switch

The following pages are copies of view graph presentation material explaining Modal Analysis methods and terminology presently in use by Motorola's Mechanical Engineering Laboratory. Several examples and explanations are also included for ease of understanding.

• GENERALIZED COORDINATE THEORY/MODAL ANALYSIS

- ALLOWS ONE TO SOLVE FOR THE RESPONSE OF A COMPLEX STRUCTURE WITH POSSIBLY THOUSANDS OF DEGREES OF FREEDOM BY TRANSFORMING THE COORDINATES FROM THE PHYSICAL COORDINATES TO MODAL COORDINATES.

STRUCTURE



- EACH MASS POINT OF THE STRUCTURE MAY HAVE UP TO 6 DEGREES-OF-FREEDOM
- EQUATIONS OF MOTION

$$[M]\{\ddot{x}_i\} + [C]\{\dot{x}_i\} + [K]\{x_i\} = \{F_i\}$$

- BECAUSE OF LARGE SIZE, SOLUTION IS DIFFICULT

- MODAL ANALYSIS

- EACH DEGREE OF FREEDOM x_i IS A FUNCTION OF SPACE (POSITION ON STRUCTURE) AND TIME. THESE VARIABLES ARE SEPARABLE SINCE ONE DOES NOT DEPEND UPON THE OTHER

$$\{x_i\} = \{x_i(s_i, t)\} = \sum_n \phi_n(s_i) q_n(t)$$

OR $\{x_i\} = [\phi_n] \{q_n\}$, $i = \text{POSITION}, n = \text{MODE}$

WHERE,

$$\phi_n(s_i) = \text{MODE SHAPE}$$

$$q_n(t) = \text{GENERALIZED COORDINATE}$$

- SUBSTITUTE INTO EQUATION OF MOTION AND PRE-MULTIPLY BY ϕ^T

$$\phi^T M \phi \ddot{q}_n + \phi^T C \phi \dot{q}_n + \phi^T K \phi q_n = \phi^T F$$

LET,

$$\phi^T M \phi = m_n$$

$$\phi^T C \phi = 2 \gamma_n \omega_n m_n$$

$$\phi^T K \phi = m_n \omega_n^2$$

$$\phi^T F = q_n$$

RESULTING EQUATION OF MOTION -

$$m_n \ddot{q}_n + 2\zeta_n \omega_n m_n \dot{q}_n + m_n \omega_n^2 q_n = q_n$$

WHERE,

- m_n = GENERALIZED MASS $(m_n = 1 \text{ in SAP})$
- ω_n = NATURAL FREQUENCY
- ζ_n = CRITICAL DAMPING RATIO
- q_n = GENERALIZED FORCE

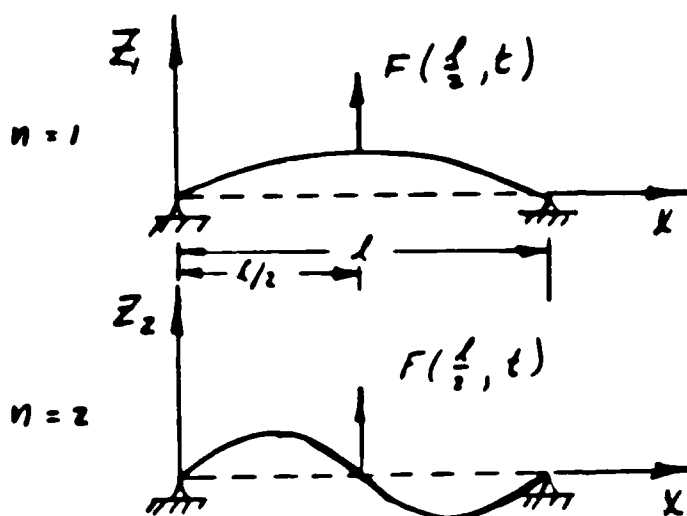
GENERALIZED FORCE

$$Q_n = \phi^T F, \quad F_i = p(x_i) f(t)$$

$$Q_n = f(t) \sum_i \phi_n(x_i) p(x_i)$$

EACH MODE RESPONDS TO ITS OWN GENERALIZED FORCE.

EXAMPLE OF GENERALIZED FORCE FOR POINT LOAD.



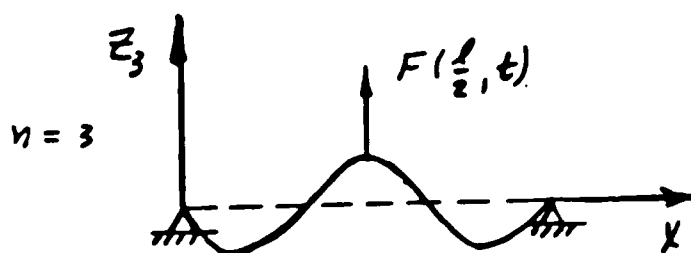
$$Q_1 = f(t) \sum_i p(x_i) z_1(x_i)$$

$$Q_1 = f(t) p\left(\frac{l}{2}\right) z_1\left(\frac{l}{2}\right)$$

$$Q_2 = f(t) \sum_i p(x_i) z_2(x_i)$$

$$Q_2 = f(t) p\left(\frac{l}{2}\right) (0) = 0$$

NOTE, THE FORCE F IN THIS CASE COULD BE FORCING MODE 2 AT ITS RESONANT FREQUENCY BUT THE MODE WOULD NOT RESPOND SINCE IT IS BEING FORCED AT A NODE POINT

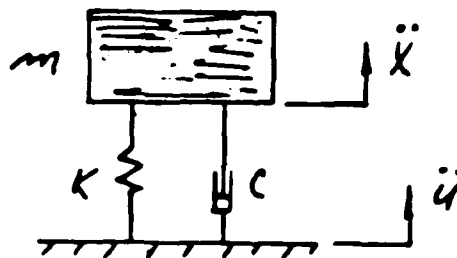


$$Q_3 = f(t) \sum_i p(x_i) z_3(x_i)$$

$$Q_3 = f(t) p\left(\frac{l}{2}\right) z_3\left(\frac{l}{2}\right)$$

GROUND ACCELERATION -

SINGLE DEGREE OF FREEDOM -



x = ABSOLUTE MOTION OF m

u = GROUND MOTION

FROM: NEWTON'S LAW,

$$\sum F = m \ddot{x}$$

$$-K(x-u) - C(\dot{x} - \dot{u}) = m \ddot{x}$$

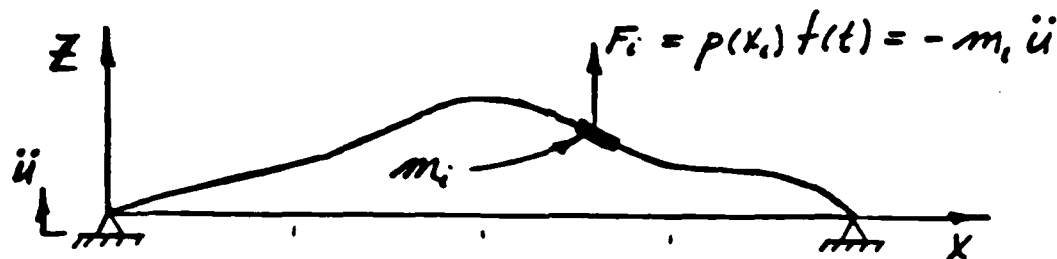
$$\text{LET } \zeta = x - u$$

$$\therefore -K\zeta - C\dot{\zeta} = m(\ddot{\zeta} + \ddot{u})$$

OR,

$$m\ddot{\zeta} + C\dot{\zeta} + K\zeta = -m\ddot{u}$$

GROUND ACCELERATION APPLIED TO PINNED-PINNED BEAM



THE LOADING ACTING ON THIS BEAM IS SIMILAR TO THE LOADING ACTING ON THE SINGLE DEGREE-OF-FREEDOM MASS. THIS IS A DISTRIBUTED LOADING, THEREFORE, THE GENERALIZED FORCE FOR MODE n IS,

$$\begin{aligned} Q_n &= \sum_i F_i z_n(x_i) = \int_0^l dF z_n(x_i) \\ &= -\ddot{u}(t) \sum_i m_i z_n(x_i) = -\ddot{u}(t) \int_0^l z_n(x) dm \end{aligned}$$

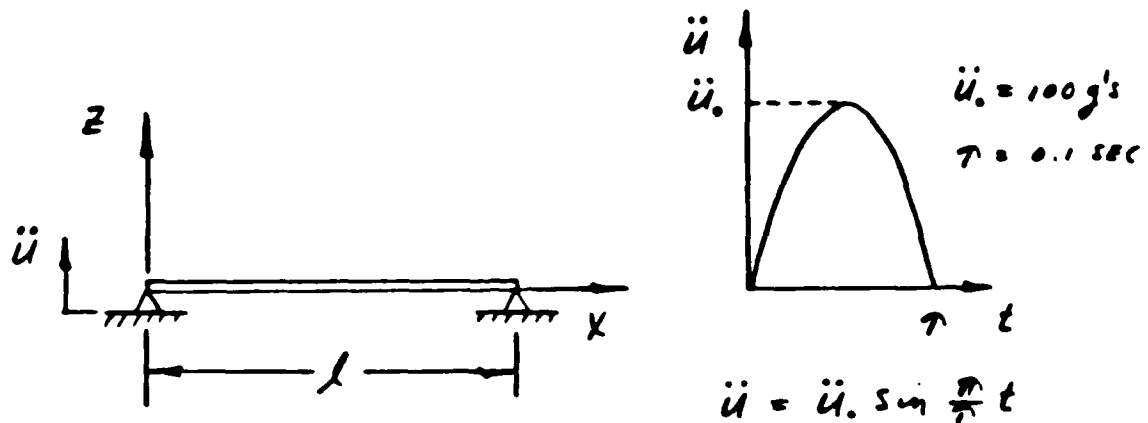
THE TERM $\int_0^l z_n(x) dm$ IS KNOWN AS THE "MODAL PARTICIPATION FACTOR Γ_n


$$Q_n = -\ddot{u}(t) \Gamma_n$$

- THE DEFINITION OF THIS FACTOR USUALLY IS DEFINED TO INCLUDE DIVIDING BY THE GENERALIZED MASS m_n .

SAMPLE PROBLEM -

- DETERMINE MAXIMUM RESPONSE OF FIRST THREE MODES OF A PINNED-PINNED UNIFORM BEAM TO A HALF SINE GROUND ACCELERATION PULSE OF 100 G'S LASTING 0.1 SECONDS.



MATERIAL - ALUMINUM
 CROSSECTION - 

$$\mu = \rho A = 0.1 (2) = .2 \text{ lb/in}, \quad l = 10' = 120''$$

$$EI = 10 \times 10^6 \frac{1}{12} (1)(2)^3 = 6.67 \text{ EG in}^2$$

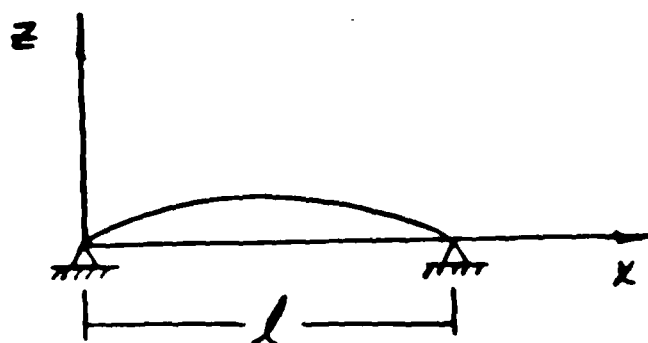
$$\omega_n = n\pi \sqrt{\frac{EI}{\mu l^4}}$$

$$\omega_1 = 77.4 \text{ RAD/SEC} = 12.4 \text{ Hz}, \quad T_1 = .0808 \text{ SEC}$$

$$\omega_2 = 311.0 \text{ RAD/SEC} = 49.5 \text{ Hz}, \quad T_2 = .0202 \text{ SEC}$$

$$\omega_3 = 699.7 \text{ RAD/SEC} = 111.4 \text{ Hz}, \quad T_3 = .0090 \text{ SEC}$$

FIRST MODE CALCULATIONS,



$$z = z_0 \sin \frac{\pi}{l} x$$

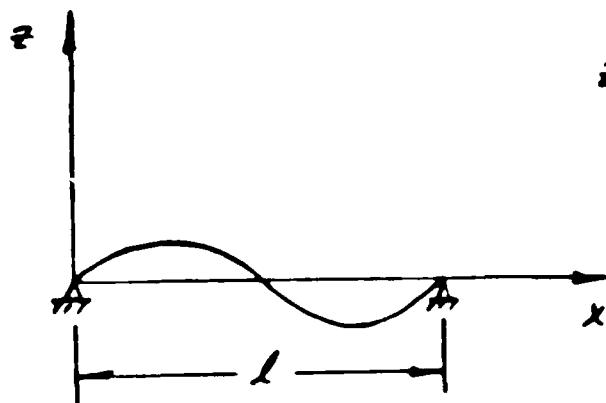
GENERALIZED MASS,

$$\begin{aligned} m_1 &= \int_0^l \ddot{z}_1(x) dm, \quad dm = \frac{\mu}{g} dx \\ &= \int_0^l z_0^2 \sin^2 \frac{\pi}{l} x \frac{\mu}{g} dx = \frac{\mu}{g} z_0^2 \left(\frac{x}{2} \right) \Big|_0^l \\ &= \frac{1}{2g} \mu z_0^2 l = \frac{1}{2g} (1.2) z_0^2 (120) = .03109 z_0^2 \end{aligned}$$

MODAL PARTICIPATION FACTOR,

$$\begin{aligned} \Gamma_1 &= \int_0^l z_1(x) dm \\ &= \int_0^l z_0 \sin \frac{\pi}{l} x \left(\frac{\mu}{g} \right) dx \\ &= \frac{\mu}{g} z_0 \frac{l}{\pi} \left(-\cos \frac{\pi}{l} x \right) \Big|_0^l \\ &= \frac{2\mu l}{\pi g} z_0 = \frac{2(1.2)120}{\pi g} z_0 = .03958 z_0 \end{aligned}$$

SECOND MODE CALCULATIONS,



$$z = z_0 \sin \frac{2\pi}{l} x$$

GENERALIZED MASS,

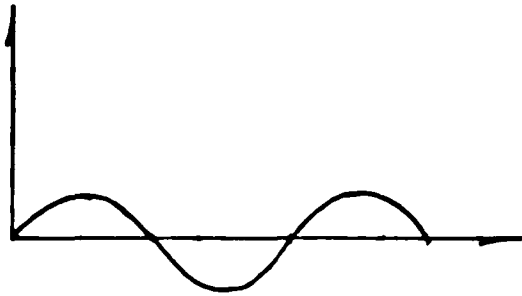
$$\begin{aligned} m_2 &= \int_0^l z_2^2 dm = \int_0^l z_0^2 \sin^2 \frac{2\pi}{l} x \frac{\mu}{g} dx = z_0^2 \frac{\mu}{g} \frac{x}{2} \Big|_0^l \\ &= \frac{1}{2} \mu z_0^2 l = 0.3109 z_0^2 \end{aligned}$$

MODAL PARTICIPATION FACTOR,

$$\Gamma_2 = \int_0^l z_2 dm = \int_0^l z_0 \sin \frac{2\pi}{l} x \frac{\mu}{g} dx$$

$$\Gamma_2 = 0$$

THIRD MODE CALCULATIONS



$$z = z_0 \sin \frac{3\pi}{l} x$$

GENERALIZED MASS,

$$\begin{aligned} m_3 &= \int_0^l z_3^2 dm = \int_0^l z_0^2 \sin^2 \frac{3\pi}{l} x \frac{M}{l} dx = z_0^2 \frac{M}{l} \left(\frac{x}{2} \right) \Big|_0^l \\ &= \frac{1}{2} \frac{M}{l} z_0^2 l \end{aligned}$$

MODAL PARTICIPATION FACTOR,

$$\Gamma_3 = \int_0^l z_3 dm = \int_0^l z_0 \sin \frac{3\pi}{l} x \left(\frac{M}{l} \right) dx$$

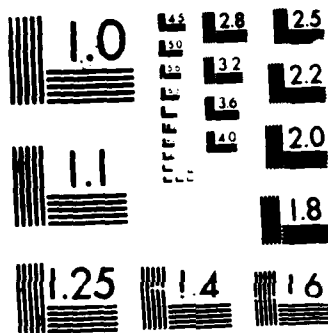
$$\Gamma_3 = z_0 \frac{M}{l} \frac{l}{3\pi} \left(-\cos \frac{3\pi}{l} x \right) \Big|_0^l = -z_0 \frac{M}{l} \frac{l}{3\pi} (-1 - 1)$$

$$\Gamma_3 = \frac{2Ml}{3\pi} z_0$$

AD-A180 112 SOLID-STATE THRESHOLD ACCELEROMETER CHIP(U) MOTOROLA 2/2
INC SCOTTSDALE AZ GOVERNMENT ELECTRONICS GROUP
L FARRACO ET AL 28 MAR 87 HDL-CR-86-146-1
UNCLASSIFIED DAAL02-85-C-0146

F/G 19/1 NL





MICROCOPY RESOLUTION TEST CHART
NATIONAL BUREAU OF STANDARDS 1963-A

EQUATION OF MOTION TO BE SOLVED FOR EACH MODE N,

$$m_n \ddot{g}_n + 2\zeta_n \omega_n m_n \dot{g}_n + m_n \omega_n^2 g_n = Q_n$$

WHERE,

$$Q_n = -\ddot{u} \Gamma_n \quad \ddot{u} = \ddot{u}_0 \sin \frac{\pi}{T} t, \quad t \leq T; \quad \ddot{u} = 0 \quad t > T$$

$$g_{n,max} = - \frac{\ddot{u}_0 \Gamma_n}{m_n \omega_n^2} (DLF)_n, \quad DLF = \text{DYNAMIC LOAD FACTOR}$$

FOR MODE 1,

$$DLF, \text{ FOR } T_1 = .0808 \text{ SEC } \dot{\text{I}} \quad T = 0.1 \text{ SEC} \quad \text{HALF SINE}$$

$$DLF_1 = 1.65$$

$$g_{1,max} = - \frac{100 (32c) .03958 \cdot 2. (1.65)}{0.3109 \cdot 2. (77.764)^2}$$

$$g_{1,max} = 13.41 / 2.$$

NOTE THE MAXIMUM PHYSICAL DEFLECTION OF A POSITION X ON THE BEAM DUE TO MODE 1 ONLY IS,

$$z(x, t) = z_1(x) g_{1,max}(t) = z_0 \sin \frac{\pi}{L} x \cdot 13.41 / 2.$$

$$z(x, t) = 13.41 \sin \frac{\pi}{L} x$$

THIS SHOWS THAT THE NORMALIZATION Z_0 IS NOT A FACTOR IN THE FINAL RESULT

THE MAXIMUM DEFLECTION AT THE BEAM CENTER DUE TO MODE 1 IS THEREFORE,

$$\begin{aligned} z\left(\frac{L}{2}, t\right) &= \sum_n z_n\left(\frac{L}{2}\right) g_{n,max}(t) \\ &= 13.41 \text{ INCHES} \end{aligned}$$

AS A CHECK THE RESPONSE TO THE STATIC LOAD CAN BE DETERMINED
USING THE EQUATION FOR A UNIFORM LOAD APPLIED TO A PINNED-
PINNED BEAM,

$$\Delta = \frac{5 w l^4}{384 EI} = \frac{5 (.2 \times 100) 120^4}{384 (6.67 \times 10^6)}$$

$$\Delta = 8.10 \text{ INCHES}$$

THE CONTRIBUTION OF THE SECOND MODE TO THE DEFLECTION OF THE BEAM AT ITS CENTER IS,

$$g_{2max} = -\frac{4 \Gamma_2}{m_2 \omega_2^2} (\Delta F)_2 = -\frac{100(386)(0)1.1}{.03109 20^2 (3.14)^2} = 0$$

$$z = z_2\left(\frac{L}{2}\right) g_{2max} = 0$$

SIMILARLY, THE CONTRIBUTION OF THE THIRD MODE IS,

$$g_{3max} = -\frac{4 \Gamma_3}{m_3 \omega_3^2} \Delta F_3 = -\frac{100(386) \cdot .03958 z_0(1)}{.03109 20^2 (699.88)^2} = -\frac{.0334}{z_0}$$

$$z\left(\frac{L}{2}, t\right) = z_0\left(1 - \frac{.0334}{z_0}\right) = -.0334 \text{ INCHES}$$

THE MAXIMUM DEFLECTION AT THE BEAM CENTER PREDICTED BY THESE THREE MODES COULD BE OBTAINED BY SOLVING EACH EQUATION OF MOTION AS A FUNCTION OF TIME ADDING THE RESPONSES OF EACH MODE,

$$z\left(\frac{L}{2}, t\right) = \sum_n z_n\left(\frac{L}{2}\right) g_n(t)$$

THIS CAN BE DONE USING PROGRAM GCR. TO OBTAIN THE MAXIMUM POSSIBLE RESPONSE, DISREGARDING PHASING OF THE THREE RESPONSES SIMPLY ADD THE ABSOLUTE MAXIMUM OF EACH MODAL RESPONSE,

$$z\left(\frac{L}{2}, t\right) = 13.41 + .0334 = 13.74 \text{ INCHES}$$

IF THE LOAD APPLIED WAS A STATIC LOAD THE RESPONSE OF THE FIRST THREE MODES WOULD BE,

$$z_1 = 13.41/1.65 = 8.12 \text{ INCHES}$$

$$z_2 = 0$$

$$z_3 = .0334/1 = .0334 \text{ INCHES}$$

THE TOTAL RESPONSE WOULD BE,

$$z\left(\frac{L}{2}\right) = \sum_n z_n\left(\frac{L}{2}\right) g_n(t) = 13.12 + 0 + .0334$$

$$z\left(\frac{L}{2}\right) = 8.15 \text{ INCHES}$$

DISTRIBUTION

	<u>No. Cys.</u>
<u>DTIC</u>	
DTIC - A (Accessions)	1
<u>LABCOM</u>	
Technical Director (Vitali)	1
<u>HDL</u>	
Director (Donald B. Dinger)	1
Chief Division 2 (John A. Rosado)	1
Chief Lab 34000 (Philip F. Ingersoll)	1
Plans/Ops (S.M. Kulpa)	1
Br. 22300 (J.L. McGarrity and R.B. Reams)	2
Br. 34200	20
	Balance
<u>National Science Foundation (Alex Schwartzkopk)</u>	
Washington, DC 20550	1
<u>Army Research Office (Michael A. Stroschio)</u>	
Research Triangle Park, NC 27709-2211	1
<u>Other DOD</u>	
• Eglin AFB, FL ATTN: Library	1
32542 ATTN: AD/DLJF: R. Mabry	1
• US NSWC/WO ATTN: Library	1
20903-5000 ATTN: Code G44: G.E. Klamm	1
• US NWC, China Lake, CA ATTN: Library	1
93555 ATTN: Code 3353: R. Perrine	1
• US ARDEC, Dover, NJ ATTN: Library	1
07801 ATTN: SMCAR-LCN: L. Horowitz	1
• Army BMD, Adv. Technology Center	
Huntsville, AL ATTN: DASD-H-QL: Roger Heatherly	1
35807-3801	
<u>DOE Nat'l Labs</u>	
• Lawrence Livermore Nat'l Lab ATTN: Library	1
Livermore, CA 94550 ATTN: MS-L-156: D. Ciarlo	1
• Los Alamos Nat'l Laboratories ATTN: Library	1
Los Alamos, NM 87544	
• Sandia Nat'l Lab ATTN: Library	1
Albuquerque, NM 87185 ATTN: C.W. Childers: Div 1617	1

Universities

No. Cy .

- U.C. Berkeley
ATTN: Prof. R.S. Muller: Berkeley Integrated Sensors Center 1
ATTN: Prof. R.F. White: Berkeley Integrated Sensors Center 1
Berkeley, CA 94720
- U. Wisconsin 1
ATTN: Prof. Henry Guckle: WCAM
Madison, WI 53706
- Stanford Univ 1
ATTN: Prof. James B. Angell: Dept. of Electrical Engineering
Palo Alto, CA 94305
- U. Washington 1
ATTN: Dr. Peter Cheung: Dept. of Electrical Engineering
Seattle, WA 98195
- Yale University 1
ATTN: Dr. Dennis L. Polla: Center for Microelectronics and
Structures
P.O. Box 2157 Yale Center
New Haven, CT 06520-2157
- Case Western Reserve U. 1
ATTN: Dr. Wen H. KO: Electronics Design Center
Cleveland, OH 44106
- U. of Michigan 1
ATTN: Prof. Kensall D. Wise: 1246 EECS Bldg
1301 Beal Ave.
Ann Arbor, MI 48109

END

6-87

DTIC